General Disclaimer

One or more of the Following Statements may affect this Document

- This document has been reproduced from the best copy furnished by the organizational source. It is being released in the interest of making available as much information as possible.

- This document may contain data, which exceeds the sheet parameters. It was furnished in this condition by the organizational source and is the best copy available.

- This document may contain tone-on-tone or color graphs, charts and/or pictures, which have been reproduced in black and white.

- This document is paginated as submitted by the original source.

- Portions of this document are not fully legible due to the historical nature of some of the material. However, it is the best reproduction available from the original submission.

Produced by the NASA Center for Aerospace Information (CASI)

NASA

Technical Memorandum 84947

The Magnetosphere of Saturn

A. W. Schardt

DECEMBER 1982

NASA
Technical Memorandum 84947

The Magnetosphere of Saturn

A. W. Schardt

Abstract. The Pioneer 11, Voyagers 1 and 2 encounters with Saturn provided a
wealth of information about its complex magnetosphere. The magnetic dipole
moment of Saturn is rotationally alligned and only one-fifth of that expected
from pre-encounter modeling. The bow shock stand-off distance is about 22 R_S
and varies with solar wind pressure proportional to $p^{-1/6}$. The satellites
Titan, Dione and Tethys are probably the primary sources of magnetospheric
plasma. For < 10 keV thermal plasma, β < 1 in most of the magnetosphere, but
contributions from ~ 20 keV plasma may increase this value significantly.
Outside of ~4 R_S, energetic particles are energized by diffusing inward while
conserving their first and second adiabatic invariants. Particles are lost by
satellite sweep-out, absorption by the E ring and probably also by plasma
interactions, which produce a slot region betwen 4 and 9 R_S. The inner
magnetosphere is characterized by a cold plasma population (<10 eV/charge),
which probably consists primarily of O^+ and has a scale height from the
Equator of only 0.2 R_S. Intense penetrating radiation exists in the inner
magnetosphere from 4R_S to 2.265 R_S, which coincides with the outer edge of the
A ring. The energetic protons >50 MeV have approximately the spectrum
expected from a cosmic ray albedo neutron decay source. A proton component
below 0.5 MeV was also found, as well as an electron flux with energies
primarily above 1.5 MeV. Submicron charged dust grains constitute a new type
of magnetospheric particle and their properties may explain the evolution of
the B ring spokes and other B ring features.

3

Introduction

Serious thought was given to the possible existence of a magnetosphere at Saturn after the discovery in 1955 of decametric radio emission from Jupiter. Between 1959 and 1962, it was shown that the decimetric emissions were due to synchrotron radiation emitted by relativistic electrons trapped in Jupiter's magnetic field. Saturn's magnetic field strength, when scaled from Jupiter's field by the "magnetic Bode's Law", was strong enough to suggest observable radiation from that planet as well. Both ground-based and pre-Voyager space observations detected radio noise that could be attributed to Saturn; but the attribution was uncertain at the time, and we now know from Voyager observations that it was incorrect.

Modeles of a potential magnetosphere of Saturn (Kennel, 1973; Scarf, 1973; Siscoe, 1978) were developed to support planning of NASA missions to the outer planets. These models were based on extrapolations from the terrestrial magnetosphere but predicted also significant differences compared to the Earth's magnetosphere, such as the presence of magnetospheric plasma out to the magnetopause, corotation-induced distortion of the magnetic field, and energetic particle sweep-out by the rings and satellites of Saturn. The modeling also showed that relatively intense electron fluxes could exist near Saturn without producing strong enough synchrotron radiation to be detectable at Earth.

The Pioneer 11 fly-by of Saturn on September 1, 1979 provided the first definitive proof that a magnetosphere surrounded Saturn. Our present knowledge is based entirely on the observations performed with Pioneer 11 and Voyagers 1 and 2 (Fig. 1a). The three spacecraft entered the Kronian magnetosphere near the subsolar point; Pioneer 11 and Voyager 1 near the Equator and Voyager 2 at a latitude of +17°. The Pioneer 11 and Voyager 2

PRECEDING PAGE BLANK NOT FILMED

4

post-encounter trajectories were toward dawn or about -90° from the Saturn-Sun direction, and Voyager 1 penetrated the pre-dawn magnetotail to exit the magnetosphere at a solar clock angle of -140°. The Kronian latitude coverage is shown in Fig. 1b. It should be borne in mind that in-situ observations were made only over a restricted region of the magnetosphere. Extrapolations to other regions, even if based on sound principles, carry a substantial risk.

Most of the primary results have been published in special issues of several journals. The following issues contain collections of Pioneer 11 results: Science, 207, No. 4429, Jan. 25, 1980; and J. Geophys. Res., 85, No. A11, Nov. 1, 1980. The Voyager results are published in Science, 212, No. 4491, April 10, 1981; Science, 215, No. 4532, Jan. 21, 1982; Nature, 292, No. 5825, Aug. 20-26, 1981; J. Geophys. Res., 87, No. A3, March, 1982; J. Geophys. Res., 88, No. A2, Feb. 1983; and J. Geophys. Res. 88, the special Saturn issue due in Sept., 1983. Tom Gehrels, editor, is preparing a book about Saturn to be published in 1983 by the University of Arizona Press. With such a wealth and diversity of new information, this review would have been unmanageable without imposing rather arbitrary limits on its scope. In particular, we will discuss neither the optical radiations from the neutral gas and plasma in the magnetosphere nor the waves generated in the energetic particle plasma interactions. For an interdisciplinary summary of results, see Opp (1980) and Stone and Minor (1981, 1982). Plasma wave phenomena are covered in a companion report by Anderson (1983).

As expected, Saturn's magnetosphere is intermediate between the magneto-spheres of Jupiter and Earth. It resembles the terrestrial magnetosphere in the magnetic field strength at the surface, the inward diffusion and energization of trapped energetic particles and the importance of cosmic ray albedo neutron decay (CRAND) as a source for inner belt protons. It resembles

Jupiter's magnetosphere by the presence of relatively dense plasma in the outer magnetosphere to the magnetopause. Titan and the inner satellites and rings appear to be important sources of magnetospheric plasma. Absorption by the rings and satellites greatly modifies the energetic particle population and, in some respects, is even more important than at Jupiter.

The positions of the bow shock and magnetopause are determined by a pressure balance between the solar wind pressure and the planetary dipole field. The magnetopause was encountered between 17.3 and 23.6 R_S (1 R_S = 60,330 km) on the inbound passes and between 30.3 and 70 R_S on the outbound passes. The magnetosphere itself can be divided into four regions with distinctly different characteristics (Fig. 1a):

(1) <u>Outer Magnetosphere and Magnetotail</u> (magnetopause to 9 R_S). This region is populated by soft (< 1 MeV) electron and proton fluxes which become more intense and harder closer to Saturn. Cosmic-ray protons above 2 MeV have free access. Titan, which is generally inside the magnetosphere, is a major source of thermal plasma with densities between 10^{-2} and 5×10^{-1} ions cm^{-3}. Plasma densities and energetic particle fluxes undergo large spatial and temporal variations and particle acceleration occurs in the magnetotail.

(2) <u>Slot Region</u> (9 - 4 R_S). The E-ring and the satellites Rhea, Dione, Tethys and Enceladus control the characteristics of this region (Fig. 1a and Table 1). They are probably the source of a relatively dense, multicomponent plasma of 0.5 - 3 ions cm^{-3} (Fig. 1b). Energetic protons, ions and low-energy electrons are heavily absorbed in this region. Inward diffusion of particles from the outer magnetosphere appears to stop at Enceladus.

(3) <u>The Inner Magnetosphere</u> (outer edge of the A ring to 3.9 R_S). The temperature of both the ion and electron plasma decreases with radius and the plasma is confined near the Equator. A source of high-energy protons (50-200

MeV) exists in this region. These energetic protons are due to the decay of neutrons resulting from the interaction of cosmic rays with the ring material. High fluxes of energetic electrons (> 1.5 MeV) are also found.

(4) The Ring Region (< 2.265 R_S). The only energetic particles observed under the A, B and C rings are galactic cosmic rays and their secondaries produced by interactions with the ring material. Because of the large energy loss in crossing the ring plane, their lifetime is 1/2 to a few bounce periods. An as yet little studied phenomenon in this region is the motion of charged dust grains in a magnetic field. The so-called spokes seen superimposed on the B-ring appear to be one manifestation of this phenomenon.

The Magnetic Field

The magnetic field defines the size and shape of the magnetosphere (Fig. 2) and is made up of the following three components:

(1) the field generated in the interior of the planet;

(2) the field from magnetospheric currents, specifically the Equatorial ring current and the cross-tail current; and

(3) the field of boundary currents at the magnetopause.

The proposed field models include primarily the planetary field and the field due to an equatorial ring current. The model fields are derived from a scalar potential which can be specified uniquely only if the field is known over a spherical shell; thus, the scalar potential derived from a single fly-by of Saturn is not unique. The Pioneer 11 data are consistent with a planetary dipole with a moment of 0.20-0.22 G-R_S^3 (or ~4.4×10^{28} G-cm^3), aligned to < 1° with the spin axis and offset by 0.04 R_S toward north (Acuña and Ness, 1980; Acuña et al, 1980; Smith et al., 1980a,b). These results require a trade-off between the strength of the ring current and the magnitude

of the dipole moment. A number of alternative harmonic expansions of the potential function give a satisfactory fit (Smith et al., 1980b).

The Voyager 1 magnetic field data are consistent with a 0.8° dipole tilt and no north-south offset (Ness et al., 1981). External ring current parameters were calculated by fitting data within 16 R_S (Acuña et al., 1981; Connerney et al., 1981), and these were used in further iteration of the planetary field. The best representation (Fig. 3) was a central dipole of 0.21 $G-R_S^3$ with a tilt of 1.0° toward an SLS longitude of 340° (for a definition of SLS longitude, see Desch and Kaiser, 1981). The internal field should not change significantly between encounters; therefore, different missions should give the same coefficients for the harmonic expansion of its potential. Connerney et al. (1982) found that this is only possible for the Voyagers 1 and 2 missions if octopole (g_3^0) and ring current terms were included (Table 2). They refer to this field potential as the "Z_3" model (Fig. 4) which was constrained to be axisymmetric; however, the low value of the residuals (3 nT r.m.s.) indicates that any asymmetric terms are small and hard to separate from the effects of external currents (Acuña et al., 1983; Connerney et al., 1983). The g_3^0 term is very important for defining the magnetic field over Saturn's surface (Fig. 5) and affects our interpretation of ionospheric, auroral and ring plane phenomena.

Energetic particle absorption signatures provide an independent check on magnetic field models. Absorption by a satellite occurs in the equatorial plane, and particles on either side of the absorption feature follow field lines to the latitude of the spacecraft. This fixes two points on the field line and tests the ability of the model to predict the field at a location where it was not observed. The Rhea signature observed by Voyager 1 confirmed the presence of a ring current (Vogt et al., 1981). The signatures of Tethys,

Enceladus and Mimas are consistent with both the spin axis-aligned offset dipole model and the Z_3 model but not with the other field models (Acuña et al., 1983; Chenette and Davis, 1982). The motion of energetic particles in the distorted field has been studied by Birmingham (1982) who also evaluated the line integrals needed in the calculations of bounce and drift periods.

Pre-encounter predictions of the intrinsic planetary field suggested a moment of 1 G-$R_S{}^3$ and a tilt of several degrees (Russell, 1980). Dynamo theories of planetary fields require at least a small departure from axial symmetry, but a tilt of only 1° may be adequate (Todoeschuck et al., 1981). The high degree of axisymmetry and relatively small magnetic moment can be explained by the model of Stevenson (1980) for the interior of Saturn. In his model the metallic H - He is differentiated into an inner He-rich core and an innomogeneous outer layer with differential rotation relative to the inner core. The smaller size of the core explains the smaller magnetic moment and the differential rotation of the outer conducting layer shields the outside from the non-axisymmetric terms of the dynamo field.

Axial symmetry of the overall planetary field leaves us without a ready explanation for the observed longitudinal asymmetry of Saturn's kilometric radio emission (Kaiser et al., 1981; Kaiser and Desch, 1982) and of auroral radiation (Sandel and Broadfoot, 1981). A localized field asymmetry at a high latitude, missed by the magnetic field observations, could be the cause.

Solar Wind-Magnetosphere Interaction

Even though significantly different plasma conditions are involved, the solar wind interaction with Saturn's magnetic field resembles, in general, that observed near Earth. All missions observed a well-defined bow shock, sheath, magnetosphere and magnetotail. Multiple boundary crossings were

observed by each mission, and the shock-to-planet distance was inversely proportional to the 1/6th power of the ram pressure of the solar wind (Bridge et al., 1981, 1982). This implies that the pressure is balanced by the planetary field rather than by magnetospheric plasma, as is the case at Jupiter.

The bow shock normal is nearly perpendicular to the magnetic field of the solar wind. The thickness of this quasi-perpendicular shock has been estimated to be 1500 - 2100 km (Smith et al., 1980b), which is a few times the ion inertial length, much larger than the electron gyroradius and much smaller than the proton gyroradius.

The shock-to-magnetopause stand-off distance at Saturn appears to be proportionately thinner than at Earth (Bridge et al., 1981). The field magnitude in the subsolar magnetosheath (Fig. 6) varies semi-periodically as the magnetopause is approached (Pioneer 11 and Voyager 1). These large changes in magnetic field are anti-correlated with the electron density in the sheath and are consistent with slow mode magnetosonic waves (Lepping et al., 1981). The Voyager 1 inbound magnetopause crossings were unique in that the average position of the magnetopause was almost stationary at that time. The five observed magnetopause crossings (Fig. 6) have been interpreted by Lepping et al. (1981) in terms of surface waves on the magnetopause with a 23-min. period. The thickness of the magnetopause was found to be $5 \pm 3 \times 10^3$ km.

The magnetopause position can be represented by a paraboloid of revolution around the Saturn-Sun line (Fig. 1a). Typically, the nose of the magnetosphere occurs at 22 R_S and the tail diameter is 80 R_S at 25 R_S behind Saturn with a typical field of 3 nT at 25 R_S. This places the boundary between the polar cap and the trapping region in the ionosphere between 75 and 78.5° (Ness et al., 1981) and agrees with the position of the southern auroral

zone which falls between 78 and 81.5° (Sandel and Broadfoot, 1981).
Magnetopause crossings observed by Voyager 2 during the outbound pass
indicated that, based on this model, the subsolar magnetopause position was at
$32 R_S$. This extremely high value may be due to an unusually low solar wind
pressure or to the possibility that Saturn entered the extended Jovian
magnetotail at that time.

The existence of a Kronian magnetotail is confirmed by the magnetic
field directions inside the magnetosphere. All the outbound passes (Fig. 1a)
were in the dawn direction (-90° to -140° from the Saturn-Sun line) and showed
the distinct onset of the tail field. The near-Equatorial current sheet moved
past Pioneer 11 several times (Ness et al., 1981; Smith et al., 1980a,b). The
field observed with Voyager 1 in the pre-dawn tail has been modeled with a
dusk-to-dawn current sheet (Fig. 7; Behannon et al., 1981). The major field
fluctuations about the average field are believed to be induced by changes in
the solar wind and are indicative of a major solar wind influence on the
properties of the outer magnetosphere and magnetotail.

Titan-Magnetosphere Interaction

The interaction between Titan and the partially-corotating magnetosphere
of Saturn is of special interest because it is a primary source of plasma in
the outer magnetosphere and because it involves a plasma regime which had not
been explored previously. The opportunity to study this interaction arose
when Voyager 1 passed 2.7 R_T (1 R_T = 2575 km) behind Titan in the sense of
corotation (Fig. 8). While the corotation velocity is 200 km/s, the actual
plasma velocity observed just outside the interaction region was 80 - 150 km/s
with a 20° offset from the corotation direction toward Saturn. The plasma
velocity went to nearly zero behind Titan (Hartle et al., 1982; Maclennan et

al., 1982). The plasma parameters give both an Alfvénic and sonic Mach number of ~ 0.5. An upper limit of 10^{21} G-cm^3 could be placed on a possible dipole moment of Titan (Ness et al., 1982). Because the inherent field of Titan is so small, the interaction with Saturn's magnetosphere takes place in Titan's ionosphere and, in that respect, resembles the solar wind-Venus interaction.

As would be expected with a Mach number below 1, no bow shock was observed by either the plasma analyzer or magnetometer; instead, Saturn's field-lines cannot pass in the ionopause of Titan's atmosphere (Fig. 9). As these field lines are stretched out by the partially corotating plasma, they drape around Titan and form a bipolar magnetic tail (Ness et al., 1981, 1982b). The plasma interaction was different on the side of Titan that faced toward the Sun than on the other side which faced Saturn. On the sunlit side, photoionization added to ionization by corotating magnetospheric plasma and the corotational electric field ($-\vec{V} \times \vec{B}$) pulled positive ions away from Titan (between points 1 and 3 of Fig. 10). Ions on the dark side were intercepted by Titan's atmosphere as shown by points 7 to 8 of Fig. 10 (Bridge et al., 1981; Hartle et al., 1982). The hot magnetospheric plasma disappeared in the wake region and was replaced by cold plasma from Titan (bite-out region of Fig. 10). Electron densities were also derived from plasma waves observed in this region (Gurnett et al., 1982; Neubauer et al., 1983). While these densities agree with plasma cup data prior to entry into the bipolar tail, they disagree in the tail where Gurnett et al. observed densities between 10 and 40 electrons cm^{-3}, as compared to ~0.5 cm^{-3} by the plasma cup (points 4 to 6 of Fig. 10). The apparent disagreement is due to the low electron temperature of ~8300K; at that temperature the plasma cup is insensitive to the bulk of the electrons. The density in the tail can also be deduced from the positive ion observations if the average ion mass is known. These

measurements are consistent with densities of 3-7 for N^+ and ~10 for N_2^+ or H_2CN^+ (Hartle et al., 1982). These ion species were chosen because Titan's upper atmosphere consists primarily of N_2 with atomic hydrogen becoming dominant only above ~5000 km.

If the interaction is subsonic, no magnetic signature should be observable 145 R_T from Titan; whereas, such a signature may have been seen by Pioneer 11 when Titan was in the morning side of the magnetosphere (Jones et al., 1980). A perturbation was observed at the same time in the angular distribution of energetic particles (Van Allen et al., 1980a). If these effects were due to Titan then the plasma regime must have been quite different from what it was during the Voyager 1 encounter; however, these observations may have been due to another cause.

The absorption of energetic magnetospheric electrons (> 0.35 MeV) and protons (> 0.43 MeV) by Titan is generally consistent with a spherical absorber having a radius of 3800 km rather than 2575 km which is the radius of Titan (Vogt et al., 1981). The larger absorption diameter is due to particle absorption in the upper atmosphere. A detailed analysis of the absorption of several electron and ion channels in the 26-100-keV range was made by Maclennan et al. (1982). They derived the mean plasma velocity and showed that the decrease in corotation speed on the illuminated side of Titan introduced an asymmetry into the absorption of ions.

The Outer Magnetosphere

The outer magnetosphere extends from the magnetopause to the orbit of Rhea where ring and satellite absorption becomes important and where particle-plasma interactions may also play a major role. Titan is believed to be the primary source of plasma in the outer magnetosphere (Fig. 11); according to a

conservative estimate, it releases into its wake on the order of 2×10^{24} ions s^{-1} (Bridge et al., 1981; Eviatar et al., 1983). Titan is also responsible for the broad neutral hydrogen torus (Fig. 1b) with a density of 10-20 cm^{-3} (Broadfoot et al., 1981; Sandel et al., 1982) which is continuously being ionized by solar photons and energetic trapped particles. Based on the composition of Titan's atmosphere, the primary components are believed to be H^+ and N^+; however, the measurements cannot distinguish between N^+ and 0^+ or other constituents with a similar charge-to-mass ratio (Bridge et al., 1981, 1982; Frank et al., 1980; Wolfe et al., 1980). Because of their different molecular weight, the two species have different scale heights in the centrifugal potential relative to the Equator; and the heavier component was hardly detectable by Voyager 2 at 17° latitude (Fig. 12). Assuming the plasma population did not change between the Voyager missions, the scale height corresponds to an ion temperature of 160 eV for an H^+, N^+ mixture.

The plasma convection is in the corotation direction (Krimigis et al., 1981), but questions remain about the degree of corotation. The Voyager observations give convection velocities (Fig. 13) between 80 and 100% of corotation (Bridge et al., 1981), while the plasma data from Pioneer 11 are most consistent with 30 to 80% of corotation (Frank et al., 1980). Angular distributions of energetic protons (0.5-2 MeV) observed with Pioneer 11 agree with rigid corotation on the average (Fig. 14) but display significant deviations (Simpson et al., 1980; Thomsen et al., 1980; Trainor et al., 1980).

For time-averaged electron densities, the quantity $N_E L^4$ is almost constant throughout the outer magnetosphere (Fig. 15) ($\sim 5.5 \times 10^3 cm^{-3}$) where N_E is the electron density and L the magnetic shell parameter (McIlwain, 1961). As shown in Fig. 16, two distinct plasma regimes have been noted, regions with high electron temperature and low density (> 60 eV and < 3×10^{-2}

(McDonald et al., 1980; Simpson et al., 1980b; Vogt et al., 1981). The spectrum is less steep below 100 keV (Krimigis et al., 1982). The two components also differ in the proton-to-alpha ratio which equals its interplanetary value at higher energies but increases to 400 - 1500 at ~0.65 MeV/n. A high p/α ratio is indicative of magnetospheric origin because the magnetospheric plasma is deficient in helium.

A low flux of H_2^+ and H_3^+ (Voyager 2 only), observed in the 0.6-1.1 MeV/n. range, was presumably due to magnetospheric acceleration of molecular ions from the ionosphere of Saturn or Titan (Fig. 23). These molecular ions had very steep spectra with γ = 7 to 21 (Fig. 24). A flux of C, N, O ions in the 0.2-0.4 MeV/n. range was also observed. Their soft spectra are indicative of magnetospheric acceleration, but their flux relative to He, at equal energy per nucleon, is consistent with solar wind composition (Hamilton et al., 1983; Krimigis et al., 1981, 1982).

The low energy proton and electron flux increases on the average from the magnetopause to ~8 R_S (Figs. 17,18,21), but large fluctuations are superimposed on this general trend. During the Voyager inbound passes a distinct flux minimum occurred at Titan's orbit (Fillius et al., 1980; Krimigis et al., 1981, 1982; McDonald et al., 1980; Simpson et al., 1980a,b; Trainor et al., 1980; Van Allen et al., 1980a,b; Vogt et al., 1981, 1982). The phase space density of protons with a constant first invariant μ between 600 and 5000 MeV/G (Fig. 25) is almost constant throughout the outer magnetosphere. This holds true also for electrons with μ = 525 MeV/G (Krimigis et al., 1981; McDonald et al., 1980; Van Allen et al., 1980b). The outer magnetosphere and/or magnetotail are probably the source region for these particles. The phase space density of protons with a first invariant above 10^4 MeV/G decreases inward as would be expected from their interplanetary origin (Fig. 25).

During the Voyagers 1 and 2 passes, substantial flux changes were superimposed on the average trend which have been attributed to external influences. When Voyager 2 (inbound) was between 16.5 and 11 R_S at a latitude of ~17°, changes in the observed magnetic field suggested a major expansion of the magnetosphere. The subsolar distance apparently moved from 19 R_S to 32 R_S and the magnetic field became much more variable than during the Voyager 1 pass (Ness et al., 1982). At the beginning of this period, the low energy electron flux increased by an order of magnitude (Fig. 26); then, at 15.5 R_S, it decreased for a few minutes to its former value. In contrast to earlier passes, the flux peaked at a dipole L ~ 14 and then started to decrease well outside the slot region (Krimigis et al., 1982). Previously, maximum fluxes in this energy range occurred at ~ 10 R_S and ~ 8 R_S, respectively, for Voyager 1 and Pioneer 11. This example of large particle flux changes in the outer magnetosphere, although larger than most, is by no means unique; and one has to conclude that changes in solar wind characteristics have a major effect.

Angular distributions are available for both protons and electrons (Bastian et al., 1980; Fillius et al., 1980; Krimigis et al., 1981, 1982; McDonald et al., 1980; Trainor et al., 1980; Van Allen et al., 1980a). These have been Fourier analyzed in the form

$$j(\theta) = j_0 [1 + A_1 \cos(\theta-\theta_1) +$$
$$A_2 \cos2(\theta-\theta_2) + A_3 \cos3(\theta-\theta_3) \ldots]$$

where θ_1, θ_2... are measured relative to the magnetic field projection into the scan plane. The results of a typical analysis are shown in Fig. 27 which gives angular distributions of 0.5-1.8 MeV protons (See also Fig. 35). The

spin averaged flux is given by j_0. The odd coefficients, A_1 and A_3, reflect the motion of the reference frame relative to the spacecraft as well as field-aligned particle flow and gradients in the flux or angular distribution. Prior to entry into the magnetosphere, $A_1 \sim 0.6$ represents field aligned flow of solar protons, $\theta_1 \sim 0°$. Inside the magnetosphere with $\theta_1 = -90°$, A_1 reflects primarily the corotation velocity, but the fluctuations in A_1 are probably due to flux gradients. The even terms, A_2 and A_4, give the pitch angle distribution. A_2 represents a pancake distribution for $\theta_2 = 90°$ and a dumbbell distribution of $\theta_2 = 0°$. Because of the symmetry of particle trajectories around field lines, θ_2 is restricted to these two values. Contributions of A_4 tend to make the distribution defined by A_2, θ_2 more anisotropic if $\theta_4 = 0°$ and produce "butterfly" distributions for $\theta_4 = 45°$.

The proton distributions between 0.1 and 2 MeV are always pancake (Fig. 27) with larger anisotropies than those normally found in the terrestrial magnetosphere. Pioneer 11 inbound observed increasing anisotropy from the magnetopause to $L = 11.8$ then a decreasing anisotropy until the distribution became isotropic at $L = 10$. From there, the anisotropy increased to $L = 7.5$ but was almost isotropic again at $L = 5.5$. The same sequence of maxima and minima in anisotropy was repeated during the outbound pass but $1 - 2$ R_S closer to Saturn (Bastian et al., 1980; McDonald et al., 1980). Absorption by dust rings could produce such changes in angular distribution, but the asymmetry between the subsolar and morning directions (0 and -90° from the Saturn-Sun line) is hard to reconcile with this interpretation.

In general, the angular distributions of electrons (0.1 - 2 MeV) were dumbbell near the magnetopause, changed to pancake near the orbit of Rhea and became even more anisotropic in the slot region (Figs. 28,29). Such a change is qualitatively consistent with inward diffusion, which selectively increases

the velocity component perpendicular to the magnetic field. The surprise was that different energy bands deviate significantly from this average behavior (Fillius et al, 1980; McDonald et al., 1980). For instance, at L ~ 9.3, the angular distribution of 0.43 · 0.80-MeV electrons was pancake, while electron channels on either side (0.16 - 0.43 and 0.8 - 1.1 MeV) had dumbbell distributions. These selective modifications of the angular distribution may be due to resonant interactions affecting only electrons over a limited energy range and do not produce major flux changes.

The predawn magnetosphere beyond ~10 R_S is strongly affected by the transition to the magnetotail. The field lines a few degrees above or below the Equator start pointing away or towards Saturn (Fig. 7). Though the plasma sheet itself has been observed only by its magnetic signature. This change in field configuration is probably responsible for many of the differences between particle fluxes on inbound and outbound passes. Outbound somewhat lower flux levels were observed at the same dipole L values (Fillius et al., ...), larger temporal flux changes occurred, and major differences were seen in the pitch-angle distribution.

Beyond ~25 R_S in the dawn direction, fluxes of > 0.4-MeV protons and > 1-MeV electrons became quite low; however, low energy ion (0.05-0.08 MeV) and electron (< 0.4 MeV) fluxes were observed to the magnetopause (Krimigis et al., 1981, 1982; McDonald et al., 1980; Simpson et al., 1980; Vogt et al., 1981, 1982). Impulsive field-aligned flow of ~0.4 MeV protons away from Saturn into the tail was observed by Voyager 1. Bursts of electrons, accelerated to above 1 MeV, were observed during the Voyager 2 outbound pass between 18 R_S and the dawn magnetopause at ~ 50 R_S (Fig. 30). All energies peaked almost simultaneously, indicating that the acceleration occurred on the field lines going through the spacecraft and may, therefore, have occurred in the plasma

sheet of the tail. During the Voyager 2 outbound pass, a periodic modulation was observed in the flux ratio between two energy channels of electrons [(22 - 35)/(183 - 500 keV)] and of ions [(43 - 80)/(137 - 215)keV]. About three cycles were observed between 20 and 50 R_S (Fig. 31). The ion period was 9h, 49m $\pm$ 59m and the electron period was 10h, 21m $\pm$ 48m (Carbary and Krimigis, 1982). One period of a similar modulation was observed by Voyager 1 in the same SLS longitude range, 0 - 90°. It turns out that this is also the range over which southern hemisphere radio emissions (SKR) have been observed (Kaiser and Desch, 1982).

The Slot Region

This region received its name from the precipitous decrease of the proton and low-energy electron fluxes between Rhea and Tethys (Figs. 20,21). The decrease in phase space density in this region demonstrates that particles are diffusing in from the outer magnetosphere and are lost locally. Particles are absorbed by the satellites Rhea, Dione, Tethys and Enceladus, and by the E ring (Fig. 1a, Table 1). They may also be lost through interactions with the dense plasma found in this region. The relative importance of the different loss mechanisms has not yet been established.

The near Equatorial plasma density rises by ~100 between Rhea and Dione (Fig. 32) and has local maxima at Dione and Tethys. It appears to drop again inside the orbit of Tethys (Frank et al., 1980), but actually the plasma temperature drops below the threshold of the instrument (Fig. 33), that is to ~10 eV (Bridge et al., 1982). The density is about 50 cm^{-3} at 4.9 R_S and ~100 cm^{-3} at 2.73 R_S. The plasma has still two ion component, the lighter being H^+ and the heavier most likely O^+, although other ions like N^+, O_2^{2+} and O_2^+ cannot be conclusively ruled out (Fig. 11). Results of the preliminary

analysis of data taken at 2.73 R_S with Voyager 2 are still contradictory. Spectral measurements are best explained by an ~10 eV O^+ plasma, but such a plasma should have a scale height of 0.9 R_S relative to the Equator and the observed scale height was only 0.2 R_S.

The plasma in the subsolar hemisphere reaches its highest temperature (Fig. 32) of 500 eV at ~7.5 R_S where $\beta \sim 1$ (Frank et al., 1980; Eviatar et al., 1983). If a newly ionized oxygen atom or molecule is picked up by the magnetic field at this distance, its temperature would be equal to the corotation energy that is 300 or 600 eV, respectively. Inside of 7.5 R_S, however, the temperature drops more rapidly than would be expected if the plasma was in equilibrium with the corotation energy. A similar situation exists in the Io torus at Jupiter and is due to radiative cooling of the plasma. Analogously, we may conclude that the plasma residence time in the magnetosphere increases closer to Saturn and becomes long enough for radiative cooling to be effective. The above observations were made in the subsolar hemisphere. A similar analysis cannot be performed for the outbound pass on the dawn side, because the unfavorable instrument aspect relative to the corotation direction restricted observation to electron measurements.

A hot plasma torus with kT ~ 50 keV was observed in the region between L = 7 and 13 (Fig. 1b) (Krimigis et al., 1982). Apparently, the plasma in this region consists not only of multiple species (H^+ and O^+) but also has low and high temperature components. As shown in Fig. 26, Voyager 2 also observed major temporal changes in the low-energy electron flux (22 - 35 keV). In analogy with phenomena in the terrestrial and Jovian magnetospheres, one would expect that various interactions occur between this hot plasma and energetic particles above 0.1 MeV.

The sources of the plasma are probably the icy satellites Tethys and Dione; Saturn's ionosphere is another potential source. Photodissociation of H_2O and sputtering of their surfaces have been suggested as the primary mechanisms for producing the initial plasma ions or neutrals which are then ionized by Satuirn's trapped radiation (Frank et al., 1980). The inner satellites and rings are other likely sources, but their importance remains to be determined.

Extensive data are available about the behavior of energetic particles in the slot region (Fillius et al., 1980; Krimigis et al., 1981, 1982; McDonald et al., 1980; Simpson et al., 1980a,b; Trainor et al., 1980; Van Allen et al., 1980a,b). As shown in Fig. 21, fluxes of electrons below 1 MeV and of protons peak at L = 7 - 8 and then decrease smoothly inwards to the orbit of Tethys at 4.88 R_S. In contrast, fluxes of electrons above 1 MeV are relatively unaffected. The flux maxima were not symmetric between inbound and outbound passes of Pioneer 11, even though the spacecraft was at the same latitude (~3.5°). The maxima in the low-energy flux may have occurred at somewhat larger L values during the Voyager encounters (Figs. 17,18,26).

One can try to identify the major loss mechanism responsible for the slot region by considering the differences in particle loss processes due to interactions with a satellite, a dust ring or plasma. The Kronian satellites probably absorb like black spheres. The micro-absorption features observed at very close encounters with Titan and Tethys have been explained in terms of geometric absorption (Fig. 34), and the somewhat more distant encounters with Rhea and Enceladus are consistent with this picture (Krimigis et al., 1982; Maclennan et al., 1982; Vogt et al., 1981, 1982). This is in marked contrast to the behavior of the Jovian satellites Io, Europa and Ganymede, where other interactions alter the particle flux (Burlaga et al., 1980; Thomsen, 1979).

Discussions of energetic particle absorption by "black sphere" satellites and of significant parameters relavent for Saturn have been published (Thomsen et al., 1977; Thomsen and Van Allen, 1979 and 1980; Hood, 1981 and 1983). Higher energy protons are lost more rapidly because of their larger gyroradii and faster drifts relative to the satellites. Absorption by a ring of dust grains has quite different characteristics if the grain size is substantially less than the particle range: lower energy particles are lost more rapidly and the spectrum becomes harder. Because of the large surface area of the grains, they would also affect the properties of the ambient plasma. Low-energy ions and electrons could attach themselves to the surface, while higher energy ions and electrons would produce secondaries and sputter material off the grains.

As yet no overall explanation has been proposed. Hood (1983) concluded on the basis of expected absorption lifetimes that satellite absorption dominates. Others concluded that the stronger absorption of low-energy protons favors absorption by the E ring. This interpretation is also supported by the disappearance of superthermal electrons (< 6 keV) in the slot region (Sittler et al., 1981). The major problem is that this interpretation does not explain why profiles differ on inbound versus outbound passes.

Energetic particle interactions with the plasma are undoubtedly also important in the slot region. This conclusion is based primarily on the energy-dependent changes of the electron-pitch angle distributions (McDonald et al., 1980). Many of these changes are inconsistent with satellite or E ring absorption; for example, during the Pioneer 11 outbound pass between 4.9 and 7.5 R_S, a large depletion of 1.1 - 2-MeV electrons was observed within $\pm$ 22 $\frac{1}{2}°$ of the magnetic field direction (Fig 29). This depletion decreased with energy and was small or absent below 0.8 MeV.

The Inner Magnetosphere

The decrease in the energetic particle flux stops at ~4 R_S (Fig. 35). Inside the orbit of Enceladus, a flux of penetrating radiation appears and increases rapidly as L decreases. This radiation consists of at least two components; one is heavily absorbed by the satellites Mimas and the coorbital satellites 1981 S1/S2 discovered by Voyager and originally classified as a single satellite 1979S2 by the Pioneer investigators. The other component shows little or no absorption (Fig. 36). The first component was found to consist of protons and the other of electrons with energies above ~1.5 MeV (Fillius et al., 1980; Fillius and McIlwain, 1980; Krimigis et al., 1982; Schardt and McDonald, 1983; Simpson et al., 1980a,b; Van Allen et al., 1980b; Vogt et al., 1982). Because many of the detectors had not been designed for this environment, a clear-cut identification of the particle type and energy was not always possible. Publications written before this problem was fully realized may, therefore, give incorrect intensities or energies for protons between 0.5 and 5 MeV and electrons above 2 MeV. As yet, only Simpson et al. (1981) have issued a revised analysis.

Substantial progress has been made in characterizing the energetic proton component found in the inner magnetosphere. Its flux starts to increase just inside the orbit of Tethys at about 4.9 R_S. It is heavily absorbed by Enceladus, Mimas, 1979S2 and the F ring (Figs. 36,37). Three-point spectra show that the flux at 70 MeV is higher than at either 10 or 120 MeV. In addition, a soft proton component exists below 0.5 MeV (Fig. 38; Krimigis and Armstrong, 1982).

The proton absorption features at Mimas and 1979S2 are so strong that all phase space analyses, regardless of the assumptions made, show increasing phase space density on either side (Fig. 39) (McDonald et al., 1980; McKibben

and Simpson, 1980; Schardt and McDonald, 1983; Van Allen et al., 1980b). Two explanations have been proposed: a local Cosmic Ray Albedo Neutron Decay (CRAND) source or energization by inward diffusion from the outer magnetosphere in a process called episodal diffusion. The latter invokes rapid transport past the satellites during interplanetary disturbances and retrapping inside the satellite orbits. This process has been evaluated quantitatively by McKibben and Simpson (1980) and was favored by them over a CRAND source which would be too weak if their preliminary diffusion coefficients are correct (Simpson et al., 1980a,b; Cooper and Simpson, 1980). However, the preliminary values may have to be revised in view of further analysis (Simpson et al., 1981).

Calculations of the strength of the CRAND source have shown that the cosmic-ray interactions with the rings constitute a source $\sim 10^2$ times stronger than interaction with Saturn's atmosphere. The total neutron source strength is comparable to that at Earth; and scaling the magnetosphere from Earth radii to Saturn radii (10×) has no effect because the neutron lifetime is long, compared to the transit time through either magnetosphere. The 63-160 MeV proton flux observed by Voyager 2 locally in the Mimas absorption slot can be maintained by a CRAND flux which falls into the range of expected source strengths (Blake et al., 1983; Cooper and Simpson, 1980; Schardt and McDonald, 1983). Based on this neutron flux, the residence time of > 63 MeV protons is 30 years at 2.73 R_S and is comparable to that found in the terrestrial magnetosphere.

The energy spectrum of CRAND protons should be relatively flat between 10 and 100 MeV and drop rapidly above 100 MeV (Fig. 40), provided the rings' particles consist of ice, rather than rocks such as olivine (Blake et al., 1983). The limited data above 48 MeV agree with this prediction; and the e-

folding energy for an exponential spectrum ($j \propto \exp -E/E_0$) is between 20 and 50 MeV, in agreement with values found at Earth between L = 2 - 2.3 (Lavine and Vette, 1970). The decrease at lower energies may be due to a higher loss rate by absorption in the G and E rings. Pitch angle distributions are $\sin^4\theta$ to $\sin^5\theta$ inside the orbit of Mimas except in the G ring where they are less peaked (Krimigis and Armstrong, 1982; Schardt and McDonald, 1983; Van Allen et al., 1980). Depending on assumptions about neutron absorption at the source in the ring plane, the theoretical angular distribution varies from slightly pancake to $\sin^6\theta$ (Blake et al., 1983). Due to preferential absorption of ~90° pitch angle particles by the G ring, a flatter angular distribution is expected at 2.82 R_S; and Krimigis and Armstrong (1982) observed a "butterfly" distribution peaked at an intermediate θ for 28 - 43 keV protons (insert, Fig. 38).

Considerably less is known about energetic electrons in the inner magnetosphere, in part, because it is difficult to identify them uniquely in the presence of an intense proton flux above 80 MeV. No macro-absorption features in the electron flux have been seen with detectors having thresholds between 0.04 and 4.5 MeV; however, such features are seen at Mimas and 1979S2 in > 7-MeV electron channels (Krimigis et al., 1982; Simpson et al., 1980a,b). At the orbit of Mimas, the electron flux below ~1.5 MeV appears to be quite small. The only phase space density analysis performed for electrons (Fig. 41) assumed a power law spectrum with $\gamma = 4$ and shows an increase with decreasing L for > 3.4-MeV and for 7-17-MeV electrons (McKibben and Simpson, 1980). This requires an internal source and would be consistent with the episodal diffusion mechanism proposed by them. Other data giving an integral flux rise less rapidly and are consistent with inward diffusion. The resolution of this conflict depends on a definition of the electron spectrum

in the inner magnetosphere and a careful estimate of the instrumental response to bremsstrahlung, penetrating electrons and energetic protons.

Many micro-absorption features were observed, most of them in the electron flux (Fig. 34). In addition to identifying pairs of points on the same magnetic field line, these observations also made major contributions toward the discovery of the smaller satellites (Fillius et al., 1980; Simpson et al., 1980a,b; Van Allen et al., 1980a). Because these results are not primarily of interest to magnetospheric physics, the reader is referred to Marsden (1980) for a situation report after the Pioneer 11 mission and to Van Allen (1982) for a review of his findings in light of the Voyager imaging results.

The micro-absorption features observed at the orbit of Mimas have no clearly identified optical counterpart and their explanation is still controversial. The processes involved in satellite absorption and in the drift of micro-absorption signatures in longitude can be illustrated by a discussion of the various interpretations of these features. The Pioneer 11 observation, shown in Fig. 42a, was attributed by Simpson et al. (1980b) to diffuse matter concentrated at the Lagrangian point of Mimas. The reason for invoking diffuse matter was that the depth and extent of the feature was inconsistent with the absorption by a solid body on the same flux tube. Relative to a satellite, the drift of high energy electrons is in the opposite direction from that of protons, therefore, absorption on the same flux tube as the observer is required to give simultaneous signatures in both rates (Fig. 42a). Van Allen et al. (1980c) proposed that this feature was entirely due to a decrease of the electron flux (Fig. 42b) and that the proton feature observed by Simpson et al. could have been due to a residual electron sensitivity. This removes the requirement that Pioneer crossed the flux tube

of the absorber and raises the possibility that Mimas was the absorbing body. Because Mimas has an eccentric orbit, the exact radial position of the micro-signature depends on the absorption time. Mimas had been at the correct radial distance 5 h 44 min. prior to the Pioneer crossing. For the signature to be observable this long after it was produced required a monoenergetic electron flux of 1.59 MeV ($\sim$ 90° pitch angle) with an energy spread of no more than 0.1 MeV. If the energy spread is much larger, the absorption feature would have been spread over a larger range in L and its depth correspondingly decreased. This effect is produced by the radial component of the orbital velocity of Mimas, coupled with the energy dependence of the electron drift time and the broad energy window of the detector.

At the orbital location of Mimas, a peak in the electron energy spectrum at 1.59 MeV is not unexpected. The electron drift velocity is in the opposite direction to the corotation velocity; therefore, there is an energy at which electrons have the same total drift velocity as the absorbing satellite. Most of the electrons at this resonant energy can, consequently, diffuse freely past the orbit of that satellite, while the absorption probability of higher and lower energy electrons increases with departure from the resonance energy (Fig. 43). 1.00-MeV electrons with 90° pitch angle are in resonance with Enceladus and would be accelerated to 1.6 MeV by inward diffusion to Mimas. Van Allen et al. (1980) conclude the required energy filtering would occur at Enceladus if the electron diffusion coefficient is $\sim 1\times10^{-10}$ R_S^2 s^{-1}; however, there is no indication that electrons are heavily absorbed at Enceladus.

Micro-absorption features between 3.02 and 3.14 R_S were also observed with Voyager 2 (Vogt et al., 1982). The Voyager 2 encounter with a substantially different geometry from the Pioneer 11 encounter made observations which cannot be explained in terms of Van Allen's model (Vogt et al., 1982).

A plausible explanation of the Voyager observations requires an object at a longitude opposite that of Mimas; if this is the same object proposed by Simpson, it would not be phase-locked with Mimas. A quantitative explanation of these signatures is difficult because both the depth and radial extent depend on the size of the object, the eccentricity and phase of the orbit, the electron energy spectrum and the radial diffusion since the signature was formed.

The Ring Region

The intense flux of penetrating radiation stops abruptly at the outer edge of the A ring. Pioneer 11 explored the region under the ring plane as close as 1.3 R_S. As would be expected from the high Störmer cutoff, counting rates of various detectors were considerably lower than in interplanetary space; however, a small flux remained which consisted of electrons between 2 and 25 MeV and of protons above 67 MeV (Chenette et al., 1980; Simpson et al., 1980a). Because the energy of most of these particles is below the Störmer cutoff, they must originate as secondaries produced by primary cosmic-ray interactions with Saturn's rings and atmosphere. The electrons are the result of $\pi \rightarrow \mu \rightarrow e$ decay. They have the expected spectrum, $E^{-0.6}$, and their intensity increases proportionally to $R^{2.8}$ (Fig. 44) because the lower Störmer cutoff means that more primaries hit the outer part of the rings. The differential proton flux increases with energy above 67 MeV. About 1/6 of the flux is due to primary cosmic rays.

Once created, the secondaries are trapped in the local magnetic field but are absorbed by the rings within a few seconds. The secondary protons will, however, contribute to the production of albedo neutrons and significantly enhance the neutron flux over what is calculated exclusively

from primary interactions. Because the albedo neutrons move both toward and away from Saturn, it has been proposed that another trapped radiation belt exists inside the C ring (Van Allen, et al. 1980b). Voyager has confirmed the existence of the D ring, whose inner edge fades out at 1.11 R_S; thus, there is little room left for an "innermost" radiation belt unless the stopping power of the D ring is low enough to permit an appreciable proton lifetime.

A rather new phenomenon in magnetospheric physics is the presence of charged dust grains in the ring region of Saturn's magnetosphere. For these particles, the gravitational, electric and magnetic forces are comparable. In a corotating coordinate system the electric potential vanishes and charged grains, as well as neutral grains, have the same Hamiltonian as a constant of the motion; but the simple laws applicable to the conservation of angular momentum are modified for charged grains because they interact with the Saturnian magnetic field. Charged grains, thus, obey the same energy conservation rules as neutral grains; but their trajectories may be quite different, and different orbit stability criteria apply. The Keplerian velocity equals the magnetic field corotation velocity at 1.86 R_S. Inside 1.86 R_S, magnetic forces are required to keep charged grains from falling into Saturn and beyond 1.86 R_S they have to prevent charged grains from escaping.

The physical processes affecting the motion of charged grains, as applicable to volcanic dust from Io, were discussed by Morfield et al. (1981). Exact equations suitable for numeric integration and adiabatic approximations describing the motion of charged grains have also been developed (Mendis et al., 1982; Northrop and Hill, 1982b). These have been applied to explain the evolution of radial spokes which have been observed above the B ring (Thomsen et al., 1982). Their results are consistent with

0.2 - 3-μm grains with a charge-to-mass ratio of ~10 coul/kg (Fig. 45). A scatter in spoke velocities is predicted by Hill and Mendis (1982a). The field lines going through the spokes are rooted in the ionosphere in a region with strong zonal winds (Carbary et al., 1982). These winds could produce a substantial potential across the B ring, which would affect the alignment of nonspherical grains and modify the trajectory of charged grains.

The stability of negatively charged dust grains inside of synchronous orbit has been investigated (Northrop and Hill, 1982a). A radius of marginal stability exists, inside of which the trajectories intercept the atmosphere. This distance depends on the charge-to-mass ratio and is 1.625 R_S for infinite q/m (submicron particles). Interestingly enough, the marginal stability limit corresponds to a sharp boundary in the B ring (Fig. 46). The optical depth of the B ring is considerably greater beyond 1.625 R_S, and it has been suggested that the stability of negatively charged submicron grains may be responsible.

Summary

Our knowledge about Saturn's magnetosphere has been acquired during the last four years and further analysis should resolve many of the questions raised to date. Other questions, such as the existence of an intense radiation belt inside the D ring < 1.11 R_S, have to wait for future missions into that region. A very promising interdisciplinary field of research has emerged in the study of charged dust grains. Many interesting features of the ring system have no ready explanation based on gravity alone, and it is likely that plasmas and charged dust grains have played a significant role in the evolution of the ring system.

CRAND is the source of energetic protons (>50 MeV) in the inner magnetosphere. The required neutron flux is in the range expected from cosmic ray interaction with the rings. However, the decrease in proton flux below 50

MeV is not an inherent property of the source and requires modification of the injection spectrum, most likely by absorption in the G and E rings. The source of the proton flux below 0.5 MeV has not yet been identified. The electron flux below ~2 MeV can be explained in terms of inward diffusion across the orbits of Tethys, Enceladus, Mimas and 1979S2. The intensities and sources of > 7-MeV electrons in the inner magnetosphere are uncertain. Especially helpful would be a more quantitative understanding of the electron absorption by the satellites and of the evolution of the micro-signature as it drifts in longitude. This will involve a better definition of the electron spectrum and a consistent set of diffusion coefficients at the inner satellites. A unique interpretation of the various micro-absorption features observed at the orbit of Mimas has yet to be proposed.

The models of Saturn's internal magnetic field are converging on an axisymmetric field containing a dipole, quadrupole and octopole term. The surprising axisymmetry has been explained in terms of differential rotation between the core and a conducting shell. Still to be found are the causes for the longitudinal asymmetries found in the kilometric radio emission, the auroral radiation, and the spectral index of low energy electrons and ion spectra. If anomalies in the magnetic field are responsible, then measurements close enough to Saturn are inadequate to define them. The presence of a ring current has been established. As yet, no asymmetric model has been proposed which properly describes the magnetic field in the outer magnetosphere and slot region. Such a model is required for assessing the role of shell splitting in producing the observed noon-dawn differences (0 and -90° from the Saturn-Sun direction) in energetic particle population.

The overall properties of the magnetospheric plasma distribution are emerging and the general agreement between Pioneer 11 and Voyagers 1 and 2 is reassuring. Yet to be resolved are the plasma composition and the degree of

corotation in the outer magnetosphere. The sudden, very large decreases in ion densities are very puzzling. Large temporal changes occur in the plasma and energetic particle population which have no exact analogue at either Jupiter or Earth. These are exemplified by the hot plasma torus near 7 R_S, the drastic decreases in energetic particle fluxes which last from minutes to hours, and strong electron acceleration events which probably originated in the magnetotail.

In spite of these and many other remaining questions, a surprisingly coherent picture has emerged of a magnetosphere that is intermediate between the terrestrial and Jovian magnetospheres, both in its size and in the processes that shape it. The data analysis from the three Saturn missions is still in a preliminary state and many of the outstanding questions will be answered as more detailed calculations are performed. Clearly, the three missions have not provided all the data required for answering some very fundamental and puzzling questions such as the reason for longitudinal asymmetry of the radio emissions. It is to be hoped that opportunities will arise in the future to revisit this interesting and intriguing magnetosphere.

REFERENCES

Acuña, M. H., and N. F. Ness, The magnetic field of Saturn: Pioneer 11 observations, Science, 207, 444-446, 1980.

Acuña, M. H., N. F. Ness and J. E. P. Connerney, The magnetic field of Saturn: further studies of the Pioneer 11 observations, J. Geophys. Res., 85, 5675-5678, 1980.

Acuña, M. H., J. E. P. Connerney and N. F. Ness, Topology of Saturn's main magnetic field, Nature, 292, 721-724, 1981.

Acuña, M. H., J. E. P. Connerney, and N. F. Ness, The Z_3 zonal harmonic model of Saturn's magnetic field: Analyses and implications, J. Geophys. Res., 88, Special Saturn Issue, September 1983.

Anderson, R. R., Plasma waves in planetary magnetospheres, IUGG Report, 1983.

Bastian, T. S., D. L. Chenette, and J. A. Simpson, Charged particle anisotropies in Saturn's magnetosphere, J. Geophys. Res., 85, 5763-5771, 1980.

Baum, W. A., T. Kreidl, J. A. Westphal, G. E. Danielson, P. K. Seidelmann, D. Pascu, and D. G. Currie, Saturn's E ring, Icarus 47, 84-96, 1981.

Behannon, K. W., J. E. P. Connerney, and N. F. Ness, Saturn's magnetic tail: structure and dynamics, Nature, 292, 753-755, 1981.

Birmingham, T. J., Charged particle motion in the distended magnetospheres of Jupiter and Saturn, J. Geophys. Res., 87, 7421-7430, 1982.

Blake, J. B., H. H. Hilton and S. M. Margolis, On the injection of cosmic ray secondaries into the inner Saturnian magnetosphere: I, protons from the CRAND process, J. Geophys. Res., 88, A2 in press, February 1983.

Bridge, H. S., J. W. Belcher, A. J. Lazarus, S. Olbert, J. D. Sullivan, F. Bagenal, P. R. Gazis, R. E. Hartle, K. W. Ogilvie, J. D. Scudder, E. C. Sittler, A. Eviatar, G. L. Siscoe, C. K. Goertz, and V. M. Vasyliunas, Plasma observations near Saturn: initial results from Voyager 1, Science, 212, 217-224, 1981.

Bridge, H. S., F. Bagenal, J. W. Belcher, A. J. Lazarus, R. L. McNutt, J. D. Sullivan, P. R. Gazis, R. E. Hartle, K. W. Ogilvie, J. D. Scudder, E. C. Sittler, A. Eviatar, G. L. Siscoe, C. K. Goertz, and V. M. Vasyliunas, Plasma observations near Saturn: initial results from Voyager 2, Science, 215, 563-570, 1982.

Broadfoot, A. L., B. R. Sandel, D. E. Shemansky, J. B. Holberg, G. R. Smith, D. F. Strobel, J. C. McConnell, S. Kumar, D. M. Hunten, S. K. Atreya, T. M. Donahue, H. W. Moos, J. L. Bertaux, J. E. Blamont, R. B. Pomphrey, and S. Linick, Extreme ultraviolet observations from Voyager 1 encounter with Saturn, Science, 212, 206-211, 1981.

Burlaga, L. F., J. W. Belcher and N. F. Ness, Disturbances observed near Ganymede by Voyager 2, Geophys. Res. Lett., 7, 21-24, 1980.

Carbary, J. F., P. F. Bythrow and D. G. Mitchell, The spokes in Saturn's rings: a new approach, Geophys. Res. Letters, 9, 420-422, 1982.

Carbary, J. F., and S. M. Krimigis, Charged particle periodicity in the Saturnian magnetosphere, Geophys. Res. Letter, 9, 1073-1076, 1982.

Chenette, D. L., J. F. Cooper, J. H. Eraker, K. R. Pyle, and J. A. Simpson, High-energy trapped radiation penetrating the rings of Saturn, J. Geophys. Res., 85, 5785-5792, 1980.

Chenette, D. L., and L. Davis, Jr., An analysis of the structure of Saturn's magnetic field using charged particle absorption signatures, J. Geophys. Res., 87, 5267-5274, 1982.

Connerney, J. E. P., M. H. Acuña, and N. F. Ness, Saturn's ring current and inner magnetosphere, Nature, 292, 724-726, 1981.

Connerney, J. E. P., N. F. Ness and M. H. Acuña, Zonal harmonic model of Saturn's magnetic field from Voyager 1 and 2 observations, Nature, 297, 44-46, 1982.

Connerney, J. E. P., M. H. Acuña, and N. F. Ness, Saturn's magnetosphere, J. Geophys. Res., 88, Special Saturn Issue, September 1983.

Cooper, J. F., and J. A. Simpson, Sources of high-energy protons in Saturn's magnetosphere, J. Geophys. Res., 85, 5793-5802, 1980.

Desch, M. D., and M. L. Kaiser, Voyager measurement of the rotation period of Saturn's magnetic field, J. Geophys. Res., 8, 253-256, 1981.

Eviatar, A., G. L. Siscoe, J. D. Scudder, E. C. Sittler, Jr., and J. D. Sullivan, The plumes of Titan, J. Geophys. Res., 87, 8091-8103, 1982a.

Eviatar, A., Yu. Mekler, and M. Podolak, Titan's gas and plasma torus, submitted to J. Geophys. Res., 1982b.

Eviatar, A., R. L. McNutt, Jr., G. L. Siscoe, and J. D. Sullivan, Heavy ions in the outer Kronian magnetosphere, submitted to J. Geophys. Res., 1983.

Fillius, W., and C. E. McIlwain, Very energetic protons in Saturn's radiation belt, J. Geophys. Res., 85, 5803-5811, 1980.

Fillius, W., W. H. Ip, and C. E. McIlwain, Trapped radiation belts of Saturn: first look, Science, 207, 425-431, 1980.

Frank, L. A., B. G. Burek, K. L. Ackerson, J. H. Wolfe, and J. D. Mihalov, Plasmas in Saturn's magnetosphere, J. Geophys. Res., 85, 5695-5708, 1980.

Gurnett, D. A., F. L. Scarf and W. S. Kurth, The structure of Titan's wake from plasma wave observations, J. Geophys. Res., 87, 1395-1403, 1982.

Hamilton, P. C., D. C. Brown, G. Gloeckler, and W. I. Axford, Energetic atomic and molecular ions in Saturn's magnetosphere, J. Geophys. Res., 88 Special Saturn Issue, September 1983.

Hartle, R. E., E. C. Sittler, Jr., K. W. Ogilvie, J. D. Scudder, A. J. Lazarus and S. K. Atreya, Titan's ion exosphere observed from Voyager 1, J. Geophys. Res., 87, 1383-1394, 1982.

Hill, J. R. and D. A. Mendis, On the braids and spokes in Saturn's ring system, The Moon and Planets, 24, 431-436, 1981.

Hill, J. R. and D. A. Mendis, The dynamical evolution of the Saturn ring spoke, J. Geophys. Res., 87, 7413-7420, 1982a.

Hill, J. R. and D. A. Mendis, On the dust ring current of Saturn's F-ring, Geophys. Res. Lett. 9, 1069-1071, 1982b.

Hood, L. L., A comparison of characteristic times for satellite absorption of energetic protons trapped in the Jovian and Saturnian magnetic fields, Geophys. Res. Lett., 8, 976-979, 1981.

Hood, L. L., Radial diffusion in Saturn's radiation belts: A modeling analysis assuming satellite and ring E absorption, J. Geophys. Res., 88, No. A2, February 1983.

Jones, D. E., B. T. Tsurutani, E. J. Smith, R. J. Walker, and C. P. Sonett, A possible magnetic wake of Titan: Pioneer 11 observations, J. Geophys. Res., 85, 5835-5840, 1980.

Kaiser, M. L., M. D. Desch and A. Lecacheux, Saturnian kilometric radiation: statistical properties and beam geometry, Nature, 292, 731-737, 1981.

Kaiser, M. L. and M. D. Desch, Saturnian kilometric radiation: source location, J. Geophys. Res., 87, 4555-4559, 1982.

Kennel, C. F., Magnetospheres of the planets, Space Sci. Rev., 14, 511-533, 1973.

Kirsch, E., S. M. Krimigis, W. H. Ip, and G. Gloeckler, X-ray and energetic neutral particle emission from Saturn's magnetosphere, Nature, 292, 718-721, 1981.

Krimigis, S. M., T. P. Armstrong, W. I. Axford, C. O. Bostrom, G. Gloeckler, E. P. Keath, L. J. Lanzerotti, J. F. Carbary, D. C. Hamilton, and E. C. Roelof, Low-energy charged particles in Saturn's magnetosphere: results from Voyager 1, Science, 212, 225-231, 1981.

Krimigis, S. M., T. P. Armstrong, W. I. Axford, C. O. Bostrom, G. Gloeckler, E. P. Keath, L. J. Lanzerotti, J. F. Carbary, D. C. Hamilton, and E. C. Roelof, Low-energy hot plasma and particles in Saturn's magnetosphere, Science, 215, 571-577, 1982.

Krimigis, S. M., and T. P. Armstrong, Two-component proton spectra in the inner Saturnian magnetosphere, Geophys. Res. Letters, 9, 1143-1146, 1982.

Lavine, J. P. and J. I. Vette, Models of one trapped radiation environment, Vol. VI: high energy protons, NASA SP-3024, 1970.

Lazarus, A., T. Hasegawa, and F. Bagenal, Long-lived particulate or gaseous structure in Saturn's outer magnetosphere?, submitted to Nature, 1982.

Lepping, R. P., L. F. Burlaga, and L. W. Klein, Surface waves on Saturn's magnetopause, Nature, 292, 750-753, 1981.

Maclennan, C. G., L. J. Lanzerotti, S. M. Krimigis, R. P. Lepping and N. F. Ness, Effect of Titan on trapped particles in Saturn's magnetosphere, J. Geophys. Res., 87, 1411-1418, 1982.

Marsden, B. G., Saturn's satellite situation, J. Geophys. Res., 85, 5957-5958, 1980.

McIlwain, C. E., Coordinates for mapping the distribution of magnetically trapped particles, J. Geophys. Res., 66, 3681-3691, 1961.

McDonald, F. B., A. W. Schardt, and J. H. Trainor, If you've seen one magnetosphere, you haven't seen them all: energetic particle observations in the Saturn magnetosphere, J. Geophys. Res., 85, 5813-5830, 1980.

McKibben, R. B., and J. A. Simpson, Charged particle diffusion and acceleration in Saturn's radiation belts, J. Geophys. Res., 85, 5773-5783, 1980.

Mendis, D. A., H. L. F. Houpis and J. R. Hill, The gravito-electrodynamics of charged dust in planetary magnetospheres, J. Geophys. Res., 87, 3449-3455, 1982.

Morfill, G. E., E. Grün and T. V. Johnson, Dust in Jupiter's magnetosphere: Physical processes, Planet. Space Sci., 28, 1087-1100, 1981.

Ness, N. F., M. H. Acuña, R. P. Lepping, J. E. P. Connerney, K. W. Behannon, L. F. Burlaga, and F. M. Neubauer, Magnetic field studies by Voyager 1: preliminary results at Saturn, Science, 212, 211-217, 1981.

Ness, N. F., M. H. Acuña, K. W. Behannon, L. F. Burlaga, J. E. P. Connerney, R. P. Lepping, and F. M. Neubauer, Magnetic field studies by Voyager 2: preliminary results at Saturn, Science, 215, 558-563, 1982a.

Ness, N. F., M. H. Acuña, K. W. Behannon and F. M. Neubauer, The induced magnetosphere of Titan, J. Geophys. Res., 87, 1369-1381, 1982b.

Neubauer, F. M. N., D. A. Gurnett, J. D. Scudder and R. E. Hartle, Titan's magnetospheric interaction, in Jupiter, edited by T. Gehrels, University of Arizona Press, Tucson, 1983.

Northrop, T. G., and M. F. Thomsen, Theory of scan plane flux anisotropies, J. Geophys. Res., 85, 5719-5724, 1980.

Northrop, T. G., and J. R. Hill, Stability of negatively charged dust grains in Saturn's ring planes, J. Geophys. Res., 87, 6045-6051, 1982a.

Northrop, T. G. and J. R. Hill, The adiabatic motion of charged dust grains in rotating magnetospheres, J. Geophys. Res., to be published, 1982b.

Opp, A. G., Scientific results from the Pioneer Saturn encounter: Summary, Science, 207, 401-403, 1980.

Russell, C. T., Planetary magnetism, Rev. Geophys. and Space Phys., 18, 77-
106, 1980.

Sandel, B. R., and A. L. Broadfoot, Morphology of Saturn's aurora, Nature,
292, 679-682, 1981.

Sandel, B. R., D. E. Shemansky, A. L. Broadfoot, J. B. Holberg, G. R. Smith,
J. C. McConnell, D. F. Strobel, S. K. Atreya, T. M. Donahue, H. W. Moos,
D. M. Hunten, R. B. Pomphrey, and S. Linick, Extreme ultraviolet
observations from the Voyager 2 encounter with Saturn, Science, 215, 548-
553, 1982.

Sauer, H. H., On Saturnian cosmic ray cutoff rigidities, Geophys. Res. Lett.,
7, 215-217, 1980.

Scarf, F. L., Some comments on the magnetosphere and plasma environment of
Saturn, Cosmic Electrodynamics, 3, 437-447, 1973.

Schardt, A. W. and F. B. McDonald, The flux and source of energetic protons in
Saturn's inner magnetosphere, J. Geophys. Res., 88, Special Saturn Issue,
September 1983.

Simpson, J. A., T. S. Bastian, D. L. Chenette, R. B. McKibben, and K. R. Pyle,
The trapped radiations of Saturn and their absorption by satellites and
rings, J. Geophys. Res., 85, 5731-5762, 1980a.

Simpson, J. A., T. S. Bastian, D. L. Chenette, G. A. Lentz, R. B. McKibben, K.
R. Pyle, and A. J. Tuzzolino, Saturnian trapped radiation and its
absorption by satellites and rings: The first results from Pioneer 11,
Science, 207, 411-414, 1980b.

Simpson, J. A., T. S. Bastian, R. B. McKibben, and K. R. Pyle, Interim report
of the re-examination of the University of Chicago measurements of low-
energy proton fluxes in the region 2.3 < L < 4 at Saturn, E. F. I.
Preprint No. 81-34, 1981.

Siscoe, G. L., Magnetosphere of Saturn, in The Saturn System, D. M. Hunten and
    D. Morrison, editor, NASA Conference Publication 2068, 1978.

Siscoe, G. L., Towards a comparative theory of magnetospheres, in Solar System
    Plasma Physics, Vol. III, eds. C. F. Kennel, L. J. Lanzerotti and E. N.
    Parker, North-Holland Publishing Co., 1979.

Sittler, E. C., Jr., J. D. Scudder, and H. S. Bridge, Distribution of neutral
    gas and dust near Saturn, Nature, 292, 711-714, 1981.

Smith, E. J., L. Davis, Jr., D. E. Jones, P. J. Coleman, Jr., D. S. Colburn,
    P. Dyal, and C. P. Sonett, Saturn's magnetic field and magnetosphere,
    Science, 207, 407-410, 1980a.

Smith, E. J., L. Davis, Jr., D. E. Jones, P. J. Coleman, Jr., D. S. Colburn,
    P. Dyal, and C. P. Sonett, Saturn's magnetosphere and its interaction with
    the solar wind, J. Geophys. Res., 85, 5655-5674, 1980b.

Stevenson, D. J., Saturn's luminosity and magnetism, Science, 208, 746-748,
    1980.

Stone, E. C., and E. D. Miner, Voyager 1 encounter with the Saturnian system,
    Science, 212, 159-163, 1981.

Stone, E. C., and E. D. Miner, Voyager 2 encounter with the Saturnian system,
    Science, 215, 499-504, 1982.

Thomsen, M.F., Jovian magnetosphere-satellite interactions: Aspects of
    energetic charged particle loss, Rev. Geophys. and Space Phys., 17, 369-
    387, 1979.

Thomsen, M. F., and J. A. Van Allen, On the inference of properties of
    Saturn's ring E from energetic particle observations, Geophys. Res. Lett..
    6, 893-896, 1979

Thomsen, M. F., and J. A. Van Allen, Motion of trapped electrons and protons
    in Saturn's inner magnetosphere, J. Geophys. Res., 85, 5831-5834, 1980.

Thomsen, M. F., C. K. Goertz and J. A. Van Allen, On determining
magnetospheric diffusion coefficients from the observed effects of
Jupiter's Satellite Io, J. Geophys. Res., 82, 5541-5550, 1977.

Thomsen, M. F., T. G. Northrop, A. W. Schardt, and J. A. Van Allen, Corotation
of Saturn's magnetosphere: evidence from energetic proton anisotropies,
J. Geophys. Res., 85, 5725-5730, 1980.

Thomsen, M. F., C. K. Goertz, T. G. Northrop and J. R. Hill, On the nature of
particles in Saturn's spokes, Geophys. Res. Letters, 9, 423-426, 1982.

Todoeschuck, J. P., D. J. Crossley and M. G. Rochester, Saturn's magnetic
field and dynamo theory, Geophys. Res. Lett., 8, 505-508, 1981.

Trainor, J. H., F. B. McDonald, and A. W. Schardt, Observations of energetic
ions and electrons in Saturn's magnetosphere, Science, 207, 421-424, 1980.

Van Allen, J. A., M. F. Thomsen, B. A. Randall, R. L. Rairden, and C. L.
Grosskreutz, Saturn's magnetosphere, rings, and inner satellites, Science,
207, 415-421, 1980a.

Van Allen, J. A., B. A. Randall, and M. F. Thomsen, Sources and sinks of
energetic electrons and protons in Saturn's magnetosphere, J. Geophys.
Res., 85, 5679-5694, 1980b.

Van Allen, J. A., M. F. Thomsen, and B. A. Randall, The energetic charged
particle absorption signature of Mimas, J. Geophys. Res., 85, 5709-5718,
1980c.

Van Allen, J. A., Findings on rings and inner satellites of Saturn by Pioneer
11, Icarus, in press, 1982.

Vogt, R. E., D. L. Chenette, A. C. Cummings, T. L. Garrard, E. C. Stone, A. W.
Schardt, J. H. Trainor, N. Lal, and F. B. McDonald, Energetic charged
particles in Saturn's magnetosphere: Voyager 1 results, Science, 212,
231-234, 1981.

Vogt, R. E., D. L. Chenette, A. C. Cummings, T. L. Garrard, E. C. Stone, A. W. Schardt, J. H. Trainor, N. Lal, and F. B. McDonald, Energetic charged particles in Saturn's magnetosphere: Voyager 2 results, Science, 215, 577-582, 1982.

Wolf, D. A., and F. M. Neubauer, Titan's highly variable plasma environment, J. Geophys. Res., 87, 881-885, 1982.

Wolfe, J. H., J. D. Mihalov, H. R. Collard, D. D. McKibbin, L. A. Frank, and D. S. Intriligator, Preliminary results on the plasma environment of Saturn from the Pioneer 11 Plasma Analyzer Experiment, Science, 207, 403-407, 1980.

Table 1. SATELLITES AND RINGS
(From Stone and Miner, 1982)

OBJECT	DISTANCE (R_S)[1]	DIAMETER (km)	PERIOD (hrs)
Titan	20.25	2,575	382.7
E Ring[2]	3 - 8		
Rhea	8.75	1,530	108.7
Dione[3]	6.27	1,120	65.7
Tethys[3]	4.88	1,060	45.3
Enceladus	3.94	500	32.9
Mimas[3]	3.01 - 3.14	392	22.6
G. Ring	2.8		
1979S1, 1979S2 1980S1, 1980S3[4]	2.51	~190, ~120	16.67
1980S26	2.349	~90	15.09
F Ring	2.326		
1980S27	2.310		
1980S28	2.282		
A Ring	2.04 - 2.265		
B. Ring	1.524 - 1.946		

[1] 1 R_S = 60,330 km

[2] A very tenuous ring with maximum density near $4R_S$ (Baum et al., 1981).

[3] Tethys has 2 co-orbital companions, Dione has one and Mimas may have one or more companions.

[4] The following three designations probably apply to the same object: 1979S1, 1979S2, and 1980S3.

Table 2. HARMONIC COEFFICIENTS OF SATURN'S MAGNETIC FIELD

	VOYAGER 1 [1]	VOYAGER 2 [1]	VOYAGER 1&2 [1]	PIONEER 11 [2]
PLANETARY FIELD, G				
g_1^0	0.2158	0.2143	0.2154	0.218
g_2^0	0.0172	0.0164	0.0164	0.022
g_3^0	0.0269	0.0258	0.0274	0.028
EXTERIOR DIPOLE, nT				
G_1^0	-11	-8	-10	-16.9
G_1^1	0	-1	-1	-1.7
H_1^1	0	-2	0	4.8

[1] Axisymmetric models of Connerney et al. (1982).

[2] The non-axisymmetric coefficients of this model are not listed above; these are small ($\leqslant 0.002$) except for $h_2^2 = 0.012$, $h_3^1 = -0.004$ and $h_3^3 = 0.007$. The exterior quadropole terms of this model are also quite small, "JGR 80 Model" of Smith et al. (1980).

Fig. 1a.   The spacecraft--Saturn distance and solar aspect are given for
           Pioneer 11, Voyager 1, and Voyager 2. Also shown are the "average"
           positions in the equatorial plane of the bow shock, magnetopause,
           outer magnetosphere, slot region, and inner magnetosphere as well as
           the radial positions of the rings and satellites. The change of
           optical density with radius is indicated schematically for the E
           ring. As shown, the orbit of Titan falls entirely inside the
           magnetosphere; however, the magnetopause occurs at times inside the
           subsolar part of Titan's orbit. Because of the high inclination of
           the Voyager 1 trajectory, that spacecraft left the magnetotail about
           45 R_S in the predawn direction.
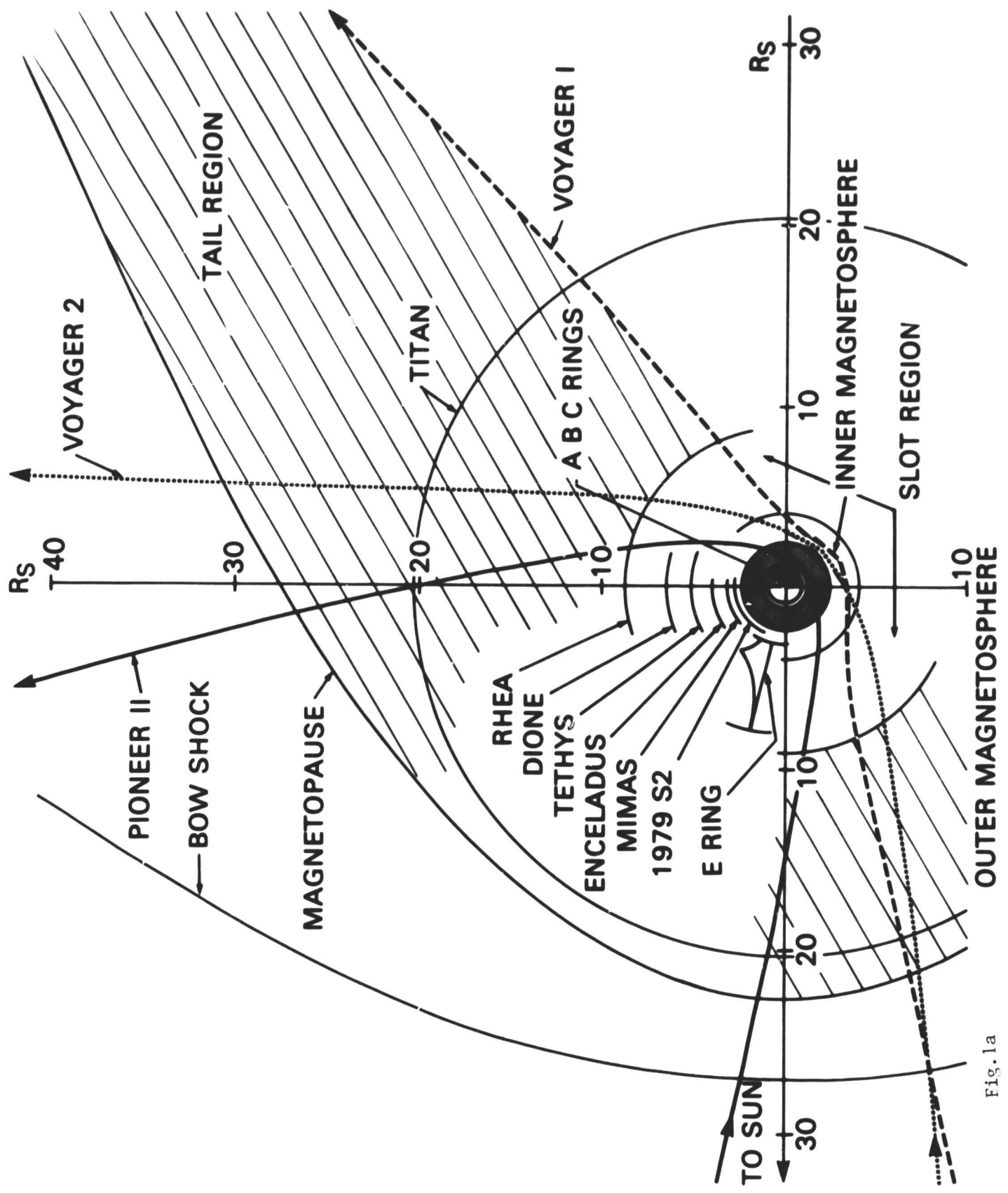
Fig. 1a

Fig. 1b.   Meridional projections of the Pioneer 11, Voyager 1, and Voyager 2
           trajectories (times are shown in hours from closest approach). The
           sunward boundary of Saturn's magnetosphere, the neutral hydrogen
           torus, the extended plasma sheet, the hot ion region, the inner O^+
           plasma torus, and the magnetic field line going through Enceladus
           are shown schematically (courtesy of Stone and Minor, 1982).
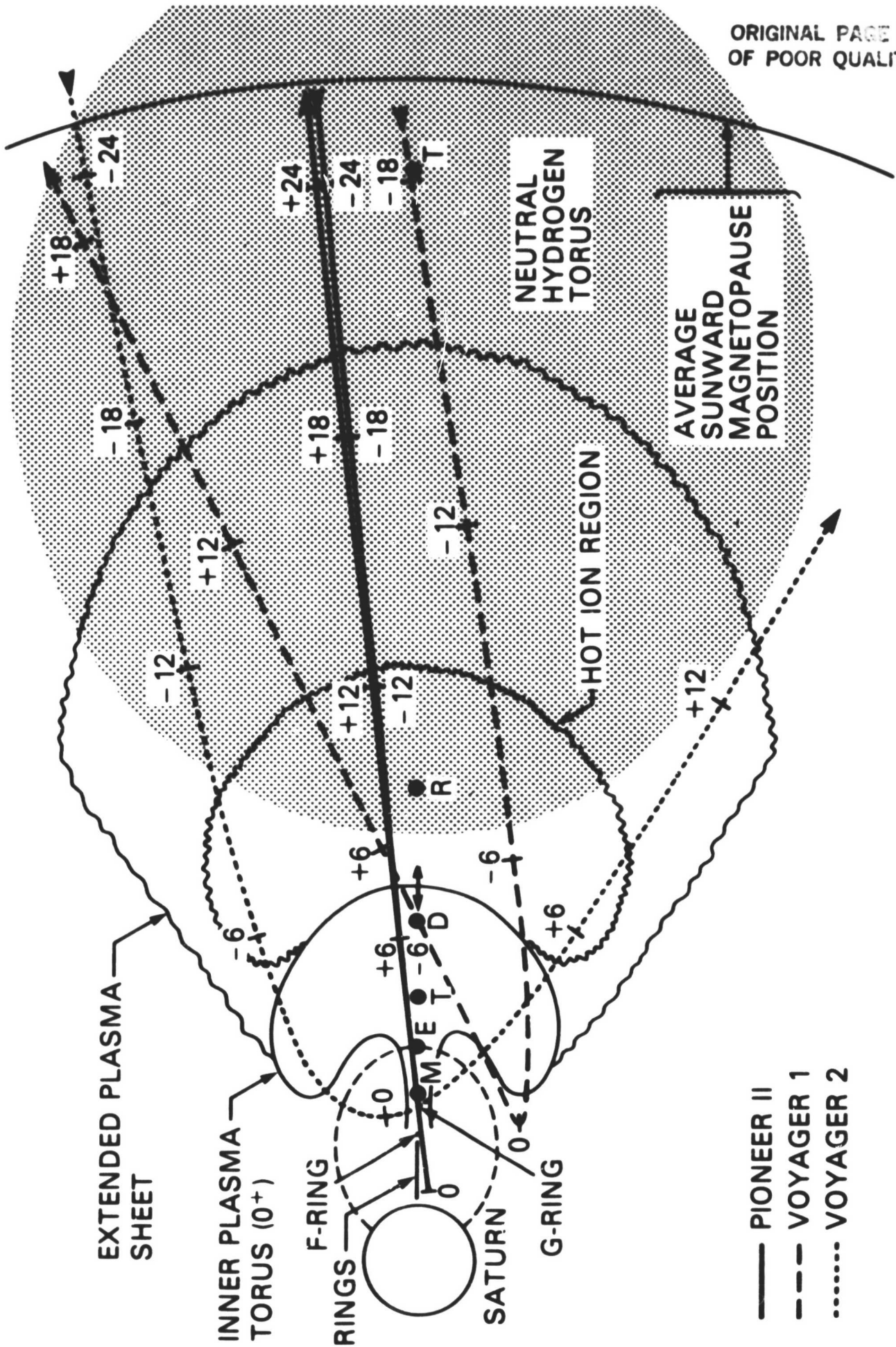
Fig.1b

Fig. 2.   The magnetic field near Saturn as observed by Pioneer 11. A maximum
          field of ~ 8,000 nT was reached at periapsis. The heavy smooth
          curve gives the magnitude of a matched dipole field. The arrows
          denoted by S and M identify the bow shock and magnetopause
          crossings, respectively. The data gap just after periapsis is due
          to the occultation of the spacecraft by Saturn (courtesy of Smith et
          al., 1980b).

ORIGINAL PAGE IS
OF POOR QUALITY.
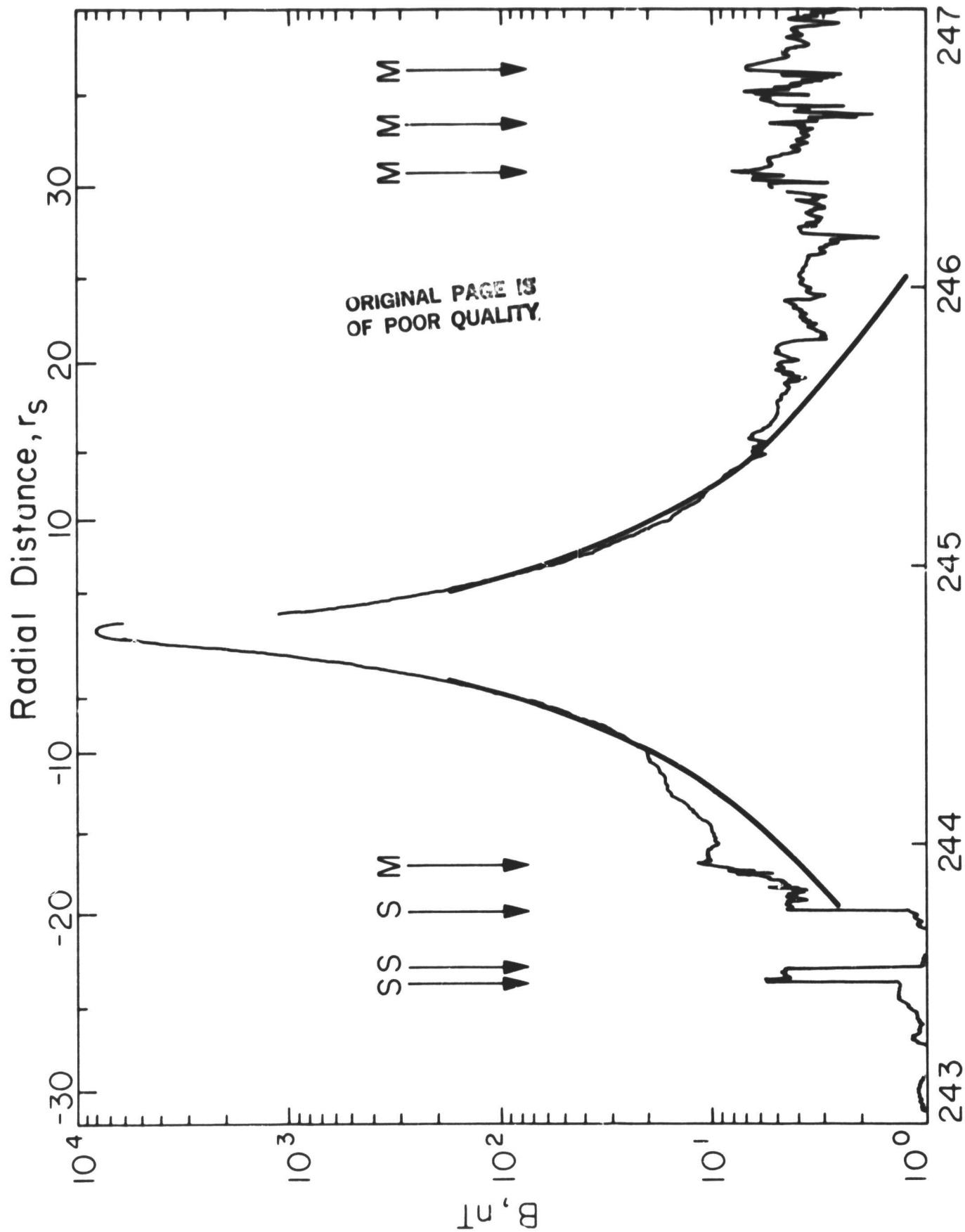
Fig. 2

Fig. 3. Voyager 1 magnetic field model of a centered internal dipole (dashed lines) plus external ring-current field (solid lines). Field lines are drawn for 2° increments in colatitude. The position of the ring current is shown by the shaded rectangle between 8.5 and 15.5 R_S. The current is distributed uniformly in Z and decreases inversely proportional to the distance from Saturn's spin axis. The solid dots at the Equator indicate (left to right) the positions of Mimas, Enceladus, Tethys, Dione, and Rhea (courtesy of Connerney et al., 1981).
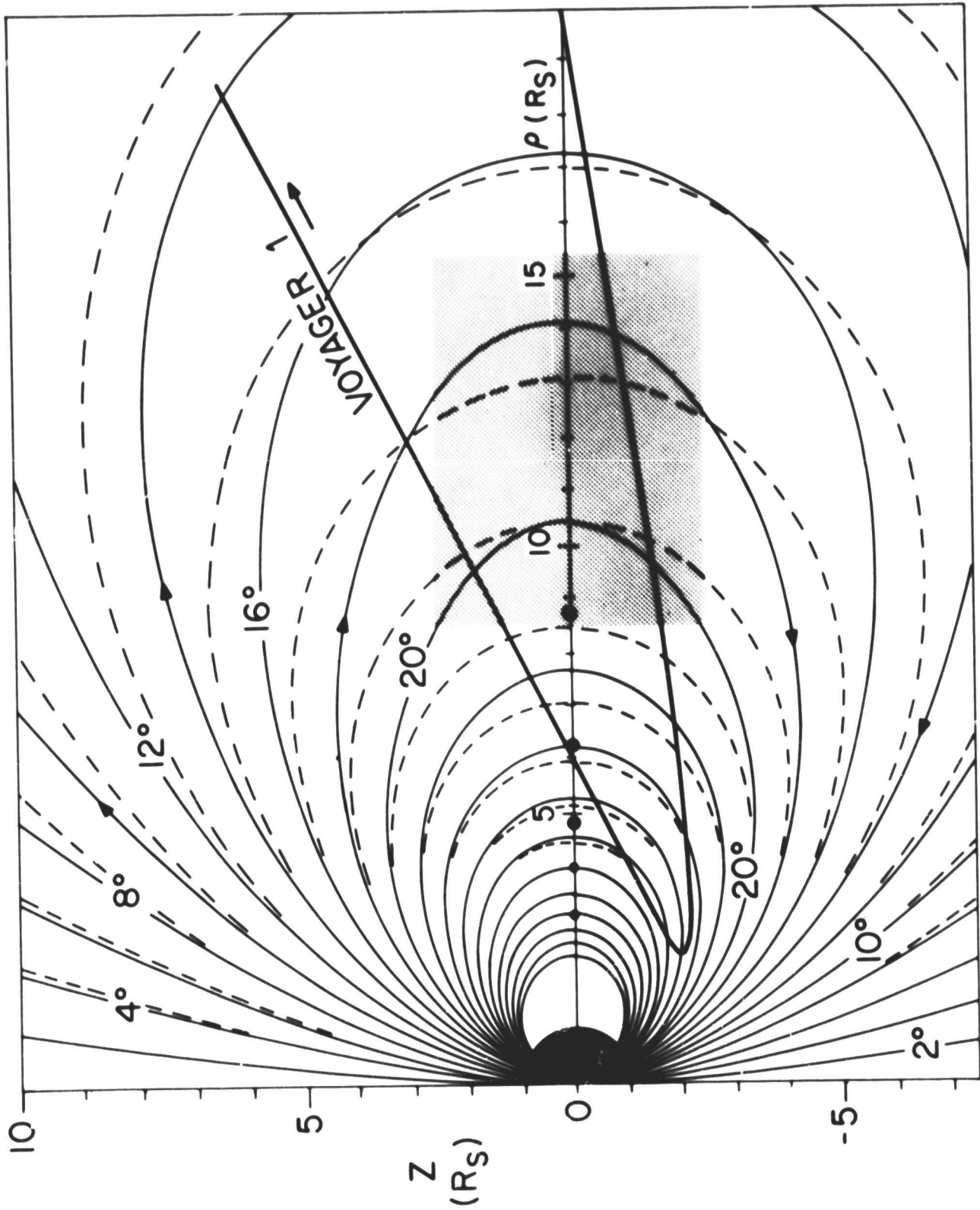
Fig. 3

Fig. 4.   Comparison of field lines from an off-set dipole and the Z_3 model. Field lines were chosen which cross the ring plane at the same distance from Saturn (courtesy of Acuña et al., 1983).

Fig. 4

50
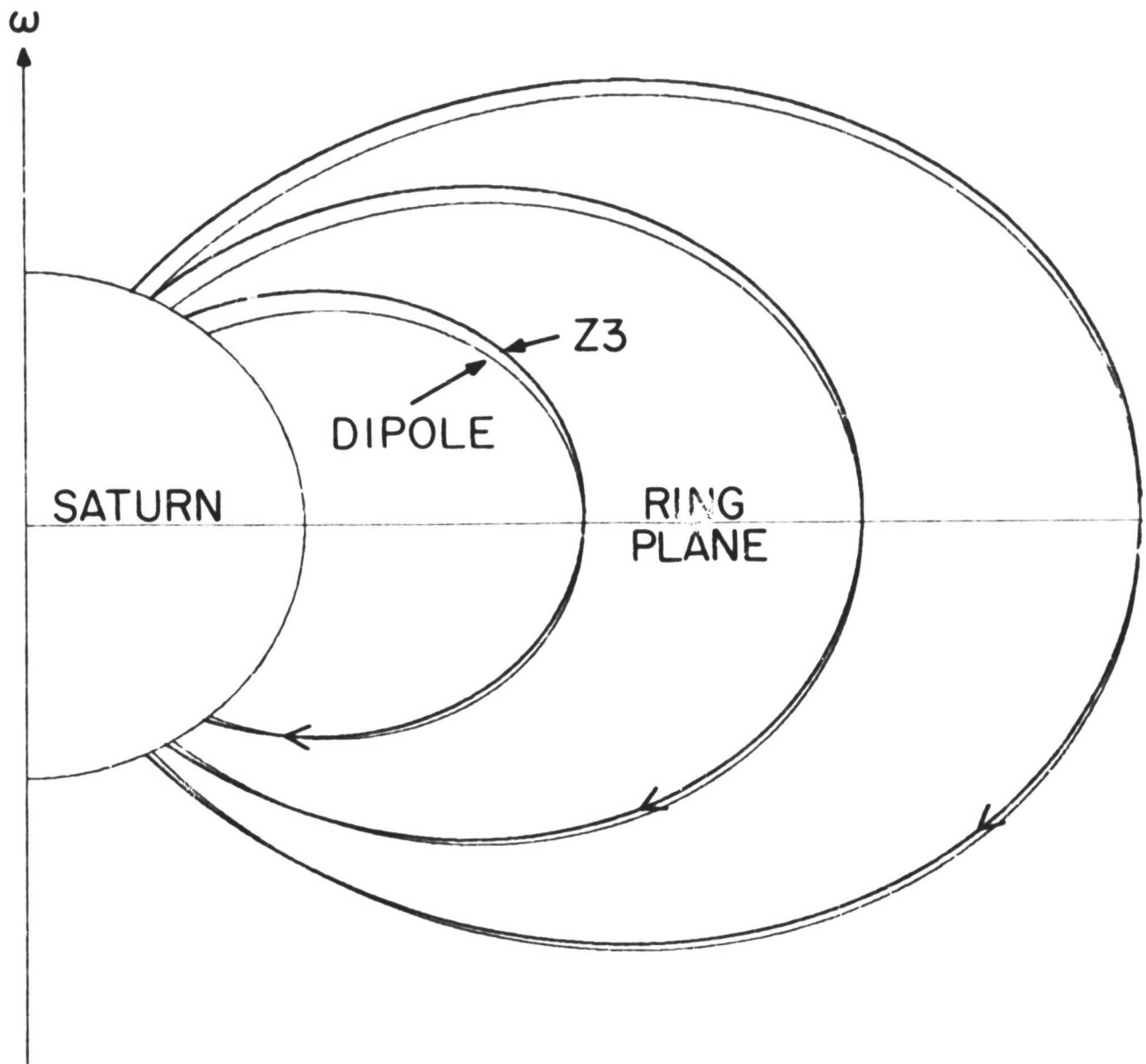
Fig. 5.   Comparison of Saturn's surface field predicted by different models. The latitude dependence of the magnetic field intensity is shown (a) for a centered dipole field with a 0.21 G-R_s^3 moment, dotted line; (b) for an off-set (~ 0.04 R_s) dipole field, light solid line for the northern hemisphere and light dashed line for the southern hemisphere; and (c) for the Z_3 model in heavy solid and dashed lines (courtesy of Connerney et al., 1982).

SURFACE MAGNETIC FIELD MAGNITUDE
(FLATTENING = 10.6)
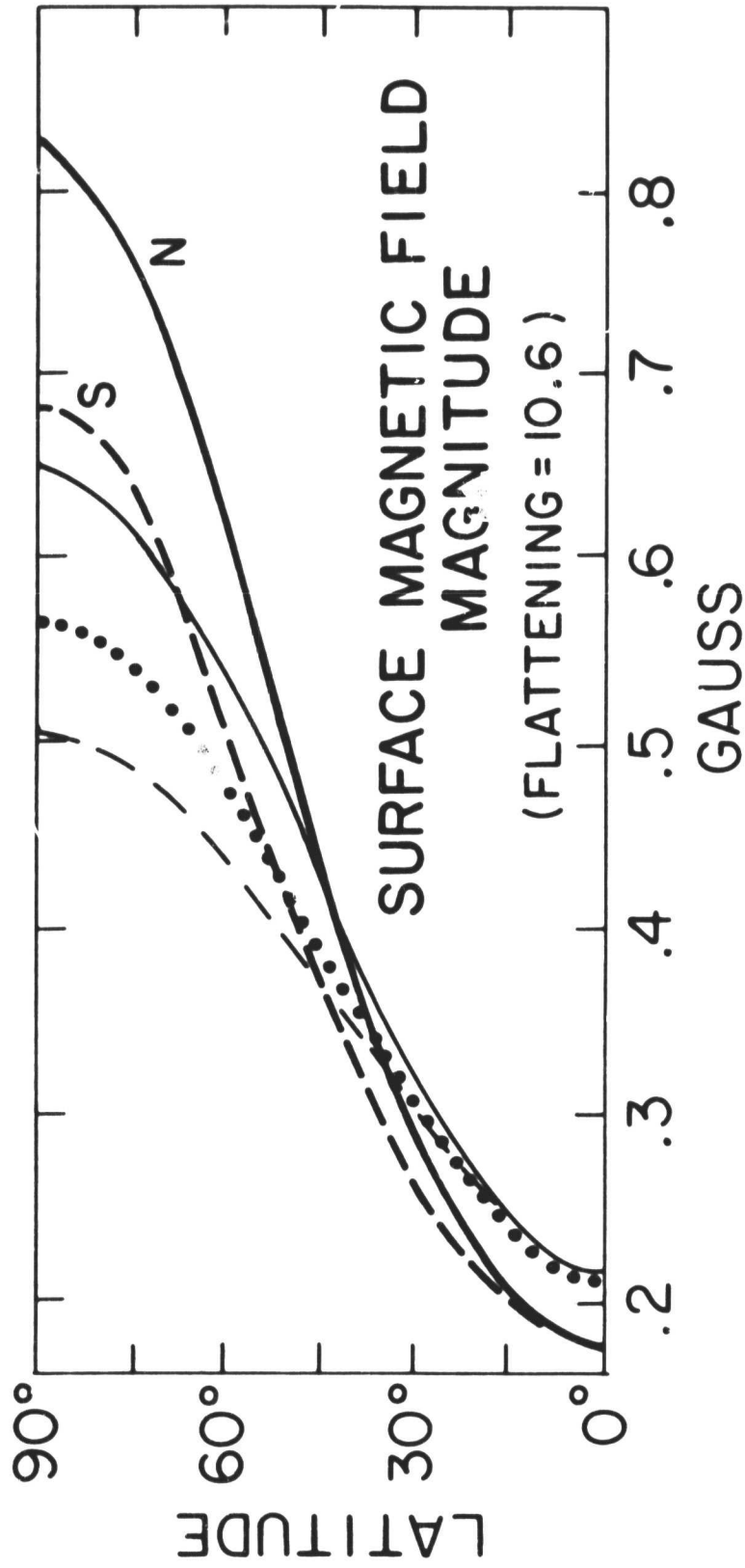
Fig. 5

Fig. 6.   The magnetic field (9.6s averages) observed while Voyager 1
traversed the bow shock, magnetosheath and entered the magnetosphere
of Saturn. Notice the absence of a systematic change of the field
direction (λ and δ) at the bow shock and the major change in
direction that occurred at the magnetopause. The semi-periodic
changes in field intensity in the magnetosheath are anticorrelated
with the electron density and are consistent with slow mode
magnetosonic waves which originated at the magnetopause. The angles
λ and δ are expressed in a heliographic, spacecraft-centered
coordinate system, such that $\lambda = \tan^{-1} B_T/B_R$ and $\delta = \sin^{-1} B_N/B$.
The vector R is radially away from the Sun; T is parallel to the
Sun's equatorial plane, normal to R and positive in the direction of
Saturn's orbital motion; and $N = R \times T$ is within 2° of being normal
to the ecliptic plane. The day numbers in the trajectory insert
refer to spacecraft positions at the start of the referenced day.
(courtesy of Lepping et al., 1981).

Fig. 6

52
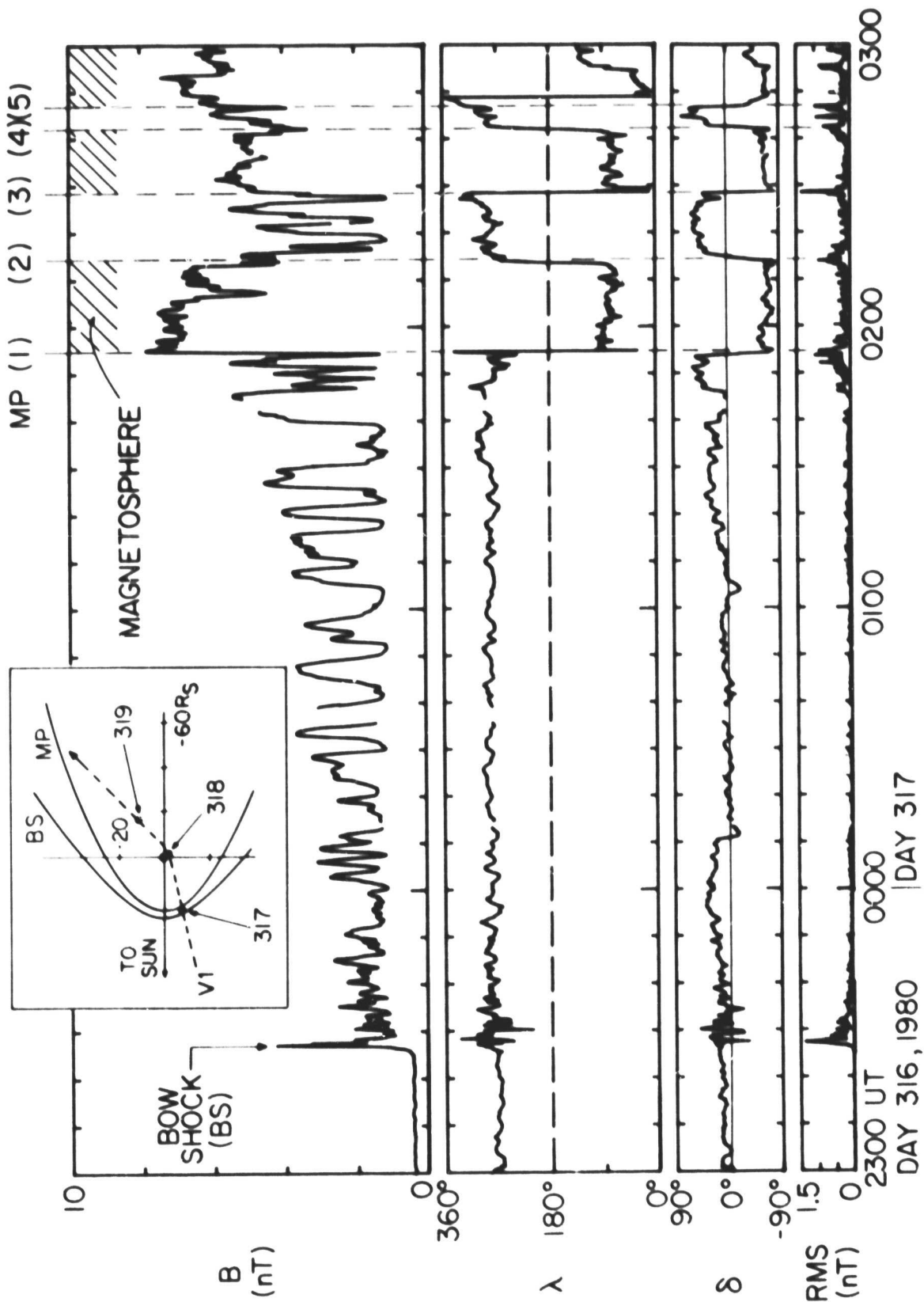
Fig. 7.   Model of Saturn's magnetic field in the noon-midnight meridian plane
           (solar magnetospheric coordinates). The model is based on a
           centered dipole planetary field, an azimuthal ring current between
           8-16 R_S (stippled) and a cross-tail current extending from 16 to 100
           R_S which closes on the magnetopause boundary. Field lines are drawn
           every 2° of invariant latitude, and the projections of the observed
           magnetic field vectors (Voyager 1 outbound) are shown. The insert
           illustrates the cross-tail current in the solar magnetospheric x-y
           plane (courtesy of Behannon et al., 1981).

Fig. 7

53
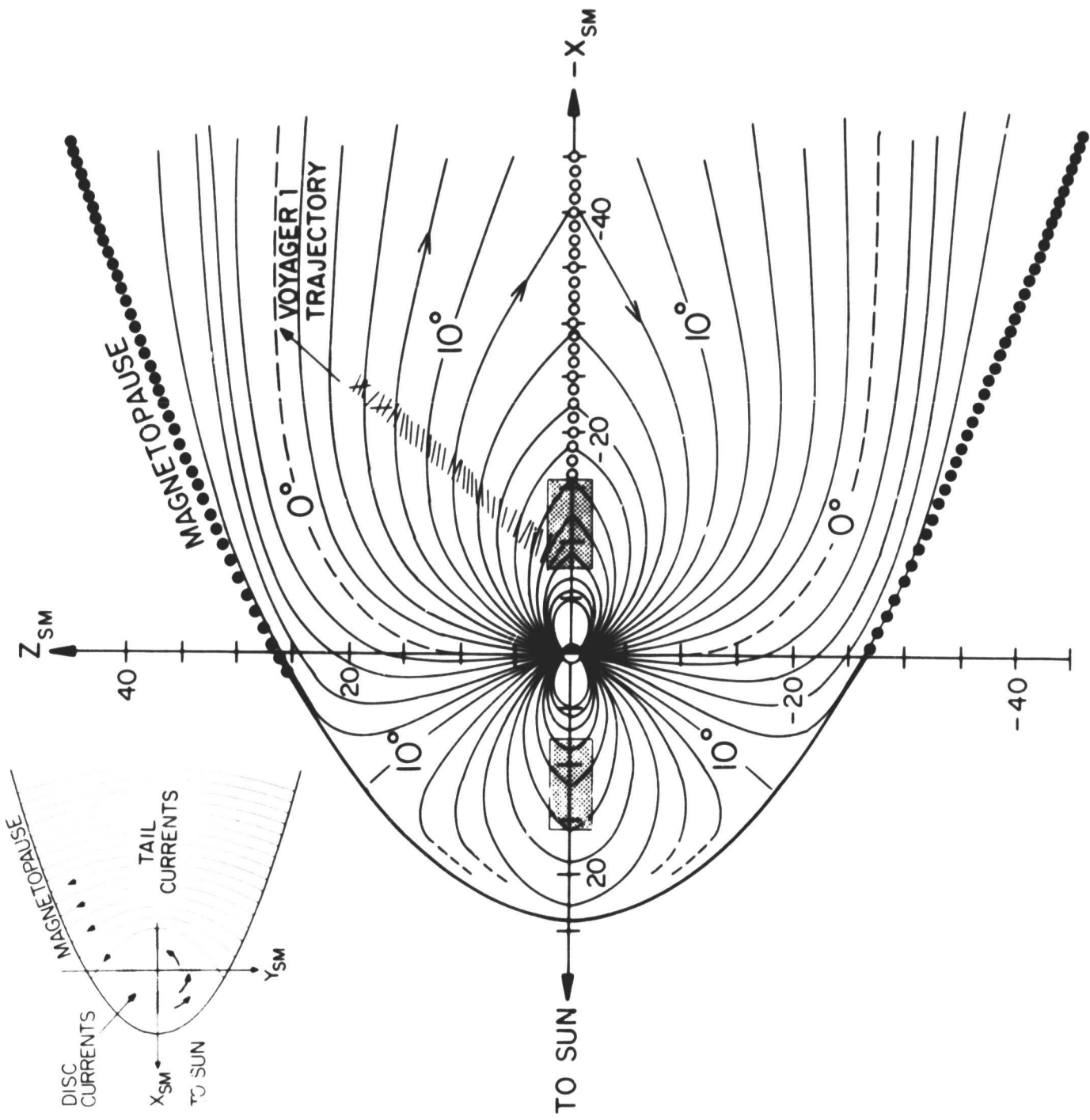
Fig. 8.   Geometry of the Titan encounter in Titan-centered coordinates with
the y axis pointing radially away from Saturn, Z parallel to
Saturn's rotation axis, and x "upstream" from the corotating
magnetosphere. The lower panel shows the magnitude of the magnetic
field with sharp minima when Voyager 1 crossed the boundaries of the
tail and the neutral sheet in the tail. The field in the tail lobes
was observed at L_1 and L_2 (courtesy of Ness et al., 1981).
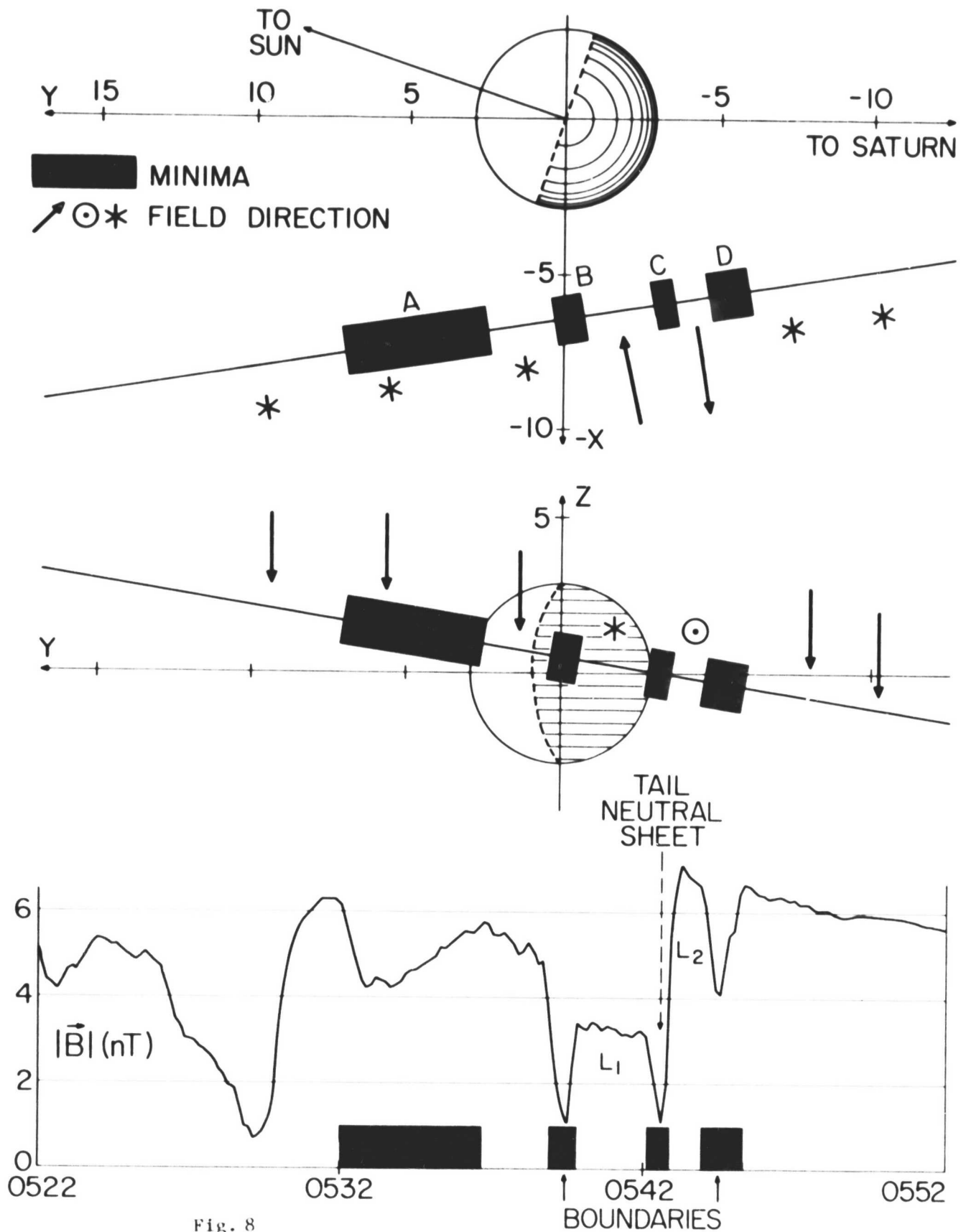
Fig. 8

Fig. 9.   Sketch of the magnetic field distortion caused by induced currents
           in the vicinity of Titan. The field lines are "draped" around
           Titan's ionosphere and form a bipolar magnetic tail which leads
           Titan in its orbit around Saturn (courtesy of Ness et al., 1981).

$\vec{\Delta V} = \vec{V}_{CR} - \vec{V}_{TITAN}$

PLASMA FLOW

FIELD LINES

TO SATURN

TITAN

Fig. 9

55
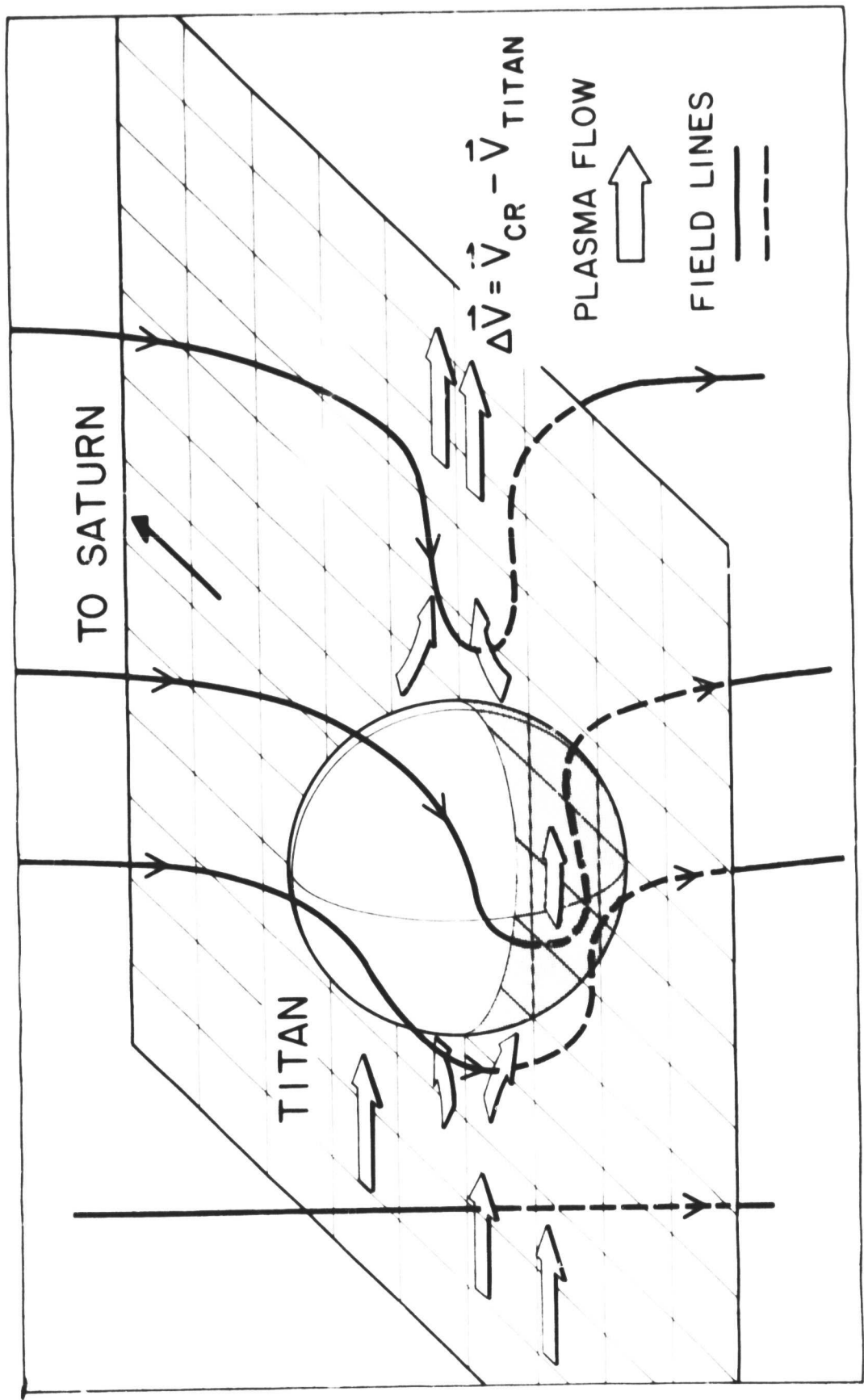
Fig. 10.   Model of the flow of magnetospheric plasma past Titan. L_1 and L_2
           refer to the lobes seen in the magnetic field, and the shaded bars
           refer to local magnetic minima (see Fig. 8). Maximum electron
           intensities were seen by the plasma wave experiment in the bite-out
           region. The incoming flow was observed at 20° to the corotation
           direction. The trajectories of H^+ ions on the sunlit side is
           approximately to scale (courtesy of Hartle et al., 1982).
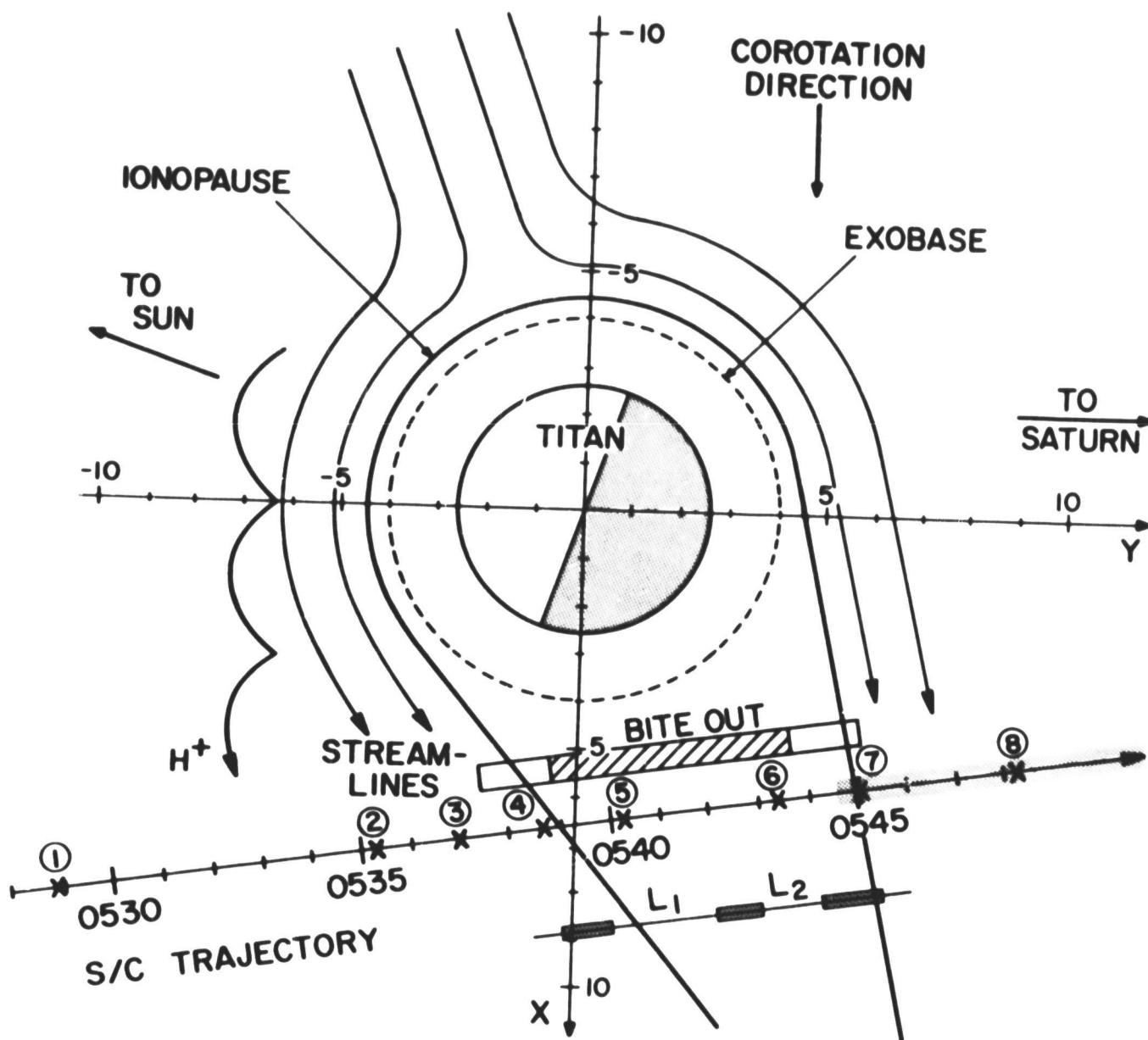
TITAN INTERACTION
NOV 12, 1980

Fig. 10

Fig. 11. Average plasma electron densities observed with Voyager 2 are shown
          in the lower panel, and the upper panel shows the height of the
          Voyager 2 trajectory above the equatorial plane as well as dipolar
          field lines. The darker region inside of 15 R_s in the upper panel
          represents O^+ plasma and the lighter region H^+ plasma. The
          horizontal scale gives the distance from Saturn's spin axis (ρ in
          cylindrical coordinates) in units of Saturn radii. The values of ρ
          at which the spacecraft crossed the L shells of the different
          satellites are indicated above the abscissa. R stands for Rhea, D
          for Dione, T for Tethys, E for Enceladus and M for Mimas (courtesy
          of Bridge et al., 1982).

VOYAGER 2 PLASMA ELECTRONS
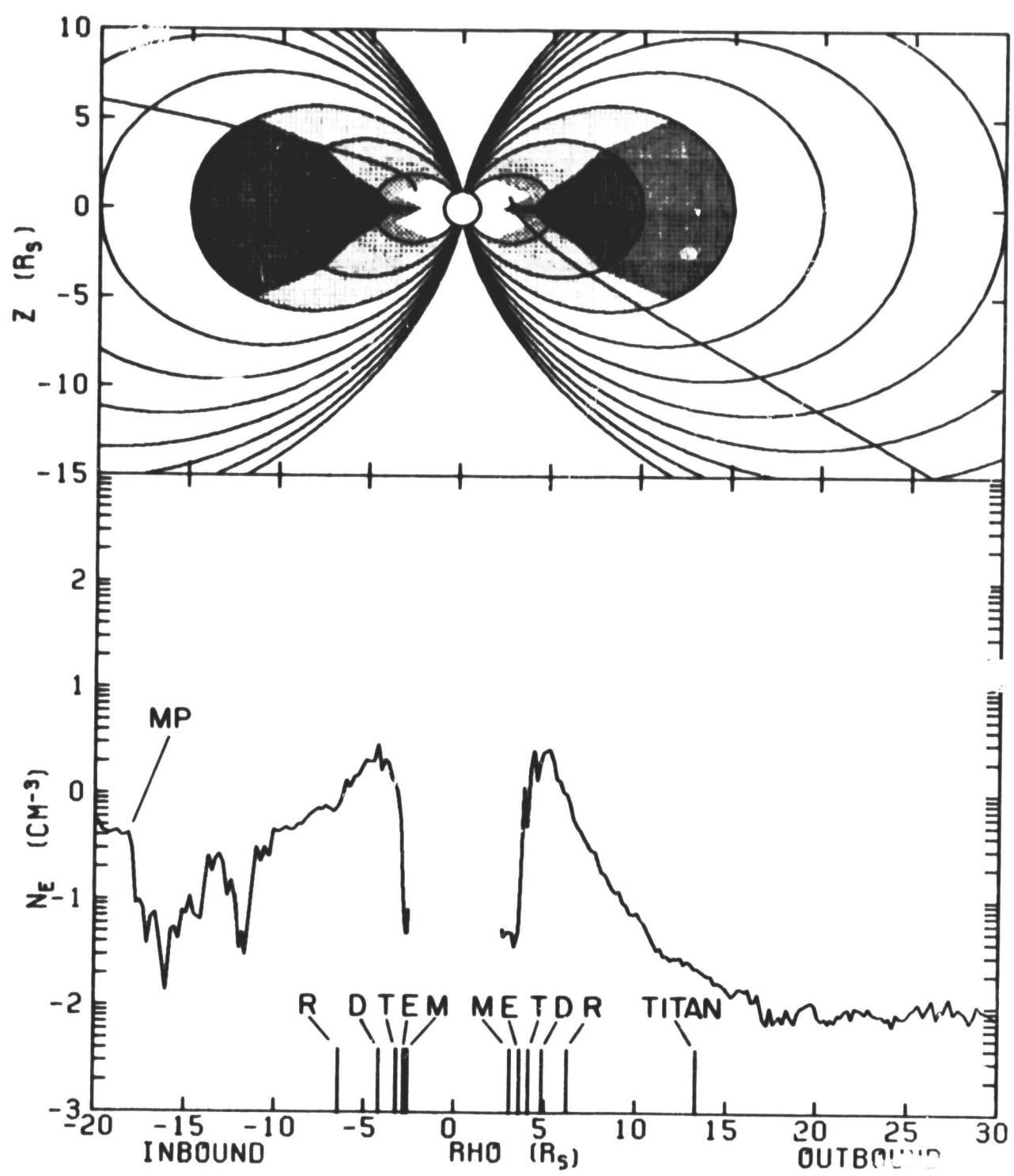
Fig.11

Fig. 12. Relative plasma distribution functions between 14-18 R_S observed
during the inbound passes of Voyagers 1 and 2. The distribution
functions were derived from low resolution mode spectra of the side-
looking plasma cup (D sensor). Peaks appearing at a low energy per
charge (10-100 volts) are attributed to H^+ and those at high values
(> 800 volts) are attributed to N^+. Note the higher temperature of
the H^+ ions at the latitude of Voyager 2 and the near absence of N^+
ions (courtesy of Bridge et al., 1982).
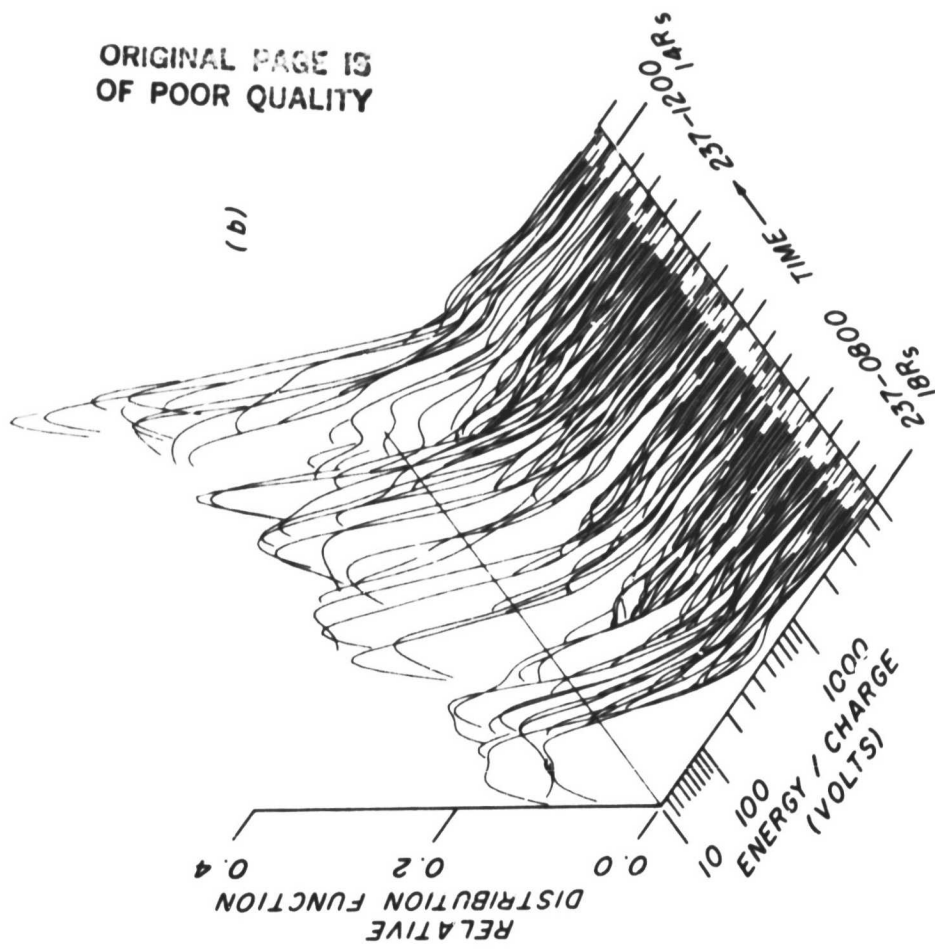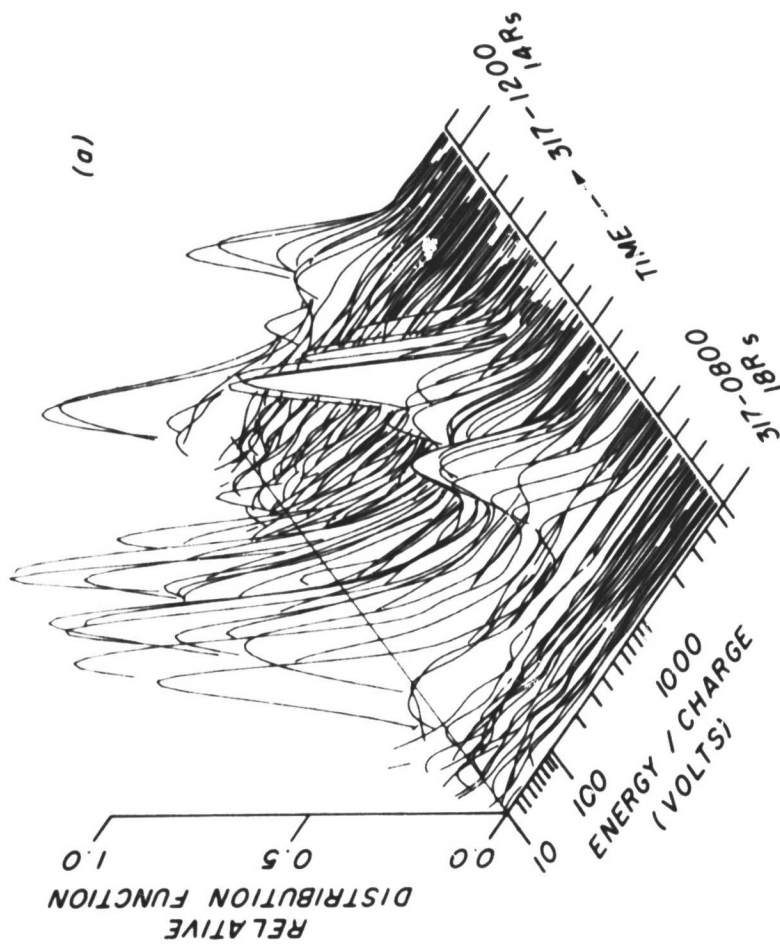
Fig.12

Fig. 13. Hydrogenic velocities of resolvable peaks in the Voyager 1 inbound
          spectra (see left panel of Fig. 12), which represent the component
          of the corotation velocity that is normal to the D sensor. Also
          shown are the expected values assuming rigid corotation for various
          values of mass to charge ratio (M/Q), with M/Q = 7 for N^+ ions.
          Values of the dipole L shells are indicated along the abscissa
          (courtesy of Dr. A. J. Lazarus).

HYDROGENIC VELOCITY OF RESOLVABLE PEAKS VOYAGER-1

EXPECTED FOR RIGID COROTATION

O = HIGH RESOLUTION
• = ISOLATED DATA POINT

M/Q = 16
M/Q = 12
M/Q = 1

ORIGINAL PAGE IS
OF POOR QUALITY

L SHELL

TIME DAY 317, 1980

SIDE SENSOR VELOCITY COMPONENT, km/s
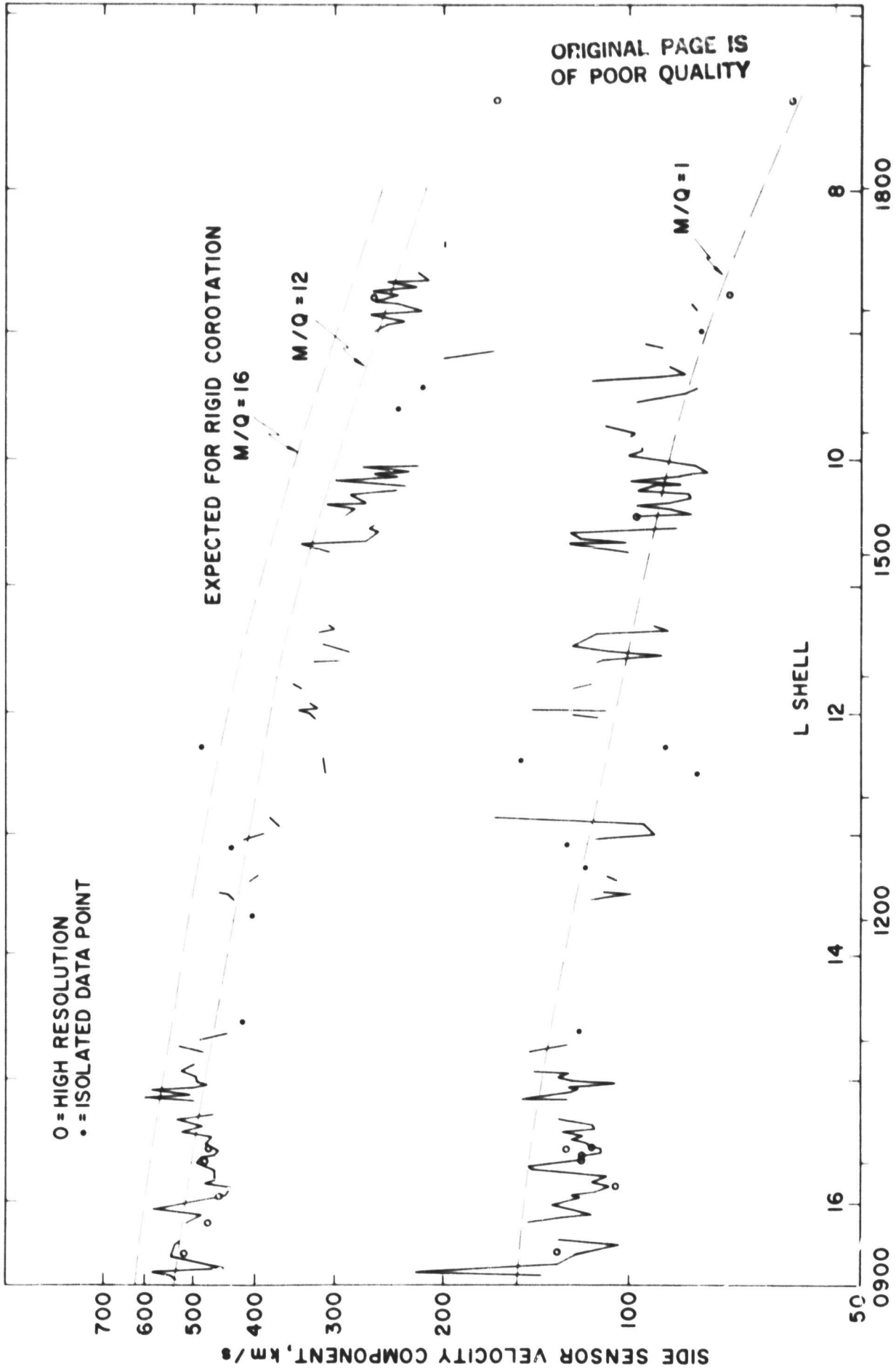
Fig. 13

Fig. 14. Corotation velocity calculated from the anisotropy of 0.61-3.41 MeV protons under the assumption of a time-stationary magnetosphere. The least squares fit to the data (dashed line) gives a corotation velocity that is ~ 5 percent higher than rigid corotation (solid line). The data have been smoothed by a 4 point running average. Error bars have been estimated by adding contributions of various experimental errors in quadrature. Deviations from the average could reflect changes in corotation velocity, but they are more probably due to temporal changes in the flux gradient or in the pitch angle distribution (courtesy of Thomsen et al., 1980).
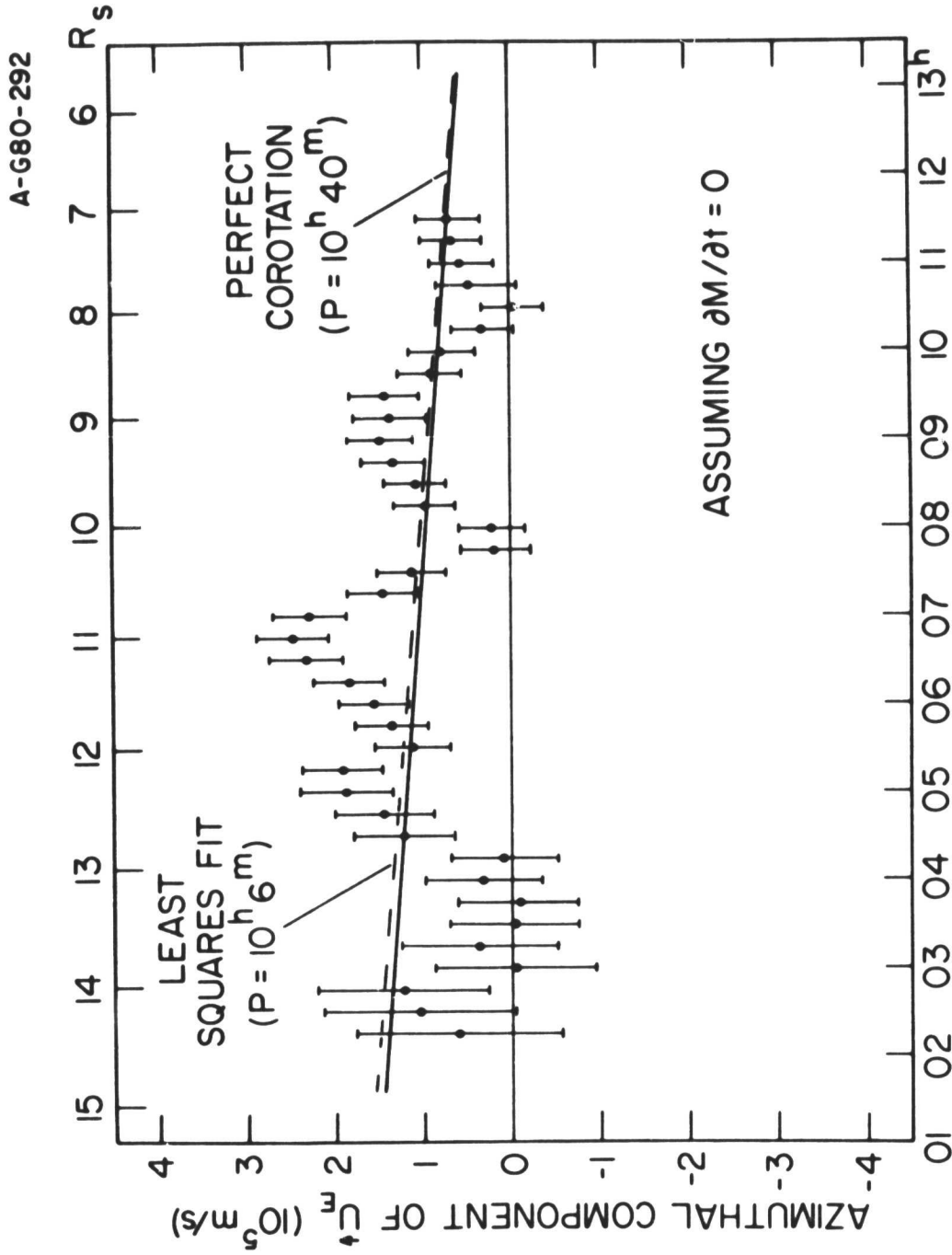
Fig. 14

Fig. 15.   Plasma electron data (15 min average) from Voyagers 1 and 2. The
           product of the density with L^4 is plotted versus the dipole L
           shell. The error bars represent extreme values of the density and L
           during the averaging period. The value of $N_E L^4$ is almost constant
           in the outer magnetosphere but decreases in the slot region
           (courtesy of Bridge et al., 1982).

INBOUND DATA
VOYAGER 1 ▲
VOYAGER 2 ■
OUTBOUND DATA
VOYAGER 1 ⋈
VOYAGER 2 ◇

DIPOLE L (R_S)

N_E (Z', L)×L^4

Fig.15

61
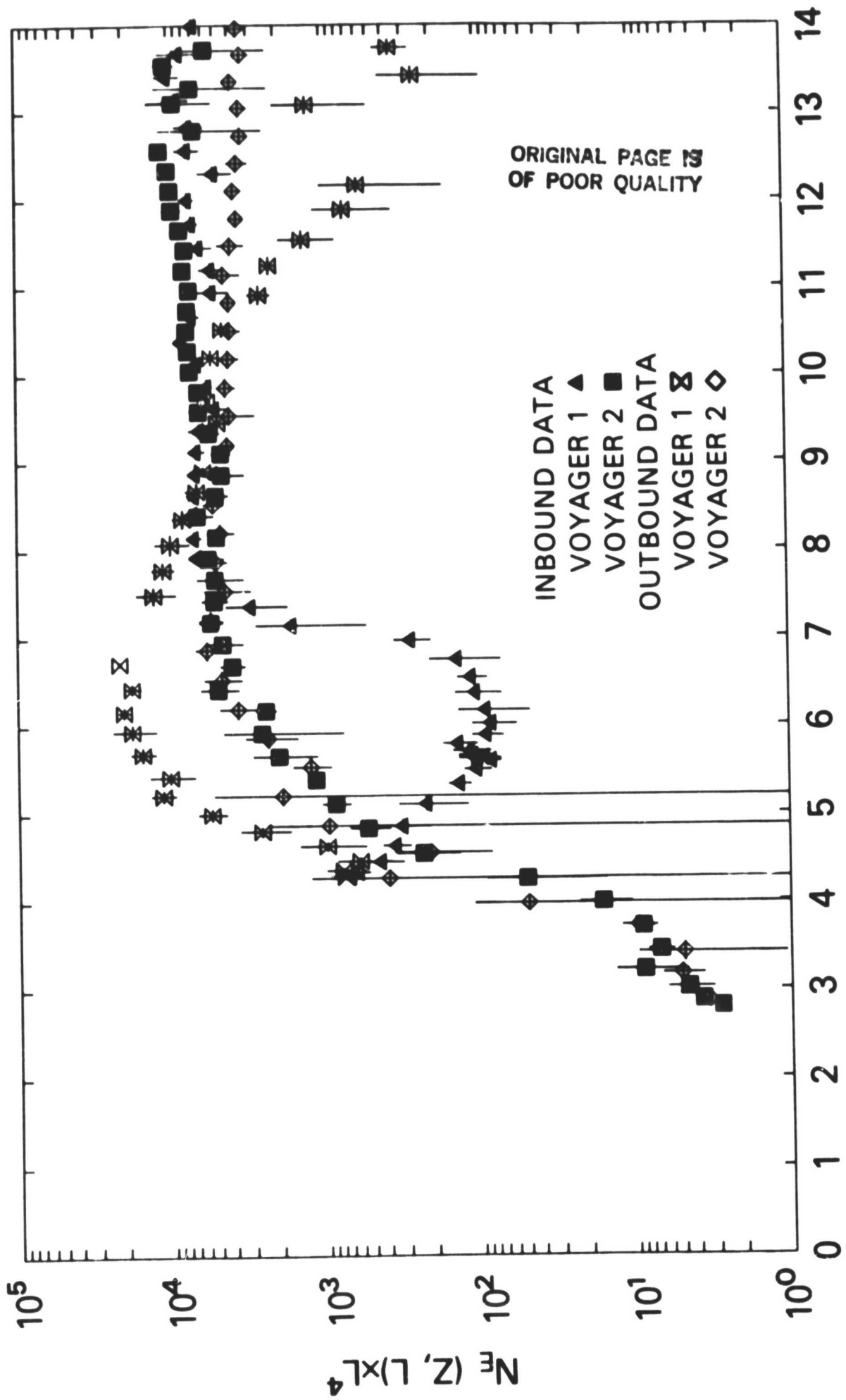
Fig. 16. Electron densities and temperatures observed during the inbound pass
          of Voyager 1. The high density and low temperature regions may be
          interpreted in terms of a plasma plume from Titan. Density maximum
          No. 1 corresponds to the most recent interaction with Titan, maxima
          2, 3, and 4 would have been produced 1, 2, and 3 Saturn periods
          earlier. Because of the variability of the solar wind pressure, the
          plume is injected into different field lines and will then move
          radially in and out with those field lines. The locations of
          density maxima 2, 3, and 4 do, indeed, correlate with the solar wind
          pressure 1, 2, and 3 periods prior to encounter. The absence of
          points between enhancements number 3 and 4 around 0700 and about
          0900 result from the absence of cold plasma rather than a data gap
          (courtesy of Eviatar et al., 1982a).
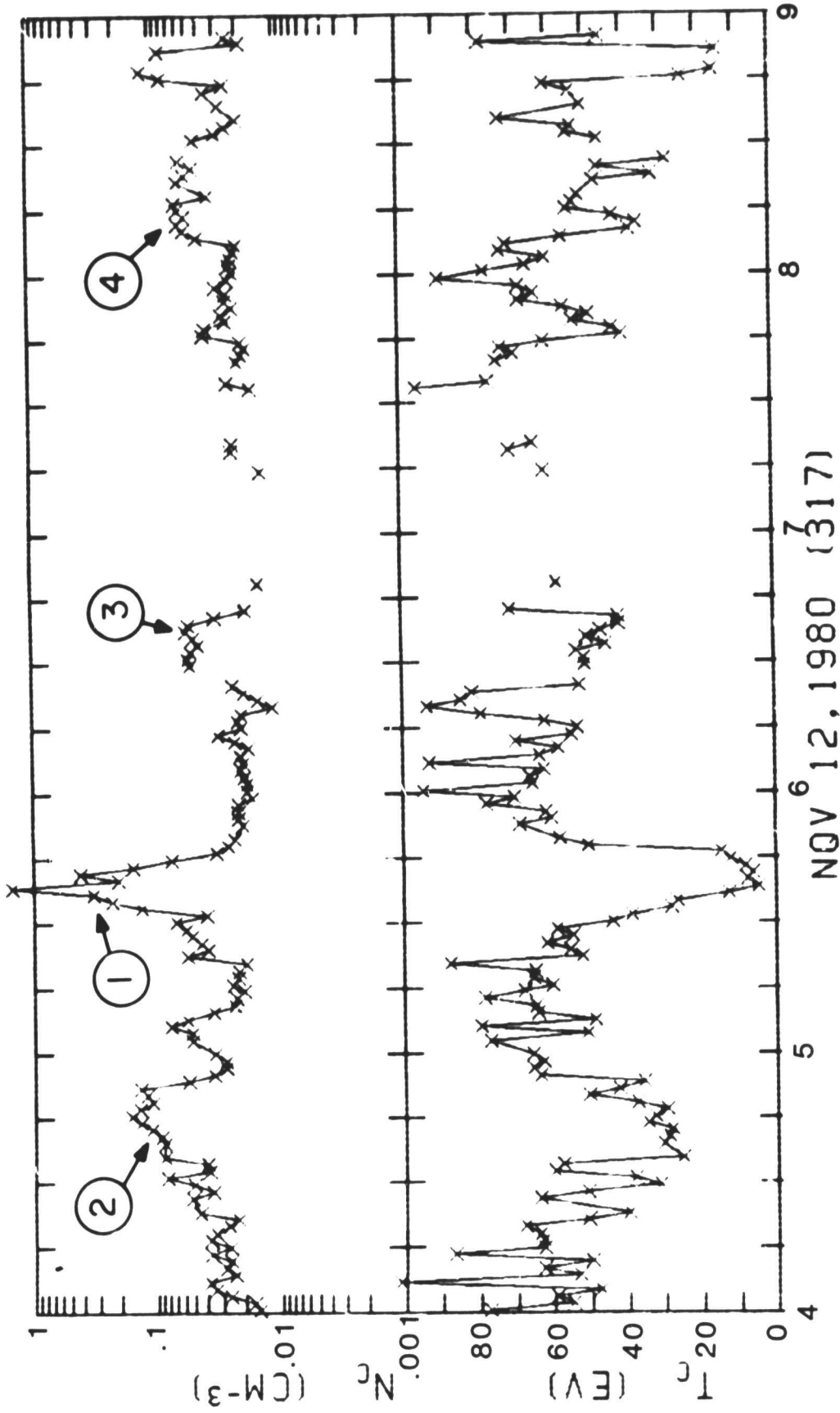
Fig.16

Fig. 17. Counting rates (1 hour average) of selected ion and electron
          channels observed with Voyager 1. The positions of the bow shock,
          magnetopause and dipole L shells of the satellites are marked
          between the two panels. The lower panel shows the exponent of a
          differential power law spectrum of the form $E^{-\gamma}$ as calculated from
          two channels at different energies. The values of γ are unreliable
          before day 317 and are uncertain for electrons from day 320 on
          (courtes of Krimigis et al., 1981).
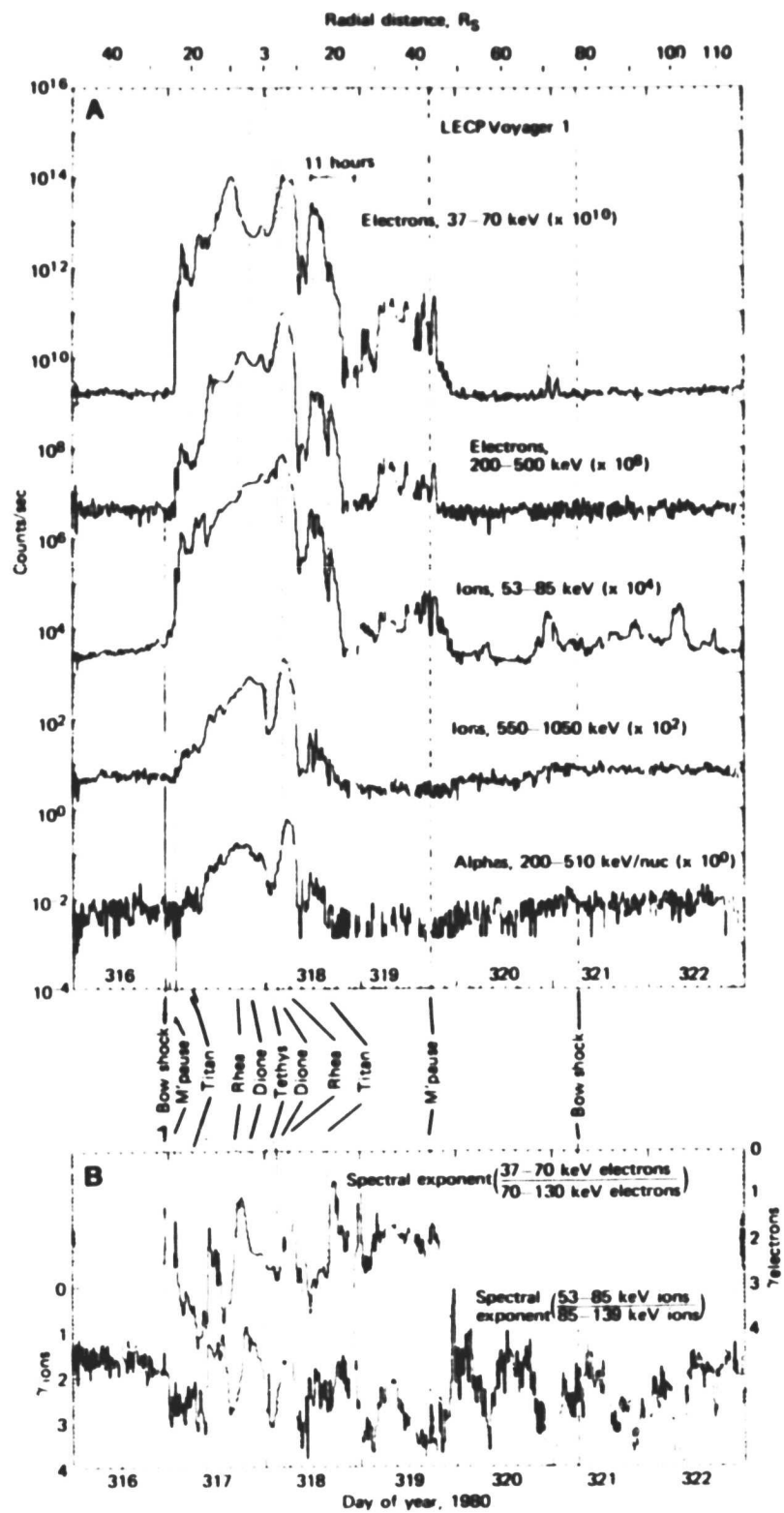
Fig. 17

Fig. 18.   Curve 1 gives the counting rate of > 0.43 MeV protons from Voyager
          1, and curve 2 gives a smiliar rate (> 0.55 MeV) from Pioneer 11
          normalized to the geometric factor of the Voyager detector (left
          scale). Curve 3 shows the Pioneer 11 1.6-5 MeV proton flux and
          curve 4 the Voyager 1 1.8-8 MeV flux (right scale); the higher
          Pioneer 11 flux (curve 3) was due to a solar proton event. On the
          inbound pass, Voyager 1 crossed the magnetopause 3 times at L ~ 24,
          and Pioneer crossed it at L ~ 17 (denoted by the circled MP). The
          Voyager 1 latitudes are shown above the distance scale. Pioneer 11
          remained with 5° of the Equator. The differential proton
          spectra from Voyager 1, shown in the inserts, are of the form
          $j = C_1 E^{-\gamma} + C_2 E^{-1/2} \exp -\sqrt{E/E_0}$. The power law contribution
          dominated at low energies and values of γ and E_0 are shown. Pre-encounter
          spectra were almost indistinguishable from the tail spectrum at L = 29.
          Note the decrease in proton intensity at L ~ 14 inbound and between L = 11
          and 14 outbound in curve 1 (courtesy of Vogt et al., 1981).

Fig. 12

64
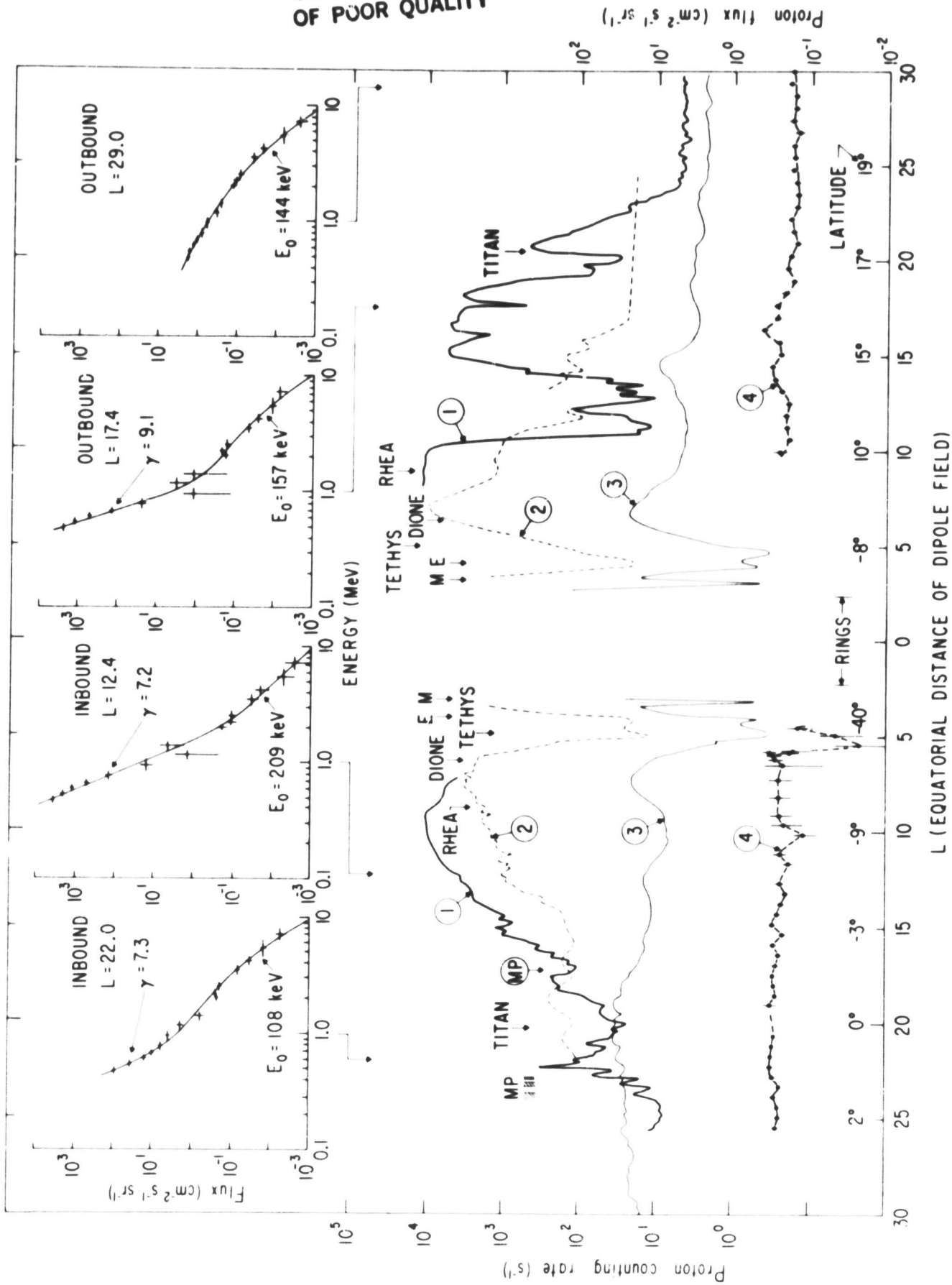
Fig. 19.   Ion number densities observed in Saturn's outer magnetosphere with Pioneer
11 in September 1979, Voyager 1 in November 1980, and Voyager 2 in July
1981.   The abscissa is the magnetic shell parameter of a centered dipole
field.   Note the low ion densities at L ~ 14 observed by the three
spacecraft and at L ~ 19 observed by Voyagers 1 and 2.   The constancy of
these features suggests the presence of particulate or gaseous structures
in Saturn's outer magnetosphere (courtesy of Lazarus et al., 1982).

Fig.19

65
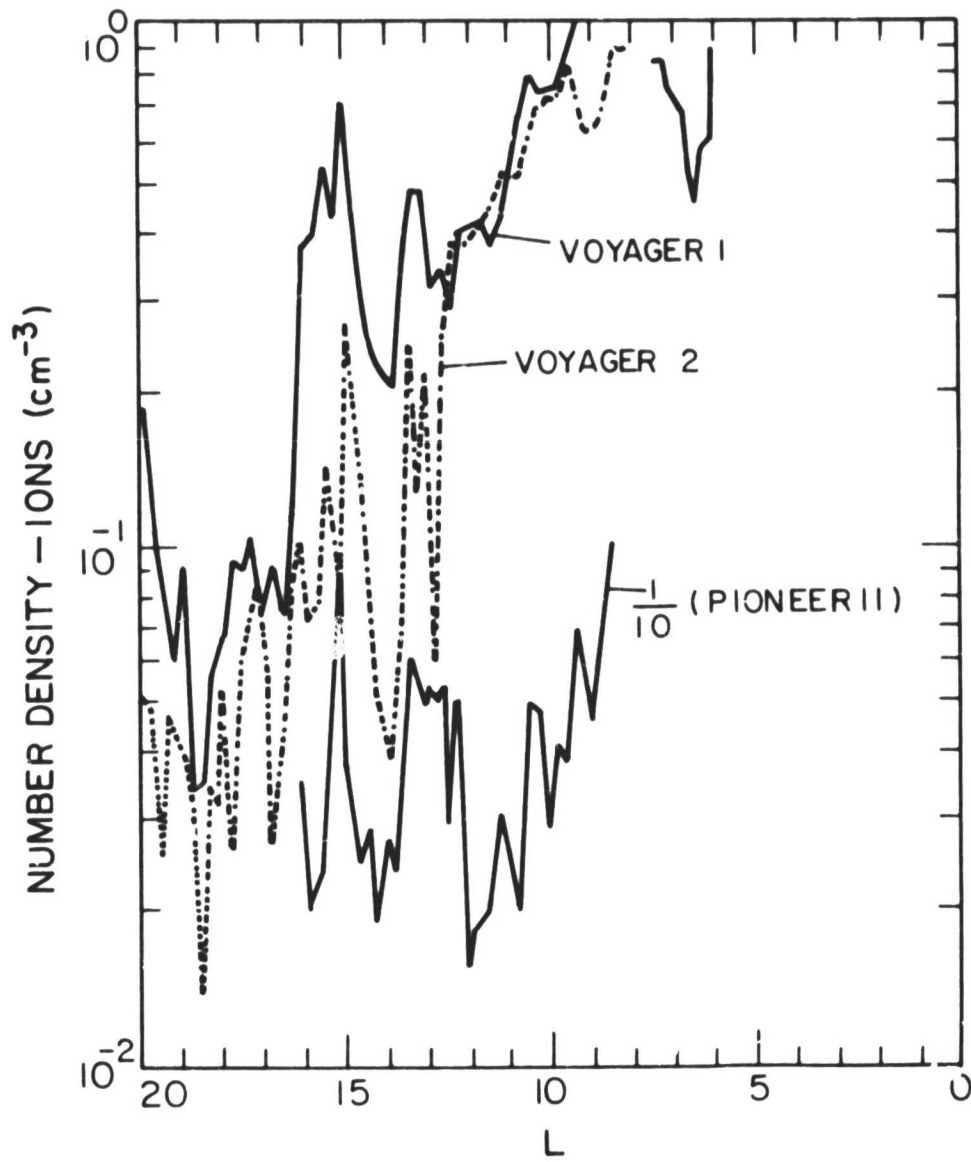
Fig. 20. Fully corrected counting rates (15-minute average) of the University of
Iowa detectors during traversal of Saturn's magnetosphere. Curve G: The
solid state detector responded to 0.61-3.41 MeV protons outside of $4R_S$ and
primarily to > 41 MeV protons inside of 4 R_S. Curve A: The GM tube
responded primarily to > 0.04 MeV electrons with possibly some contri-
bution from > 0.61 MeV protons. Curve B: The shielded GM tube responded
primarily to > 0.56 MeV electrons with possibly some contribution from > ?
MeV protons inside of 3 R_S. Curve C: The shielded GM tube responded to >
21 MeV electrons and > 80 MeV protons. Curve D: The heavily shielded GM
tube responded to electrons > 31 MeV and protons > 80 MeV. Note the large
decrease of the low energy particle rates in the slot region (courtesy of
Van Allen et al., 1980b).

Fig.20
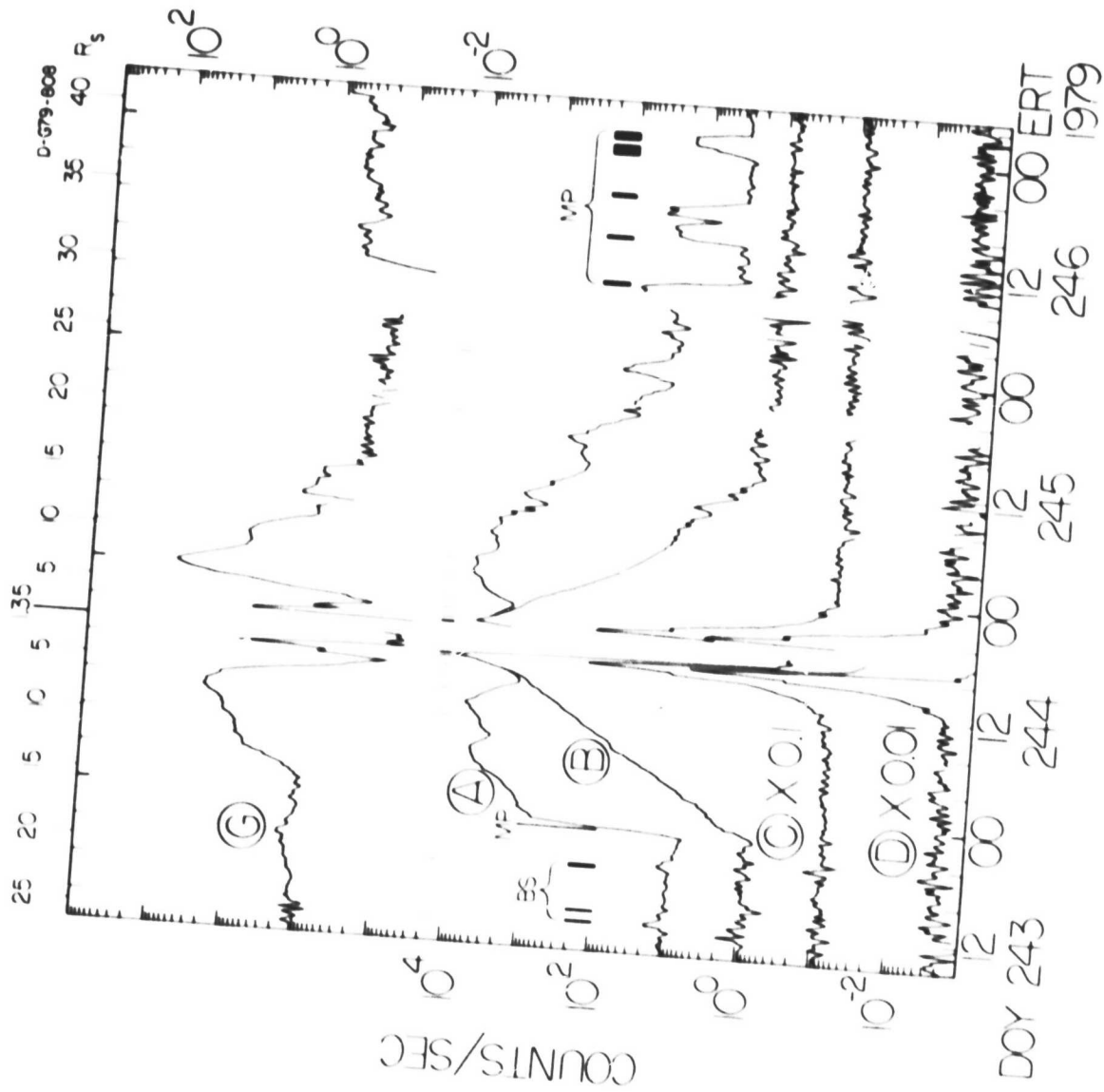
Fig. 21.   Low-energy (0.2-0.5 MeV) and high-energy (1-2 MeV) proton and electron
           fluxes observed during the inbound and outbound passes of Pioneer 11.   The
           upper arrows indicate the position of Mimas, Enceladus, Tethys, Dione,
           Rhea, and Titan.   The hatched regions mark the time spent in the dawn
           magnetosheath.   Inside of $4R_S$, the nominal 1.1-2.1 MeV proton channel
           responded primarily to > 40 MeV protons (courtesy of McDonald et al.,
           1980).

Fig. 21

- .16-.43 MeV ELECTRONS
- .2-.75 MeV PROTONS (x10)
- 1.1-2 MeV ELECTRONS
- 1.1-21 MeV PROTONS (x10)

PARTICLES / CM^2-SEC-SR-MeV
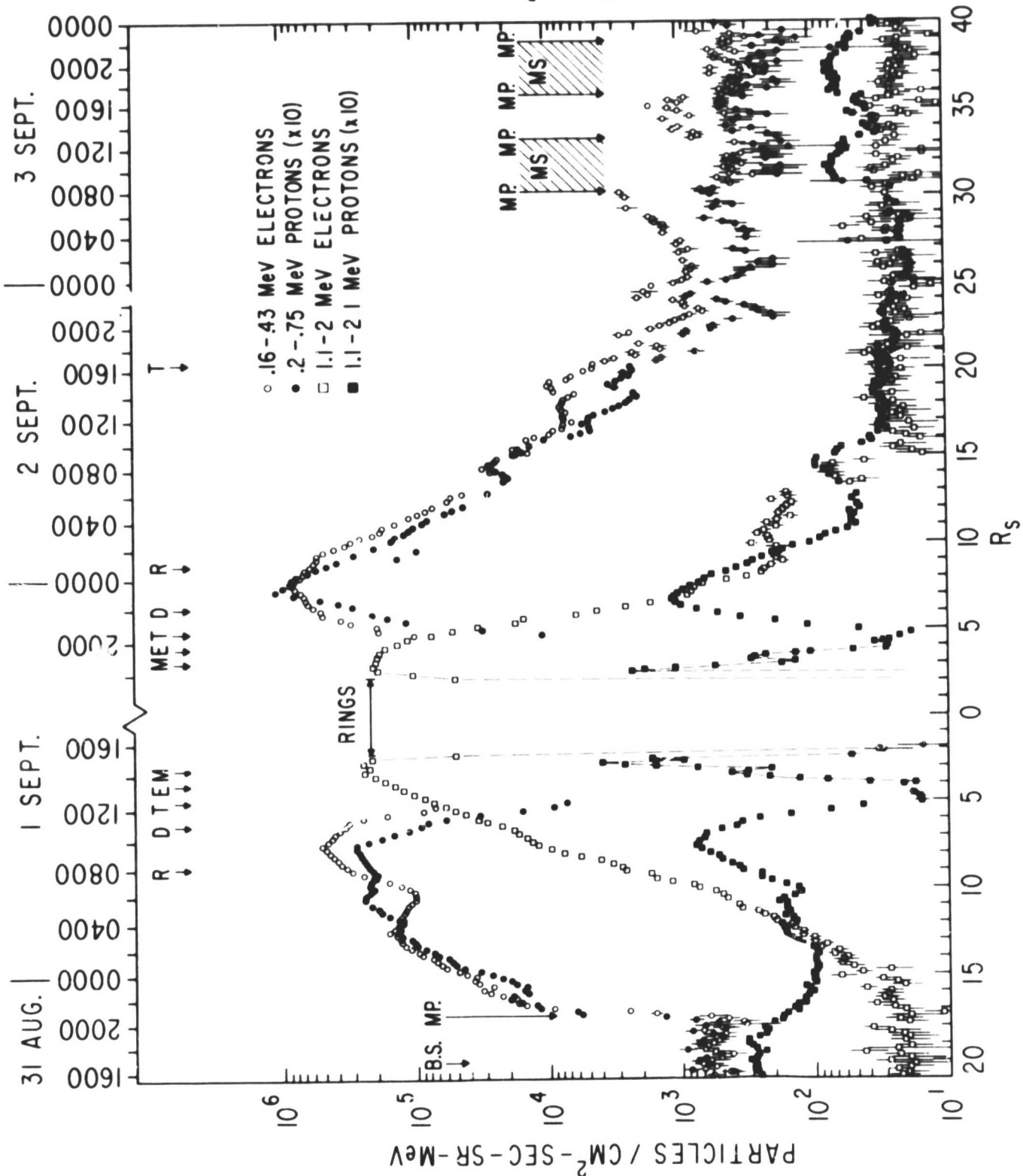
Fig. 22.   Spectral indices for proton power law spectra (32-minutes average) from
           the inbound and outbound passes of Pioneer 11. Two values of gamma at the
           same distance indicate a two component spectrum. The high energy
           component, $\gamma \sim 2$, was due to a solar proton event which was in progress
           during the Pioneer 11 encounter. During the Voyager 1 encounter
           (Fig. 18), the high energy component due to interplanetary protons was
           only $\sim$ 10 percent as intense as during the Pioneer 11 encounter and its
           spectrum was an exponential in rigidity (courtesy of McDonald et al.;
           1980).
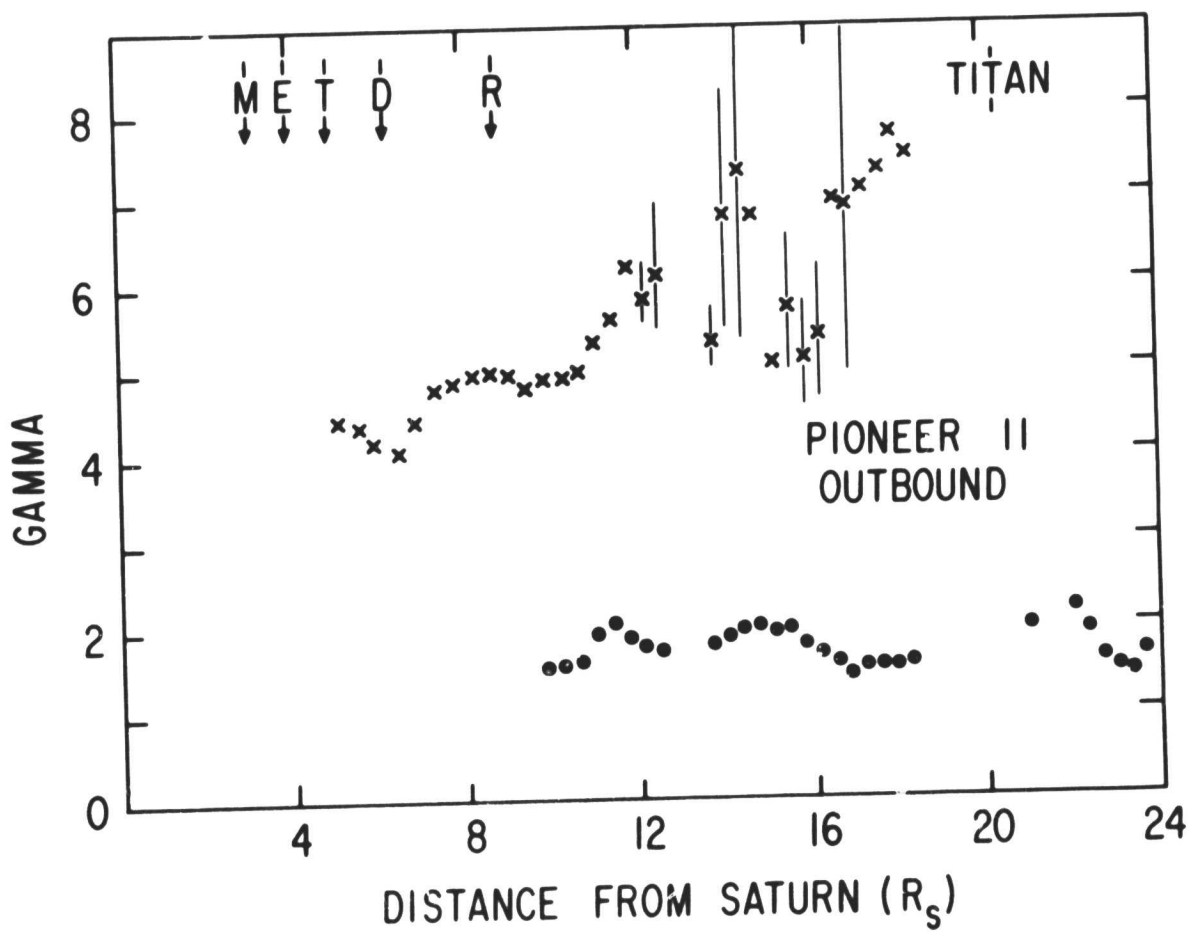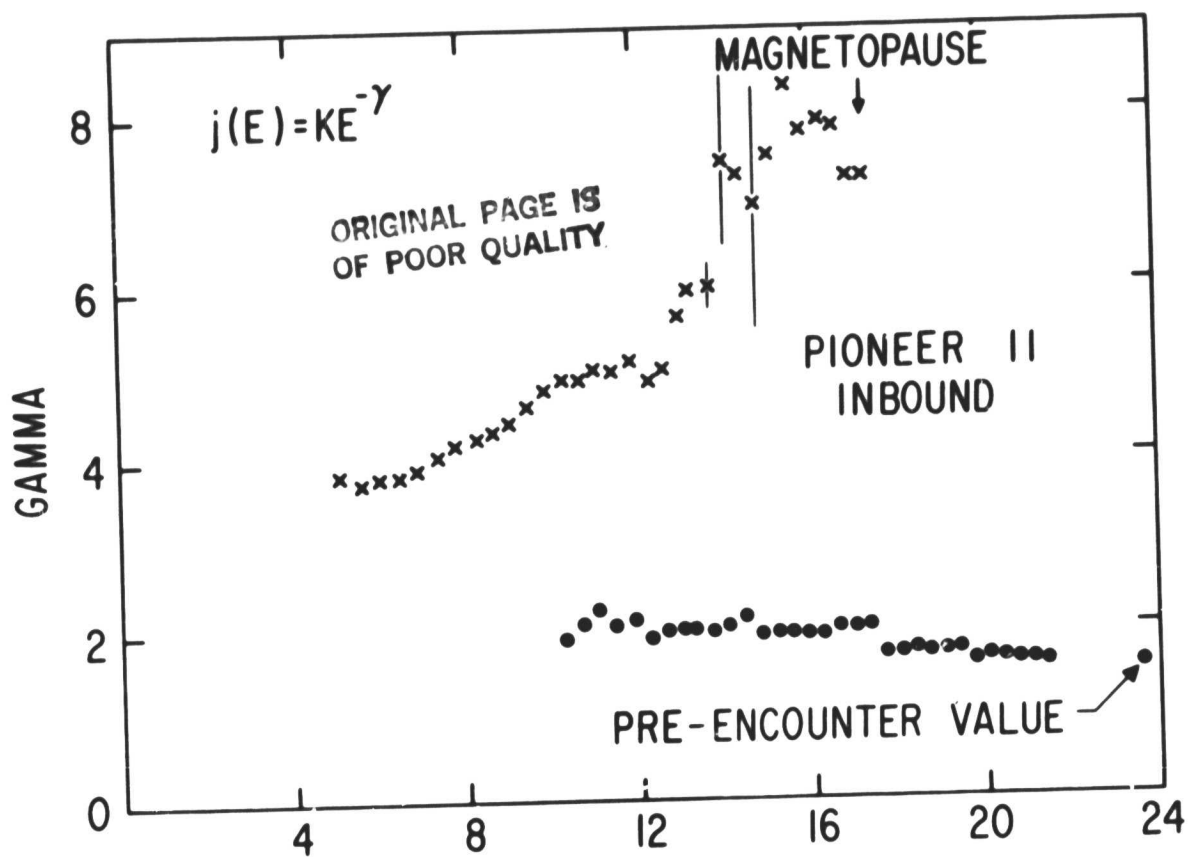
Fig.22

Fig. 23. Mass histograms of light and heavier ion species in the subsolar outer
          magnetosphere. The histograms were derived from 2-dimensional pulse-
          height matrices accumulated over 10h periods by Voyagers 1 and 2. Note
          the nearly equal abundance of H_2 molecules and He ions and the presence
          of H_3 molecules during the Voyager 2 encounter only. The flux of
          medium weight nuclei was much higher during the Voyager 2 flyby. The
          relative lack of nitrogen suggests solar wind origin rather than the
          plasma torus in the outer magnetosphere (courtesy of Hamilton et al.,
          1983).

a) Voyager 1
0.6-0.8 MeV/nuc
10.5-20.7 R$_S$

b) Voyager 2
0.5-0.7 MeV/nuc
10.6-18.7 R$_S$

c) Voyager 1
0.27-0.40 MeV/nuc
10.5-20.7 R$_S$

d) Voyager 2
0.21-0.36 MeV/nuc
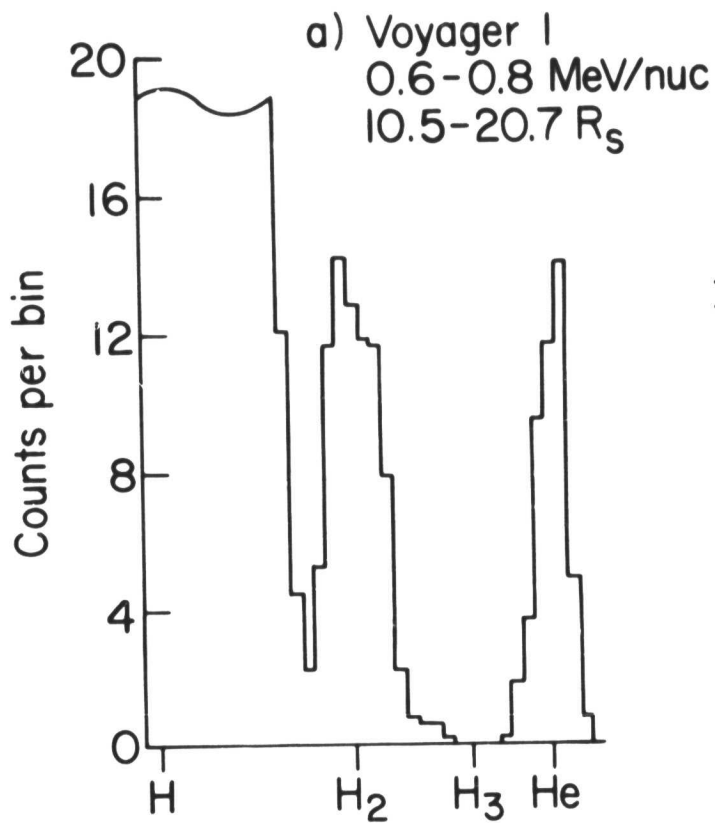10.6-18.7 R$_S$

82-24
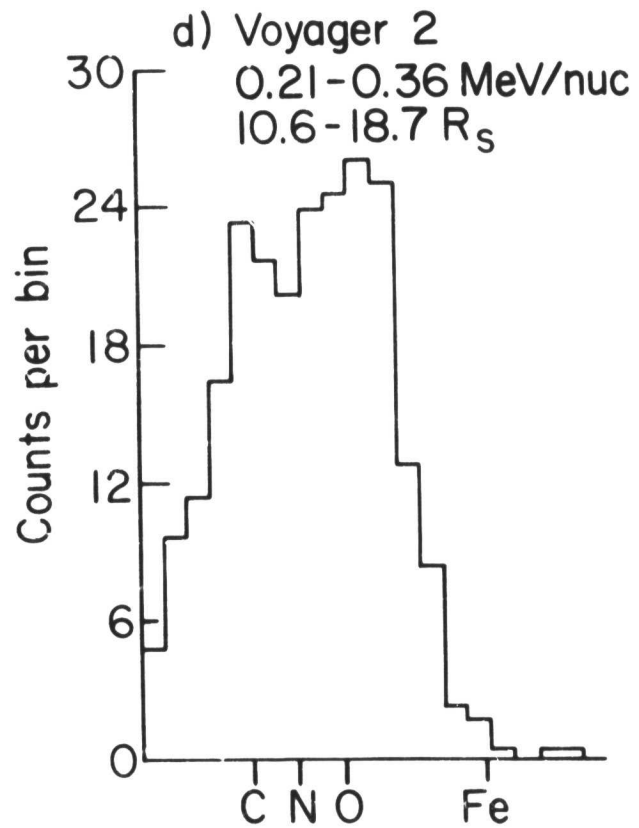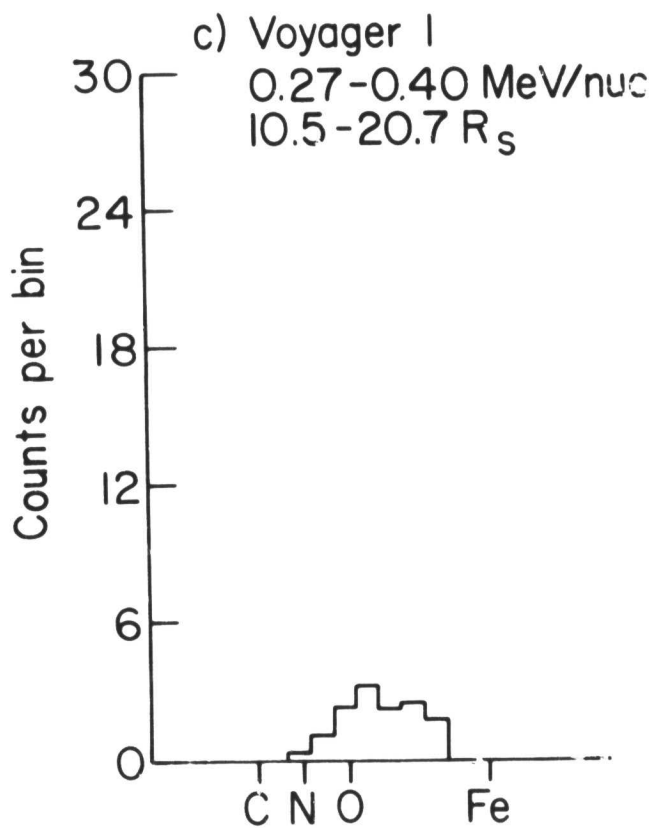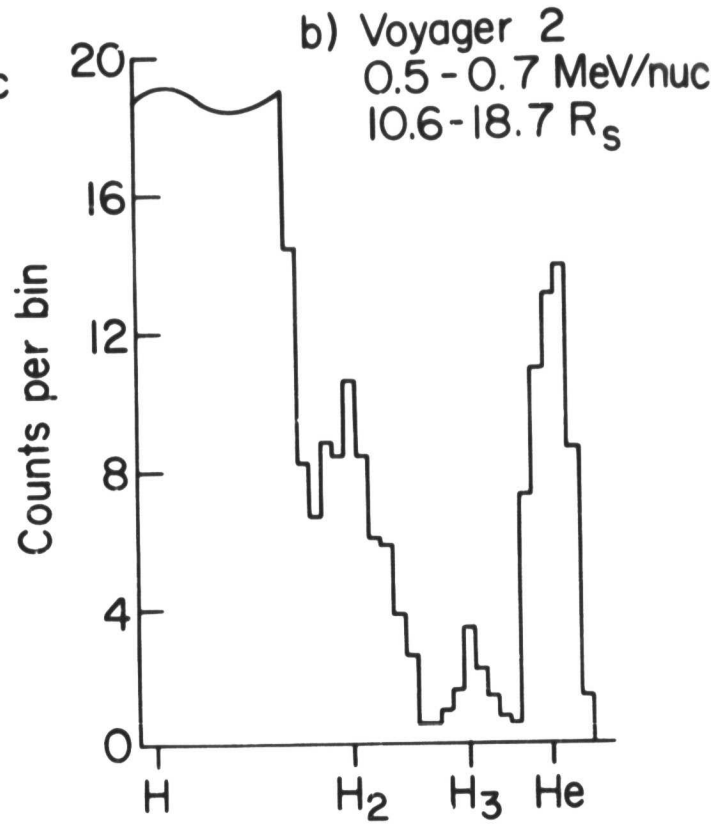
Fig. 23

Fig. 24. Energy spectra of the most abundant ion species averaged over the same 10h period as Fig. 23. A single power law in energy fits the H, He and Voyager 1 C + N + O data. The H_2 spectrum (open circles) and Voyager 2 C + N + O spectrum (triangles) requires 2 components with a cutoff above 0.4 MeV which falls at least as fast as E^{-8}. The H_3 ions were observed over such a narrow energy range that no spectrum could be derived. Interplanetary intensities and spectra of H, He and C + N + O observed just prior to encounter are shown with dashed lines (courtesy of Hamilton et al., 1983).
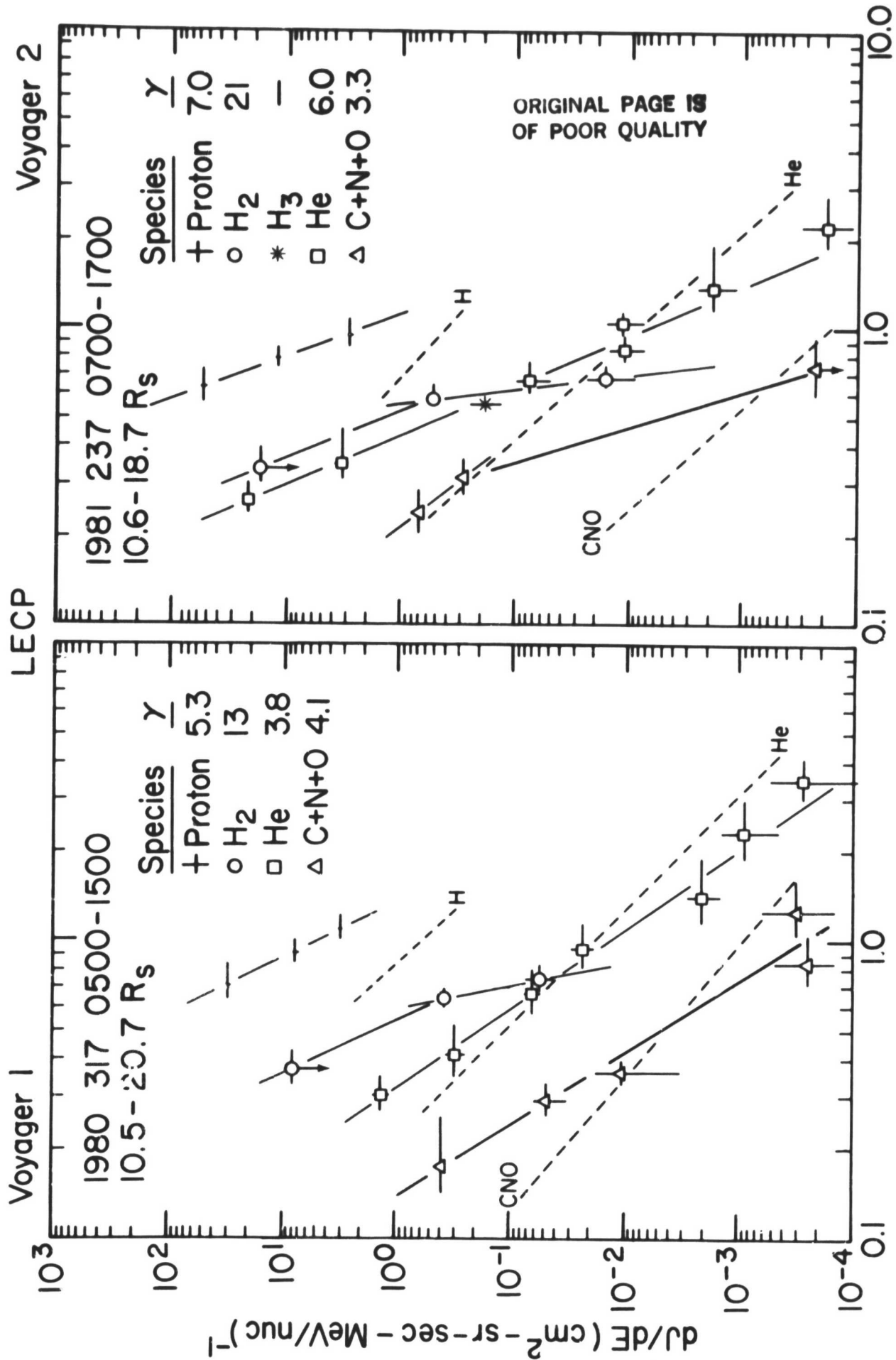
Fig. 24

Fig. 25. Relative phase space density profiles for protons with constant
          magentic moment and near Equatorial mirror points. The curves were
          calculated from a least squares fit to Pioneer 11 proton energy spectra
          and the local magnetic field strength. The inbound pass is represented
          by solid circles and the outbound pass by open circles (courtesy of
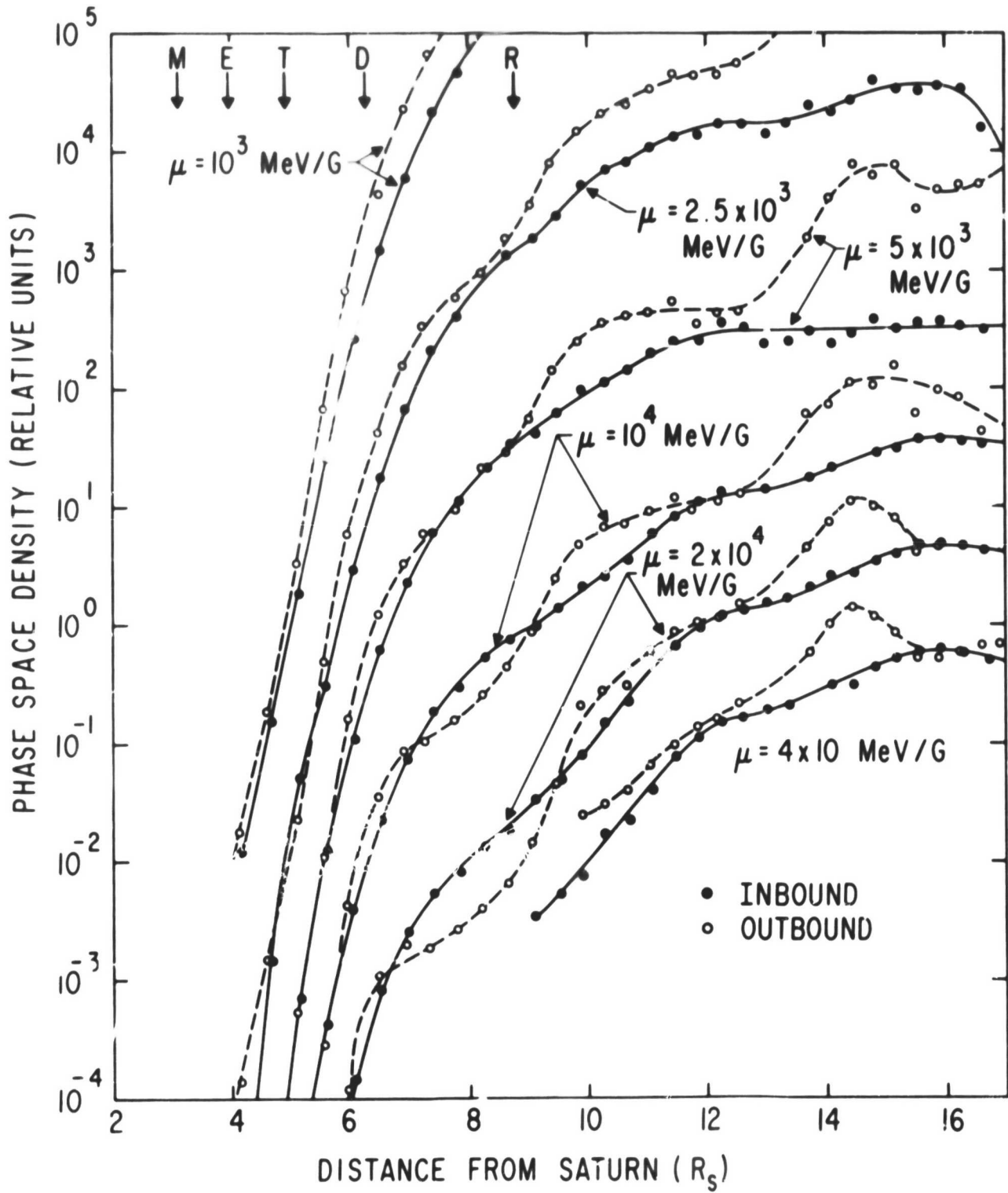   McDonald et al., 1980).

Fig.25

71

Fig. 26. Counting rates (15 minute average) of selected electron and ion rates
          observed with Voyager 2. The positions of bow shock and magnetopause
          crossings are marked by BS and MP, respectively. Dotted lines indicate
          crossings of the dipole L shells of the outer satellites (courtesy of
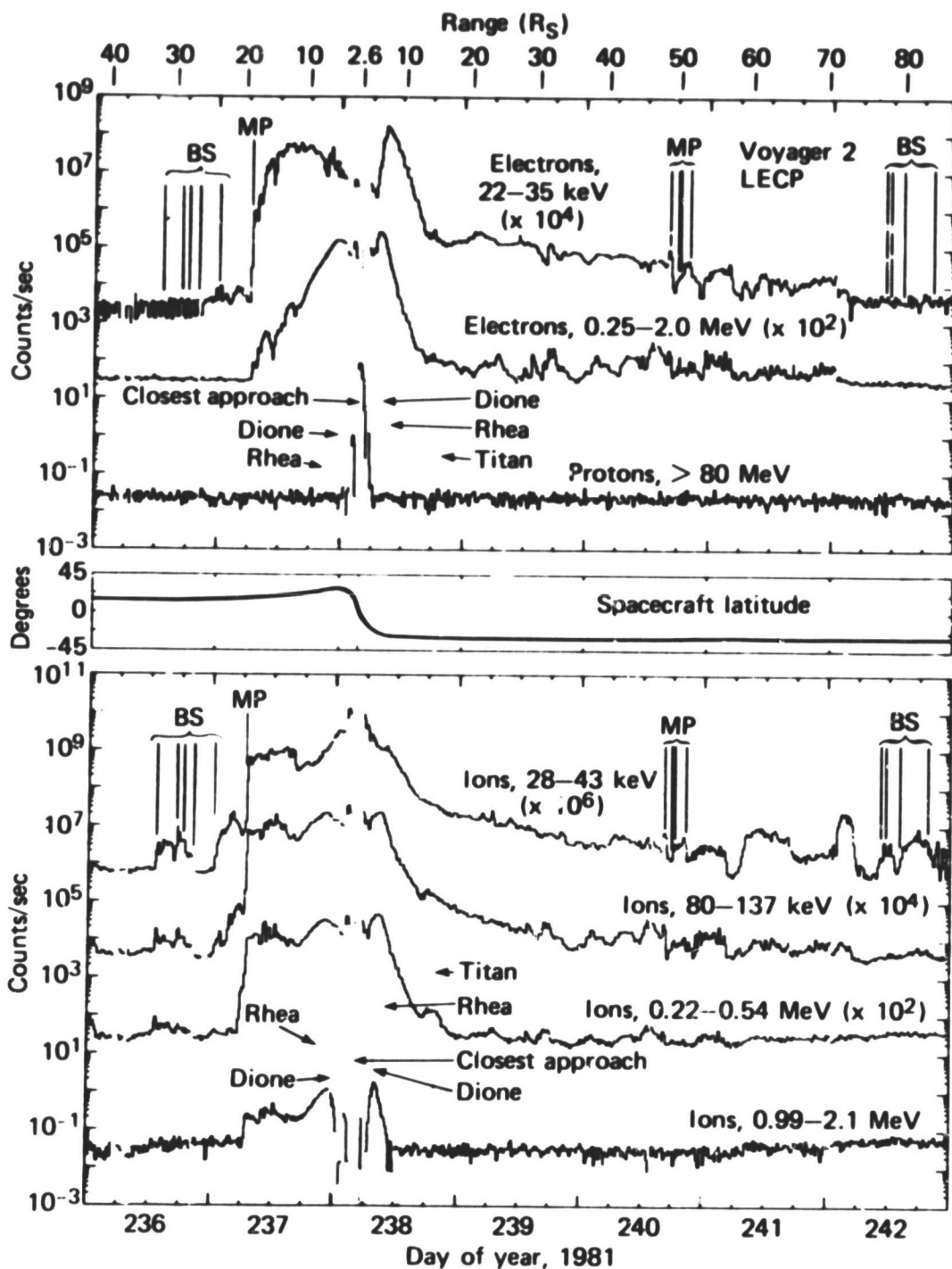   Krimigis et al., 1982).

Range (R_S)

Electrons,
22–35 keV
(x 10^4)

MP   Voyager 2
      LECP

BS

Electrons, 0.25–2.0 MeV (x 10^2)

Closest approach ⟶   ⟵ Dione

Dione ⟶   ⟵ Rhea

Rhea ⟶   ⟵ Titan   Protons, > 80 MeV

Counts/sec

Spacecraft latitude

Degrees

BS   MP   MP   BS

Ions, 28–43 keV
(x 10^6)

Ions, 80–137 keV (x 10^4)

⟵ Titan

Rhea   ⟵ Rhea   Ions, 0.22–0.54 MeV (x 10^2)

Dione ⟶   ⟵ Closest approach
                ⟵ Dione

Ions, 0.99–2.1 MeV

Counts/sec

Day of year, 1981

Fig.26

Fig. 27. Fifteen minute averages of flux intensity and anisotropy of 0.5-1.8 MeV
protons derived from the low energy telescope of the University of
Chicago on Pioneer 11. The angles θ_1 to θ_4 are measured relative to
the projection of the observed magnetic field into the scan plane. The
inclination of the magnetic field relative to the spin axis, α_B, is
shown in the top panel. Pitch angles in the range of 90 ± α_B are
scanned. Because of collimator penetration, angular distributions
inside of $4R_S$ are unreliable. The position of the bow shock crossing,
B, and magnetopause crossing, M, are indicated (courtesy of Bastian et
al., 1980).
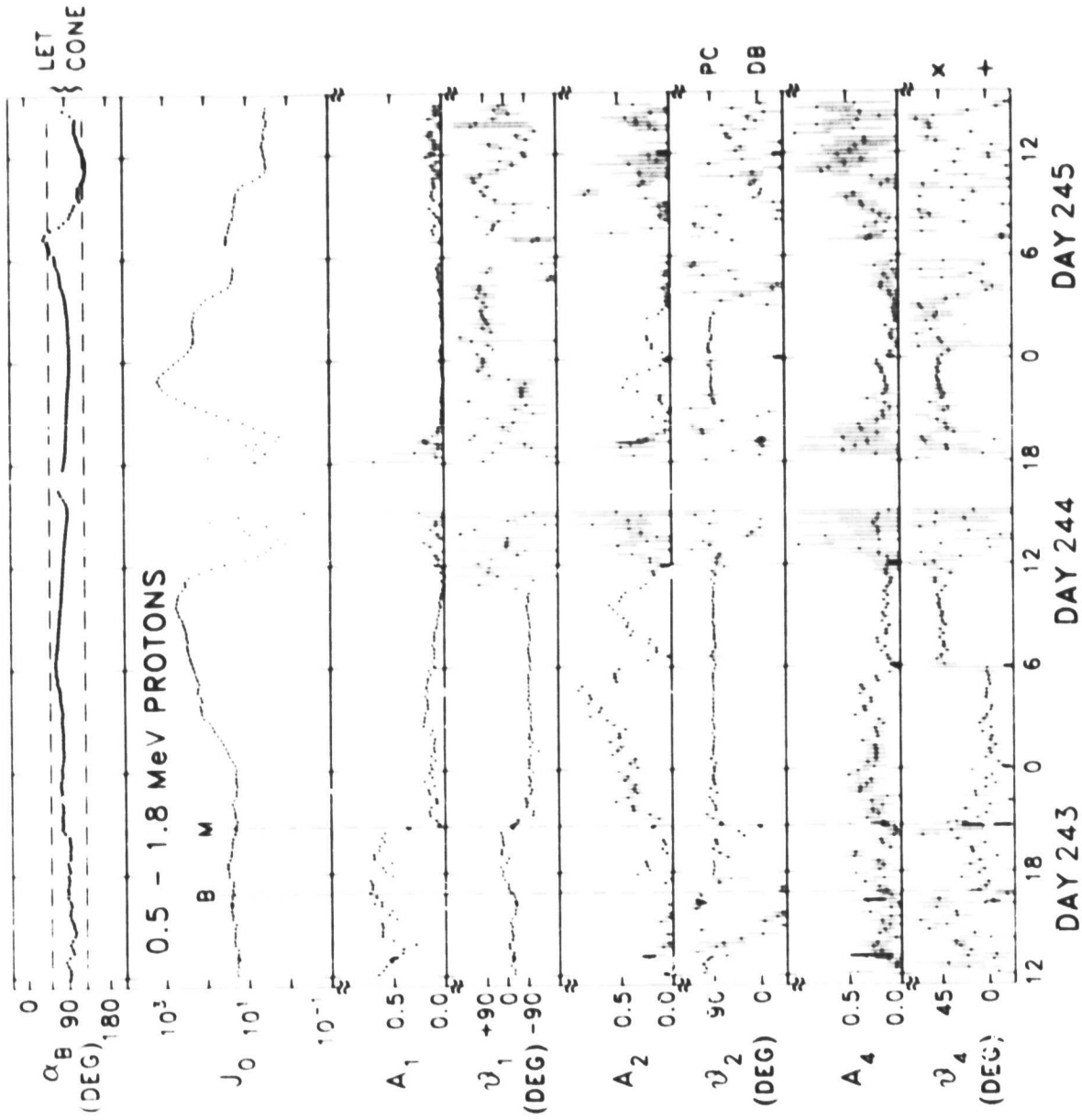
Fig. 27

Fig. 28. Thirty-two-minute averages of second-order anisotropies of electrons in three energy intervals as observed with Pioneer 11. The pancake (perpendicular to field) pitch angle distributions correspond to $1 + b \sin^2\theta$ and the dumbbell (field aligned) distributions to $1 + b \cos^2\theta$, with $b = 2A_2/(1-A_2)$. No corrections have been made for the inclination of the magnetic field relative to the scan plane. The positions of Saturn's satellites are indicated by arrows (courtesy of McDonald et al., 1980).

Fig. 23

74
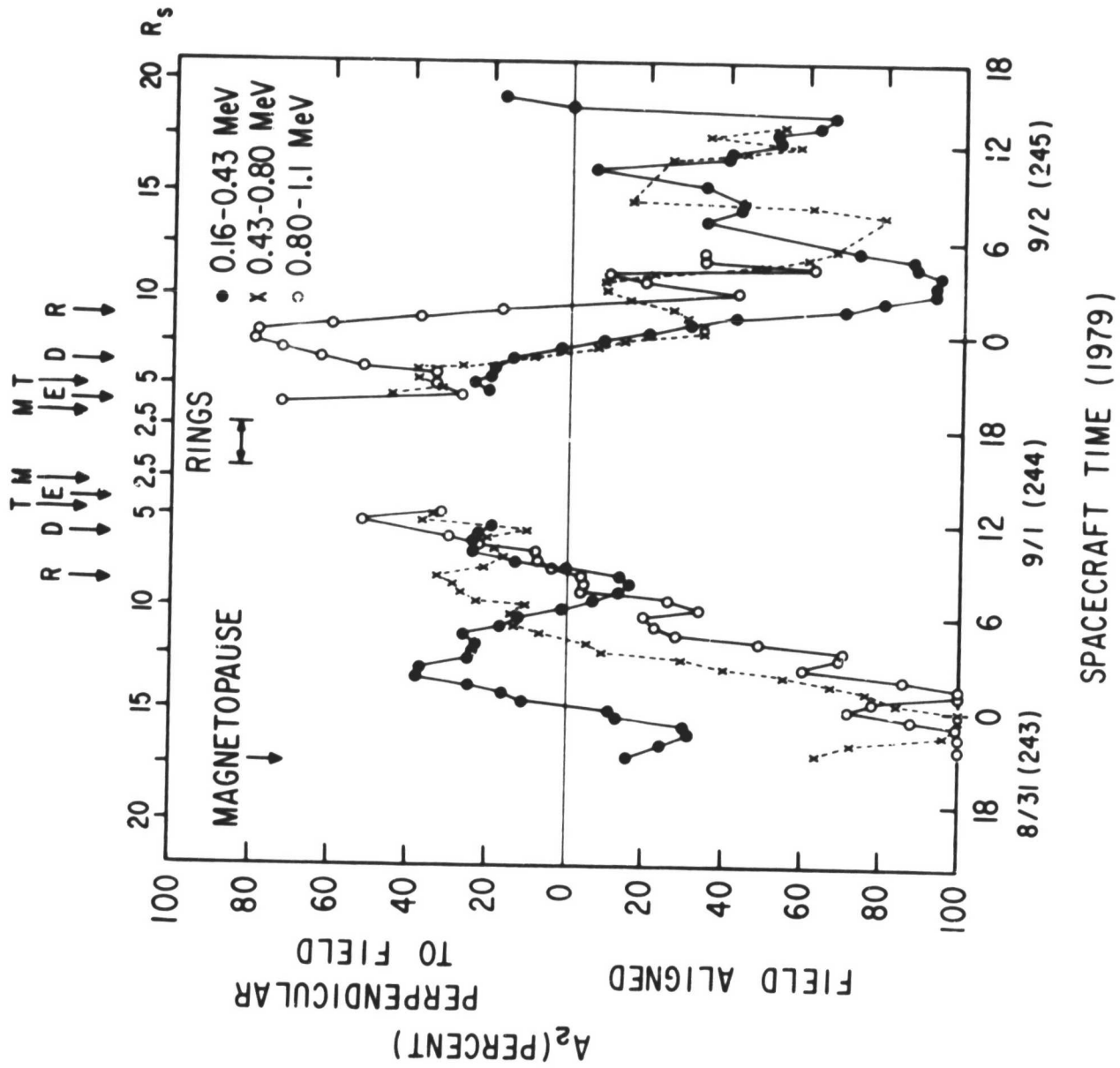
Fig. 29. Polar histograms of sectored electron counting rates (32-minute
          average) observed with Pioneer 11 during the outbound pass at -90° to
          the Saturn-Sun line. The dashed circle gives the spin averaged rate.
          The dashed arrow shows the projection of the magnetic field into the
          scan plane, and the dashed line gives the direction of the second order
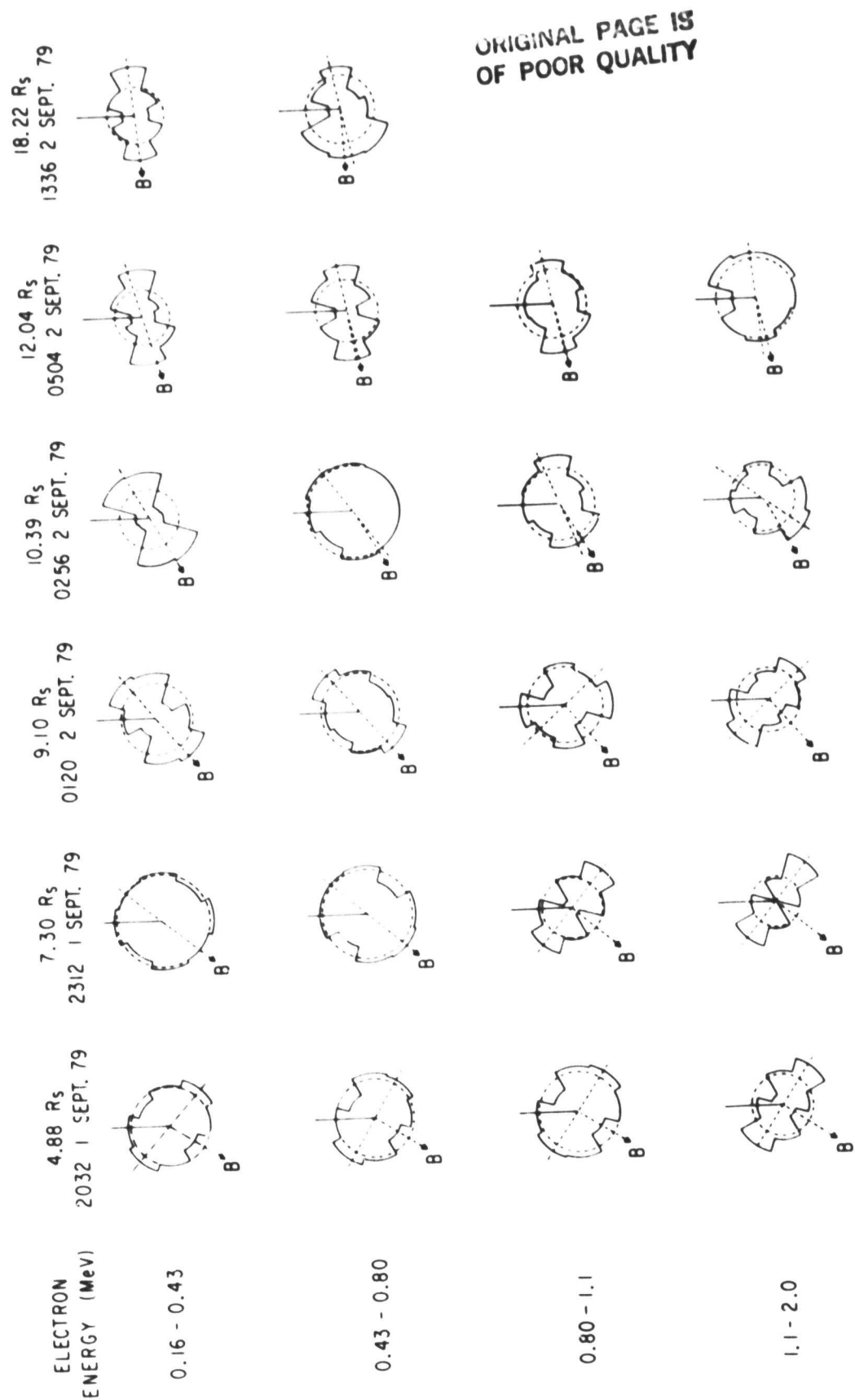   anisotropy (courtesy of McDonald et al., 1980).

Fig. 29

75

Fig. 30. Electron counting rates in the dawn side outer magnetosphere observed
          with Voyager 2 at a latitude of -29°. Curve A displays the rate of
          0.14-0.4 MeV electrons (x 10); curve B, the rate of > 0.35 MeV
          electrons; curve C, the rate of > 0.6 MeV electrons; and curve D, the
          rate of 1-2 MeV electrons (x 0.1). Typically, the electron fluxes
          increased by about an order of magnitude with a rise time of $\tau \sim 5$ min.
          The decay time was energy dependent with $\tau \sim 11$ min. above 1 MeV and
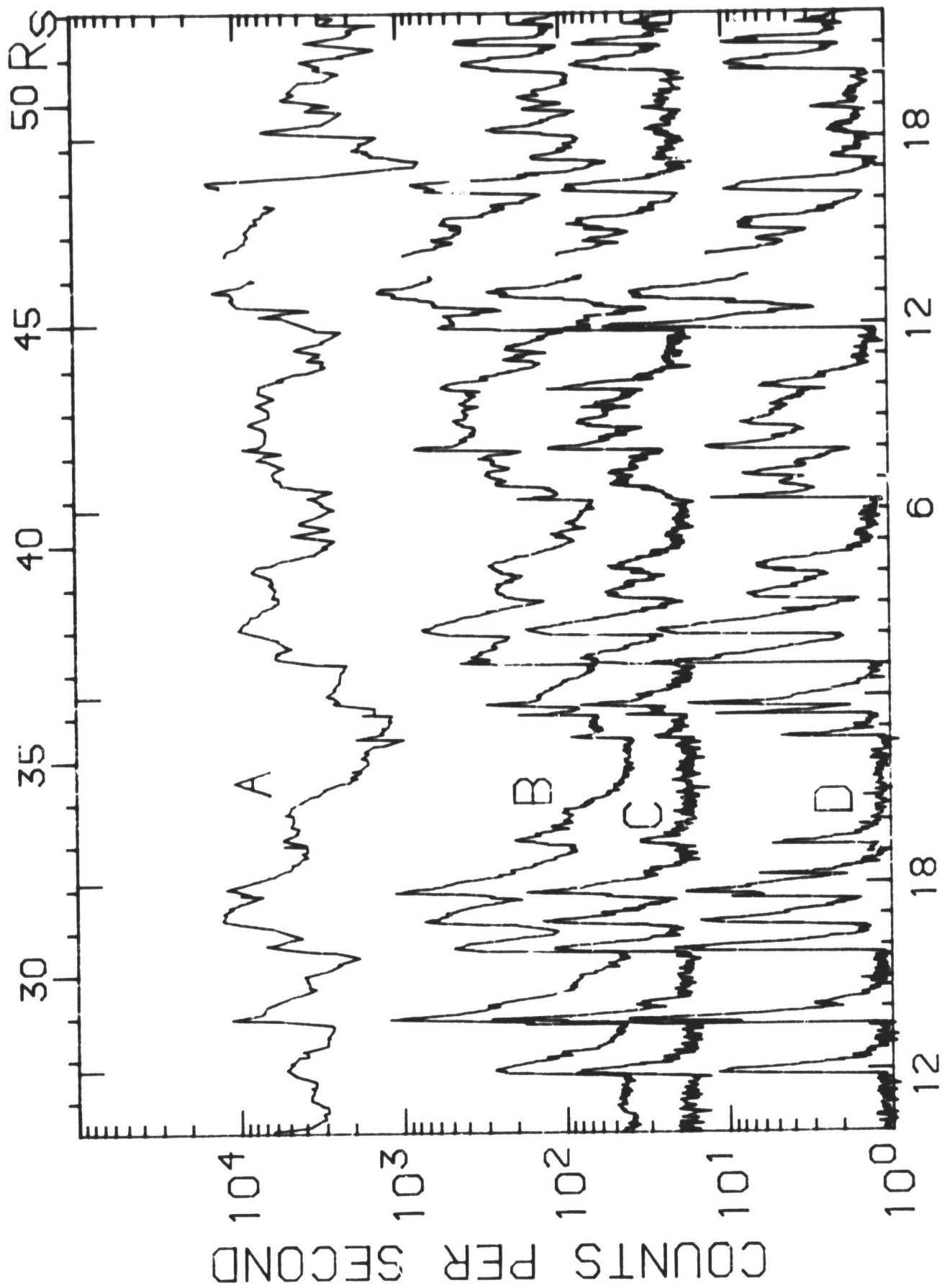 ~ 20 min. at ~ 0.4 MeV (courtesy of Vogt et al., 1982).

Fig. 30

76

Fig. 31.   Ratios of counting rates (15 minute average) in two energy channels
for electrons and ions. The dipole L shells of Rhea and Titan are
shown as dotted lines, and the tick marks identify the minima used
to determine the period. Times when the spacecraft was at an SLS
longitude of 0° are indicated at the top of the figure (courtesy of
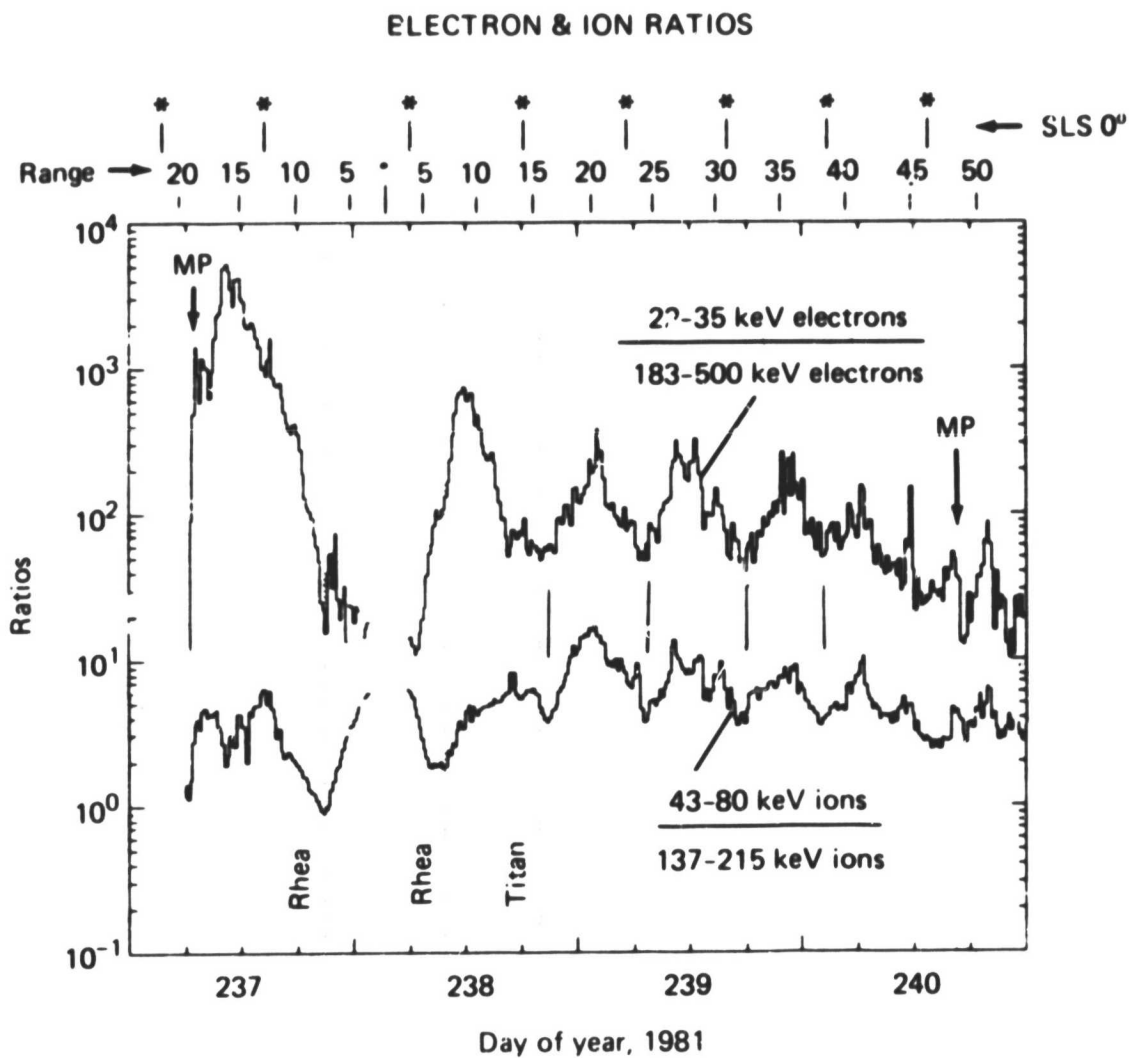Carbary and Krimigis, 1982).

ELECTRON & ION RATIOS

Fig.31

77

Fig. 32. Ion densities, temperatures, and dominant species as observed by
          Pioneer 11. The oxygen torus was observed from ~ 4 to 8 R_S. The
          apparent decrease inside of ~ 4 R_S is not real because the ion
          energies decreased to below the 100 eV per unit charge threshold of
          the plasma instruments. Ion temperatures within the plasma torus at
          4-7 R_S decreased monotonically with decreasing radial distance
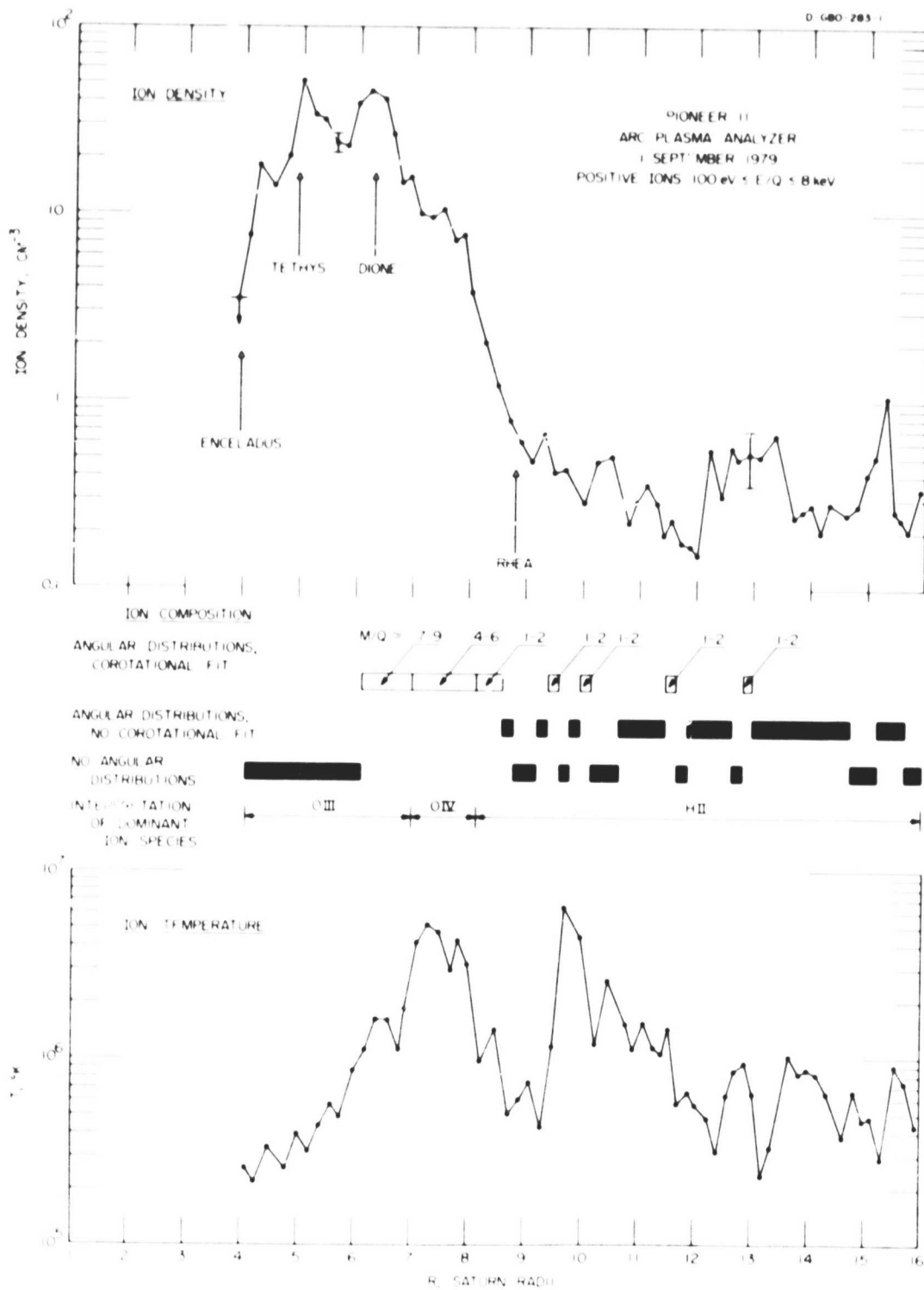   (courtesy of Frank et al., 1980).

Fig. 32

Fig. 33. Sequence of ion spectra taken within 6 R_S of Saturn by Voyager 2. The magnitude of the Saturnian magnetic fie'd at the position of the spacecraft is plotted on the back panel (Ness et al., 1982). The component into the sensor of the corotation velocity, V_A, is shown along one axis. The time of observation, the corresponding dipole L shell, and the distance from the Equatorial plane (Z in R_S) are also shown. The plasma observed at the beginning of the period (C000 to 0130) was made up of protons most of which had energies below the threshold of the instrument (~ 5 cm^{-3} with $T \sim 8$ eV at L = 4.4 inbound). The peak near periapsis has been attributed to O^+ ions, with the peak of the distribution below threshold (courtesy of Bridge et al., 1982).
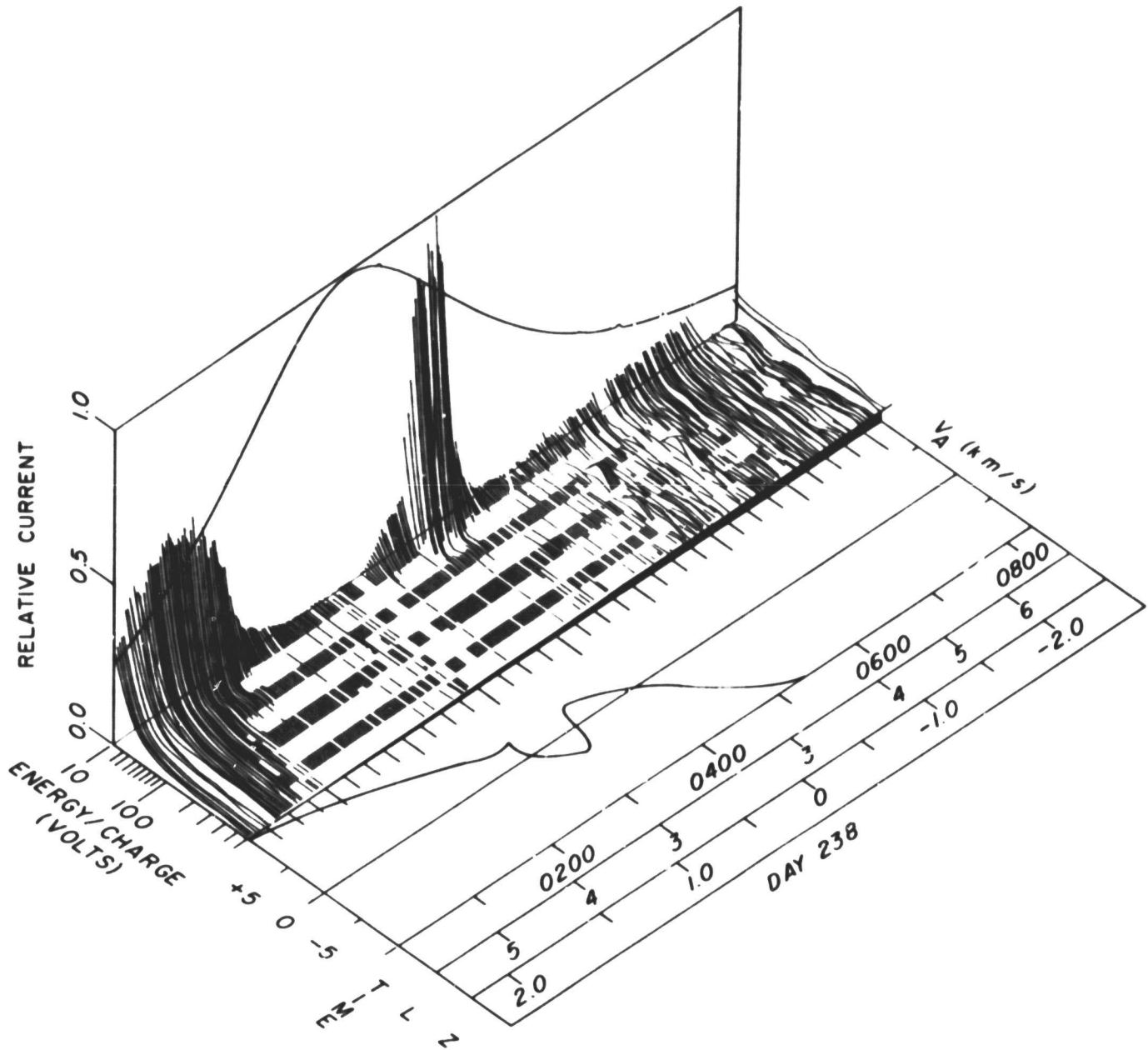
Fig. 33

Fig. 34. Microabsorption signatures of Titan, Rhea, Tethys and 1979 S2.
A. Voyager 1 observation of the microabsorption signature of Titan
    as seen in > 0.43 MeV protons and > 0.35 MeV electrons. The
    proton detector looked towards Titan in the direction shown by
    the arrows. The heavy dashed curve superimposed on the proton
    absorption feature is the expected signature of a 3800 km sphere
    in an isotropic proton flux (courtesy of Vogt et al., 1981).
B. Voyager 1 observation of the microabsorption signature of Rhea
    as seen in > 0.43 MeV protons at three different pitch angles.
    Voyager 1 was ~ 1 R_S north and 4° east (in the corotation
    direction) of Rhea, and it took the protons ~ 3 minutes to drift
    from Rhea to Voyager 1. The 4,000 km width of the signature
    would be expected from geometric absorption by Rhea (1,530 km)
    and the ~ 3,500 km gyroradius of the protons. Protons mirroring
    off the Equatorial plane have a substantial probability of
    missing Rhea, and the details of the geometric relation between
    Voyager and Rhea are believed to be responsible for the pitch
    angle dependent fine structure.
C. Voyager 2 observation of the microabsorption signature of Tethys
    in > 2.2 MeV electrons. At the time, Voyager 2 was within 1° of
    the longitude of Tethys but at -19° latitude. The Z3 model
    Equatorial field line distance is given and the nominal position of
    the orbit is indicated by the arrow. The width of the feature
    is ~ 1100 km as compared to the diameter of Tethys of 1060 km.
D. Pioneer 11 observation of the microabsorption signature of 1979
    S2 in electrons plotted versus Earth receive time. The width of
    the signature is 170 km and is comparable to the diameter of
    1980 S3 which is thought to be the same object (Van Allen, 1982;
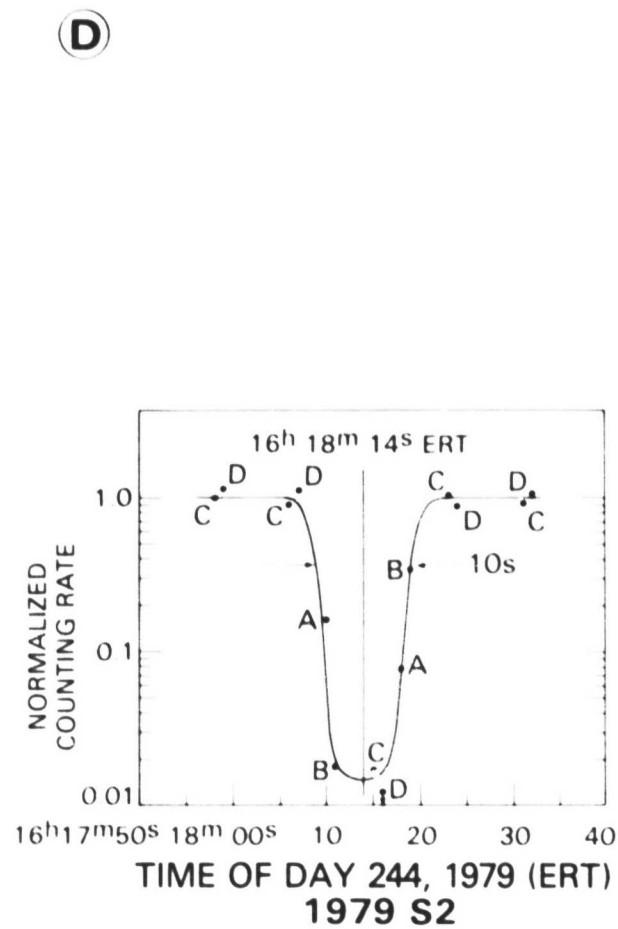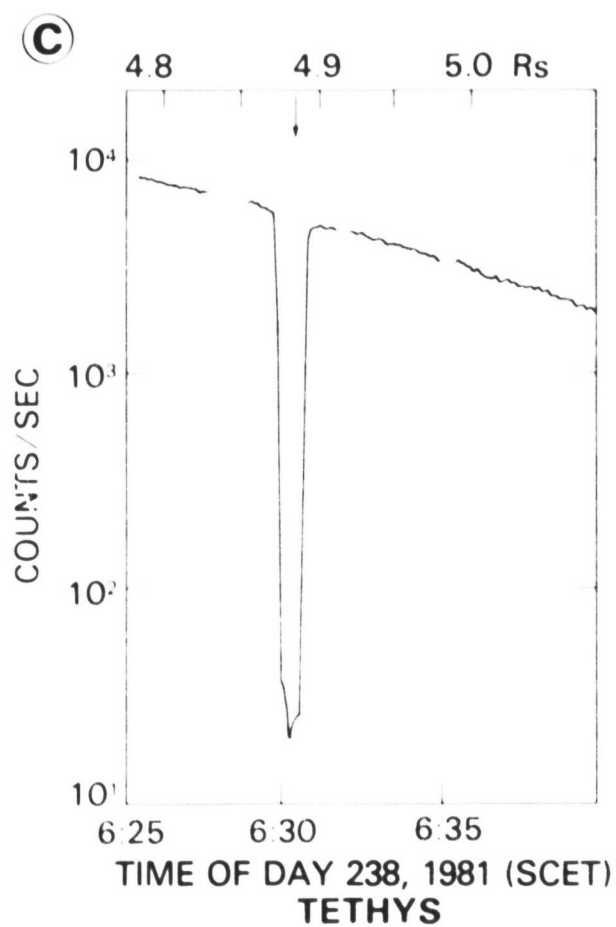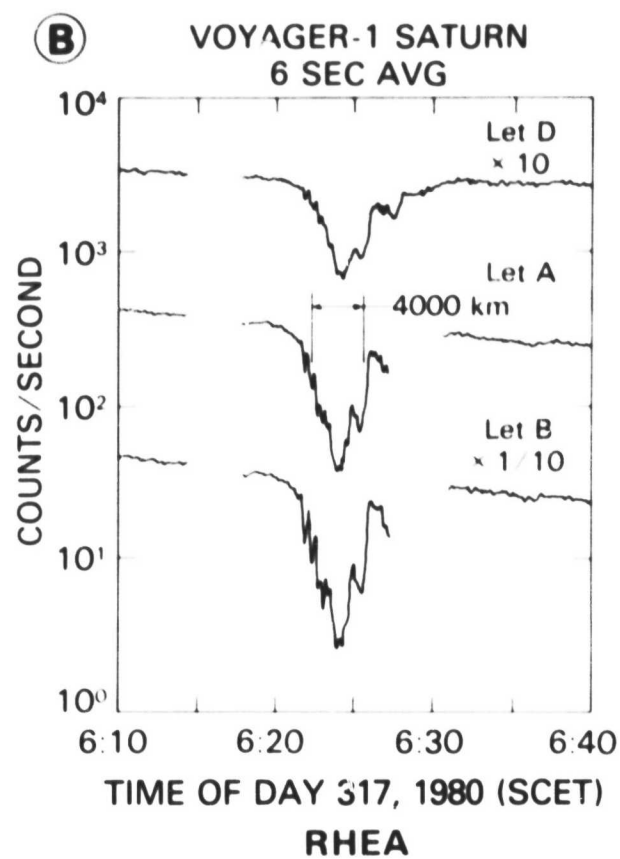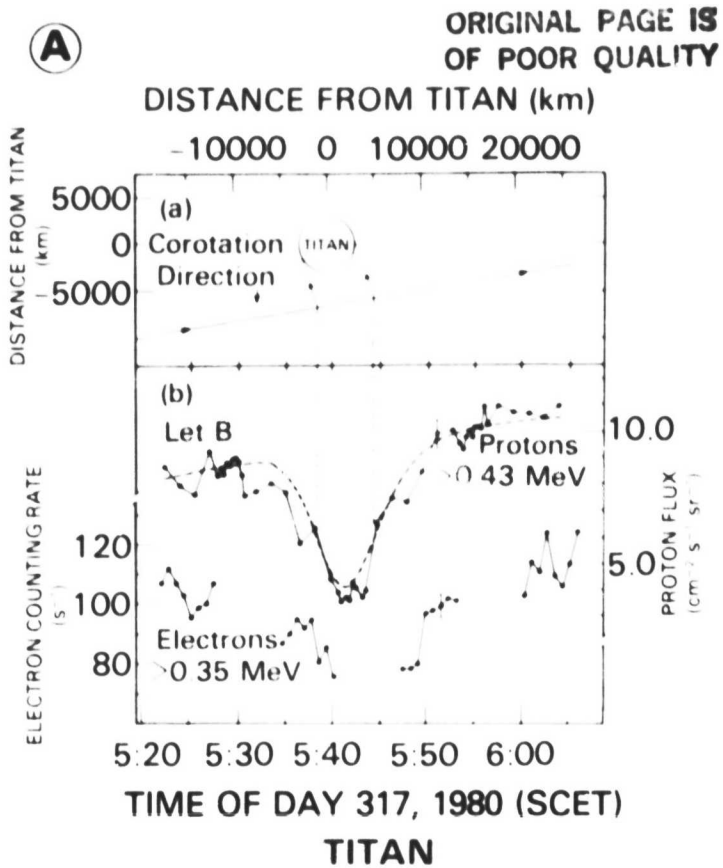   courtesy of Van Allen et al., 1980a).

(A)

DISTANCE FROM TITAN (km)

−10000 0 10000 20000

(a)
Corotation (TITAN)
Direction

(b)
Let B   Protons
                     >0.43 MeV

Electrons
>0.35 MeV

TIME OF DAY 317, 1980 (SCET)
TITAN

(B) VOYAGER-1 SATURN
6 SEC AVG

Let D
× 10

Let A   4000 km

Let B
× 1/10

TIME OF DAY 317, 1980 (SCET)
RHEA

(C)

4.8   4.9   5.0 Rs

COUNTS/SEC

TIME OF DAY 238, 1981 (SCET)
TETHYS

(D)

16h 18m 14s ERT

NORMALIZED COUNTING RATE

10s

TIME OF DAY 244, 1979 (ERT)
1979 S2

Fig. 34

Fig. 35. Counting rates of the University of Chicago 0.5-1.8 MeV proton
detector on Pioneer 11. It is now believed that the counts inside
of L = 4 are primarily due to > 30 MeV protons (Simpson et al.,
1981). Angular distributions relative to the magnetic field
direction are shown above (inbound) and below (outbound) the
counting rate curve. Note the macroabsorption features of
Enceladus, Mimas, and 1979 S2 (at L = 2.5) and the absence of such
features at the other satellites. The symmetry of the inner
magnetosphere is manifest by the agreement between the inbound and
outbound pass. The effect of shell splitting is noticeable between
the orbits of Enceladus and Dione (courtesy of Simpson et al.,
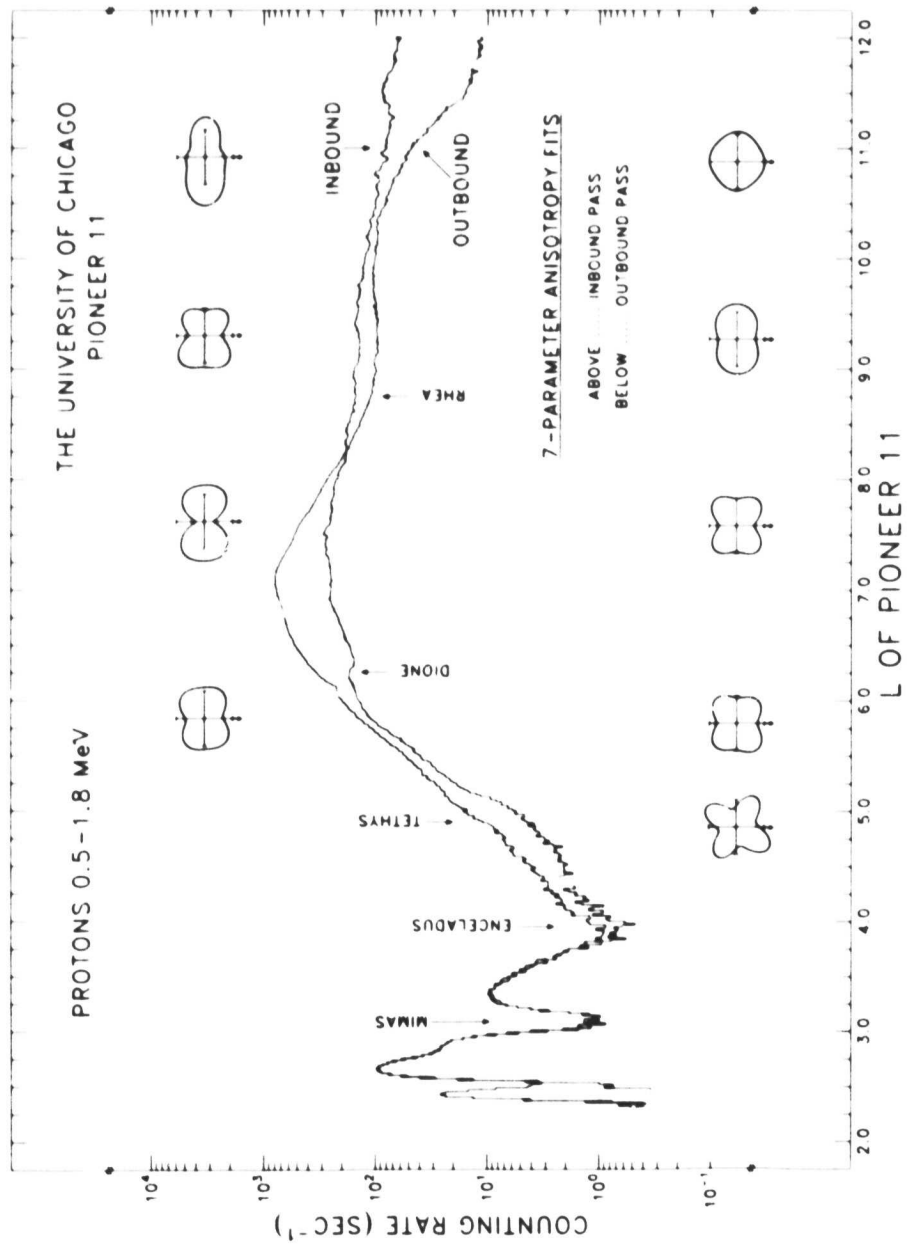1980).

Fig. 35

Fig. 36. Electron (> 0.45 MeV) and proton (> 80 MeV) intensities in the inner
          magnetosphere. To gain time resolution, data from three thresholds
          on each of the detectors have been internormalized. If the spectrum
          changes, this causes a modulation that repeats every 4th point.
          Absorption features due to Mimas, 1979S2 and the F ring are
          observable in the > 80 MeV proton flux. The electron intensities
          reflect the micro-absorption feature of 1979 S2 and absorption by
          the F and A rings (courtesy of Fillius et al., 1980).

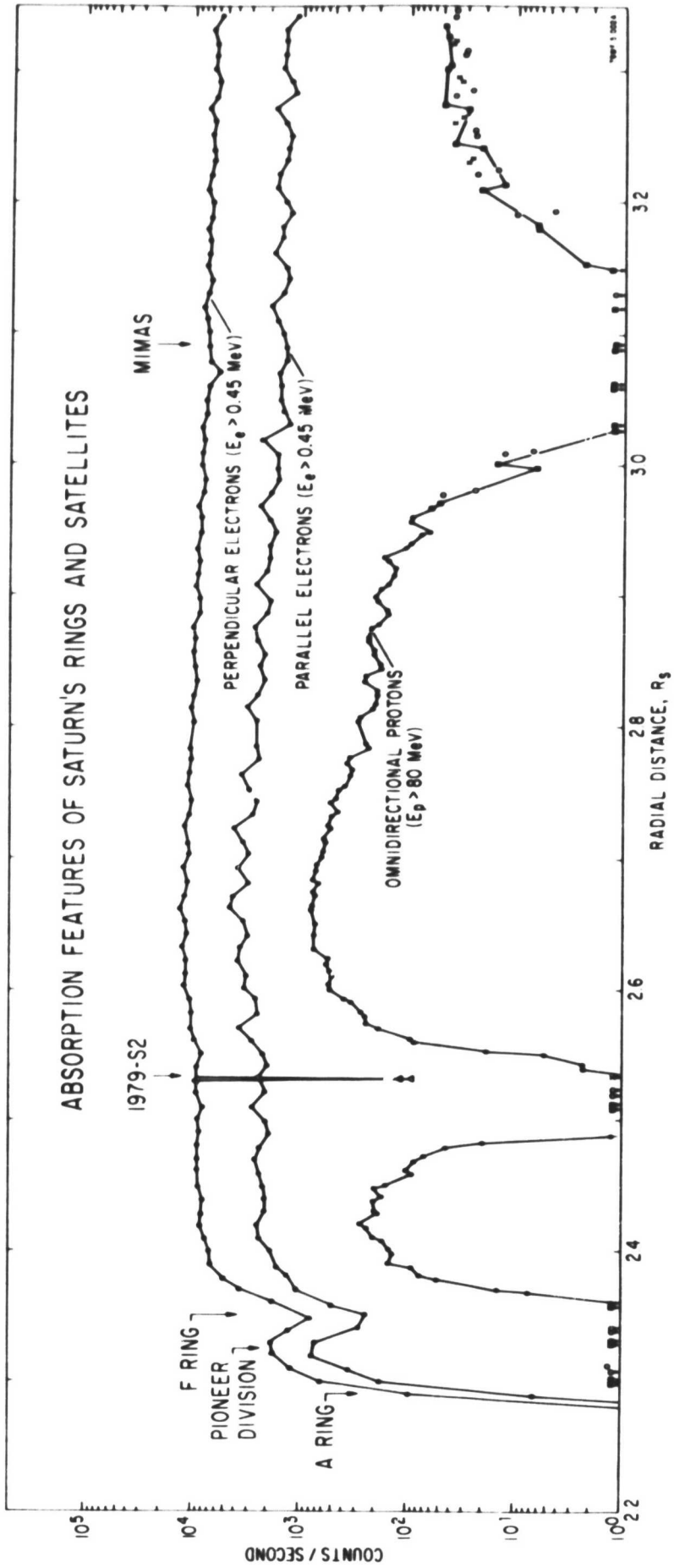ABSORPTION FEATURES OF SATURN'S RINGS AND SATELLITES

Fig. 36

Fig. 37. The flux of energetic protons in the inner magnetosphere, 48-63 MeV
          and 63-160 MeV. The 48-63 MeV flux is not shown in the Mimas and G
          ring absorption region because of uncertainties associated with
          corrections for protons going through the sides of the counter
          telescope. The dip near the G ring observed inbound just before
          peak flux was due to a spacecraft roll maneuver. At low fluxes, the
          error bars reflect statistical fluctuations and at high rates they
          represent systematic errors. The top scale giving the Equatorial
          distance of field lines and the position of satellite absorption
          features are based on the Z3 magnetic field model (Connerney et al.,
          1982). The G ring, Mimas, and Enceladus are identified by G, M, and
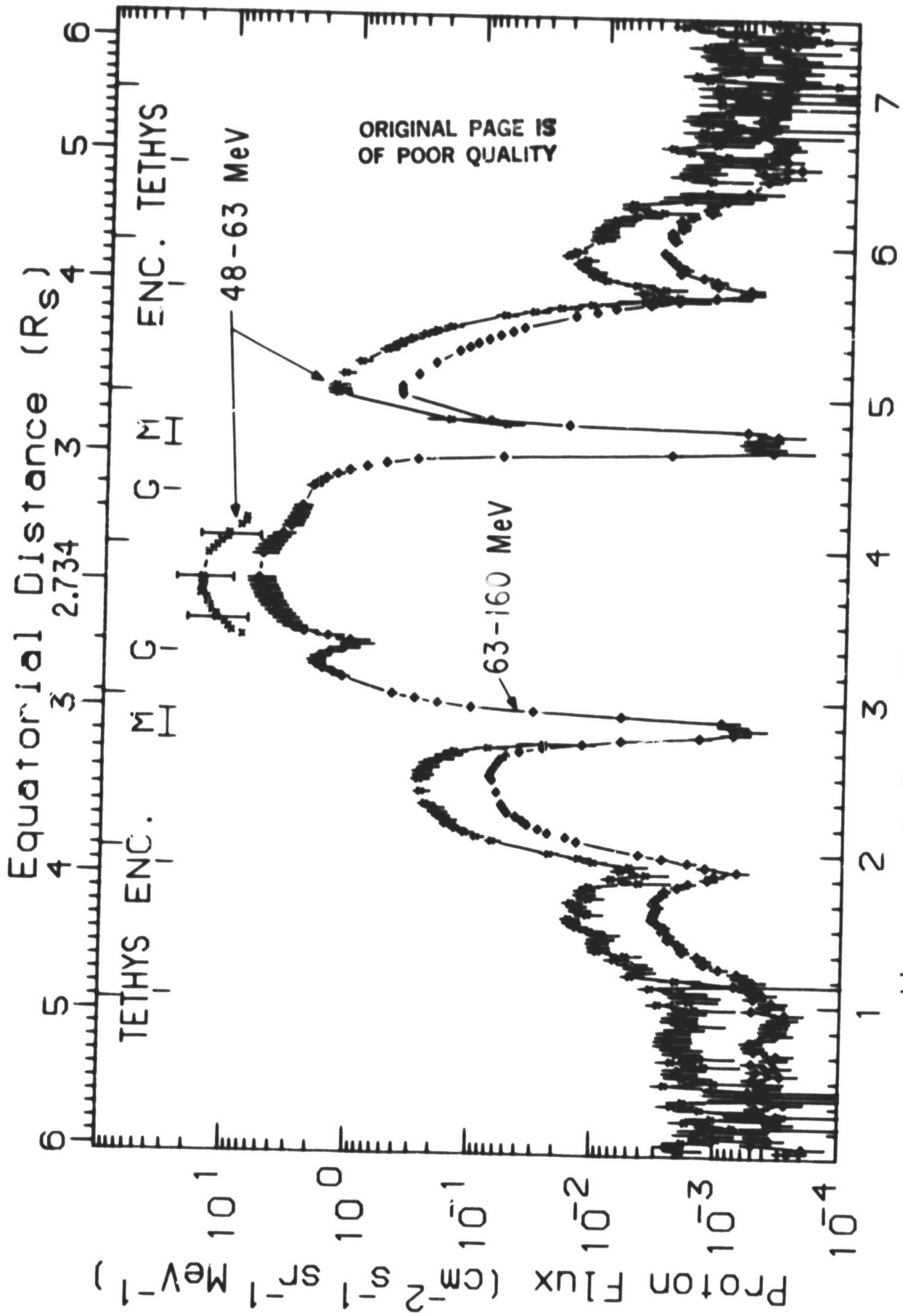   Enc., respectively (courtesy of Schardt and McDonald, 1983).

Fig. 37

ORIGINAL PAGE IS
OF POOR QUALITY

Fig. 38.   Proton energy spectra observed during the inbound pass of Voyager 2 at dipole L values of 7.80, 3.40 and 2.75 R_s. The comparison with Pioneer 11 data refers only to the 2.75 R_s curve (insert lower left hand corner). Angular distributions of 29-43 keV protons near the G ring are shown in the upper right. The preferential absorption near 90° pitch angle is clearly visible between L = 2.75 and 2.835 (courtesy of Krimigis and Armstrong, 1982).
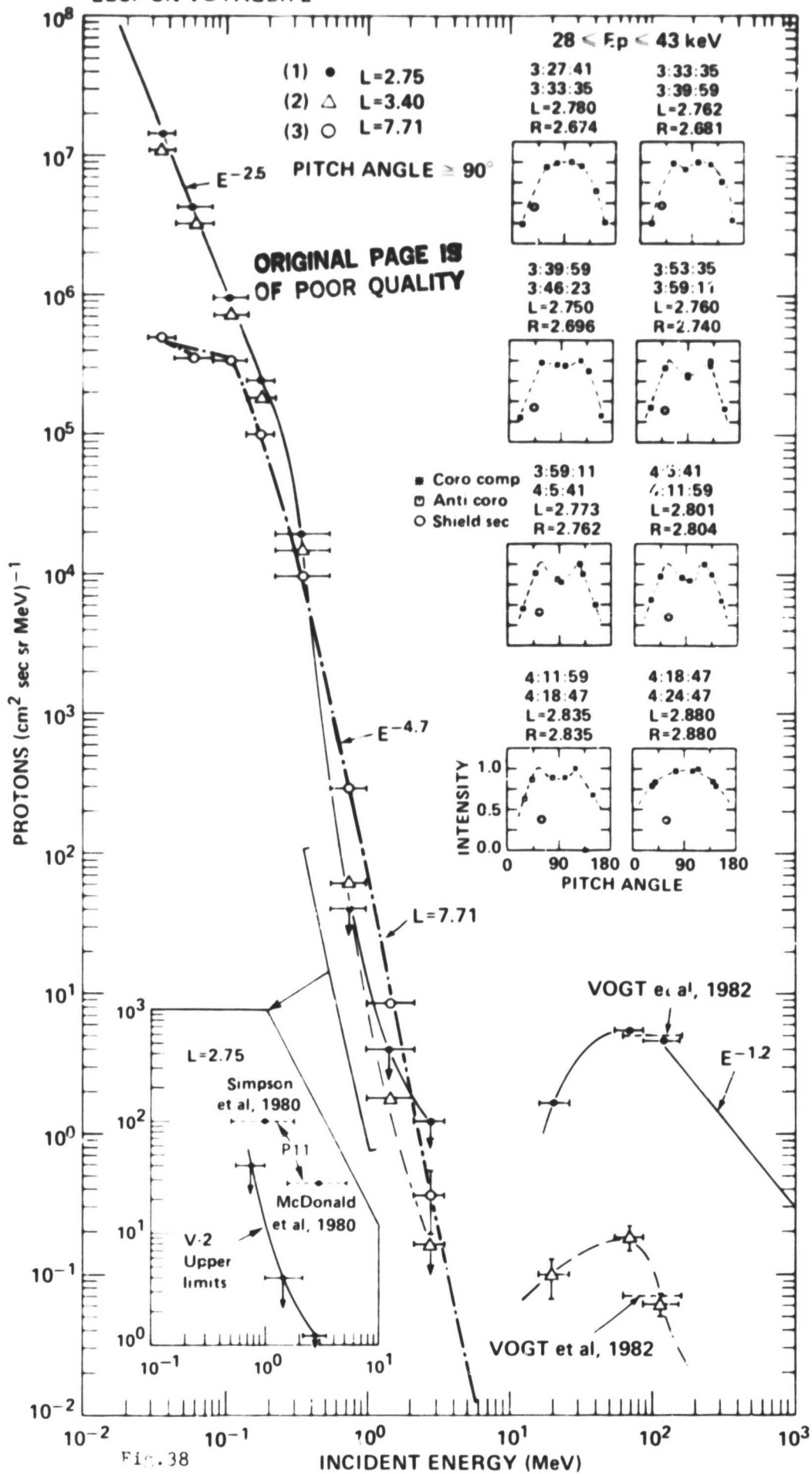
Fig. 38

84

Fig. 39. Relative phase space density profiles for protons with constant
          magnetic moment and 90° pitch angles. The curves were calculated
          for an exponential spectrum of the form $J \propto \exp - E/E_{CH}$, WITH E_{CH} =
          40 MeV for the 15 BeV/G curve and E_{CH} = 33 MeV for the 60 BeV/G
          curve. The pitch angle distribution used was of the form $\sin^{n}\theta$,
          with n reflecting the probable angular distribution. Typical error
          bars are shown. It should be noted that the curve represents only
          an upper limit beyond 5 R_S because of the presence of a substantial
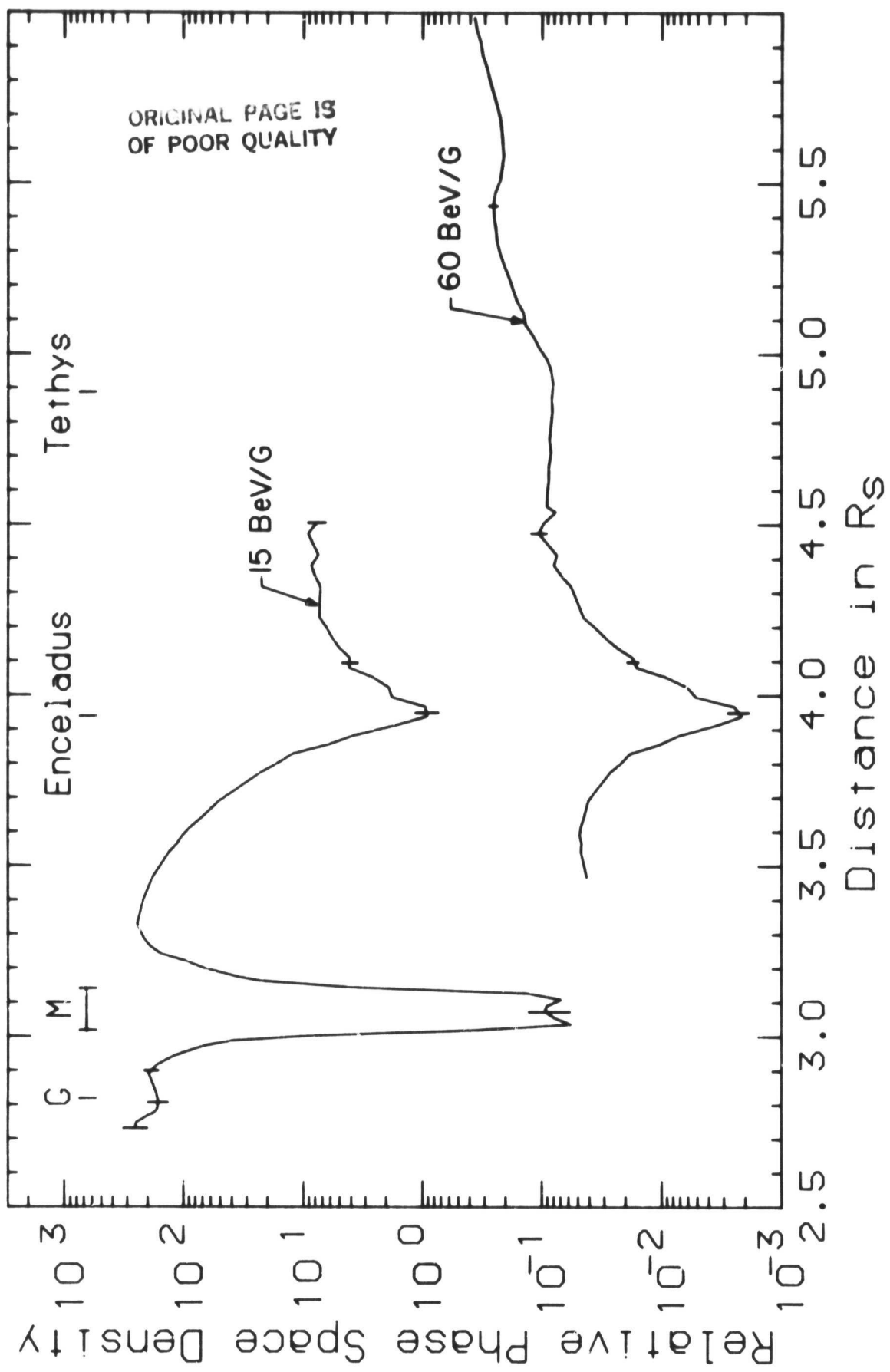   cosmic ray component (courtesy of Schardt and McDonald, 1983).

Fig. 39

85

Fig. 40. Spectra of protons injected by the decay of cosmic ray produced
          neutrons. The spectra were calculated for 20 GeV primary protons
          isotropically incident upon ice spheres of 5.5, 30 and 200 cm
          radius. The solid curve results from the decay of neutrons moving
          in the forward hemisphere relative to velocity vector of the
          incident proton; the dashed curve is for backward moving neutrons.
          Each set of spectra is normalized to unity at 12.5 MeV in the
          forward direction (courtesy of Blake et al., 1983).

Fig. 40

20 GeV 200 cm
ICE

20 GeV 30 cm
ICE

20 GeV 5.5 cm
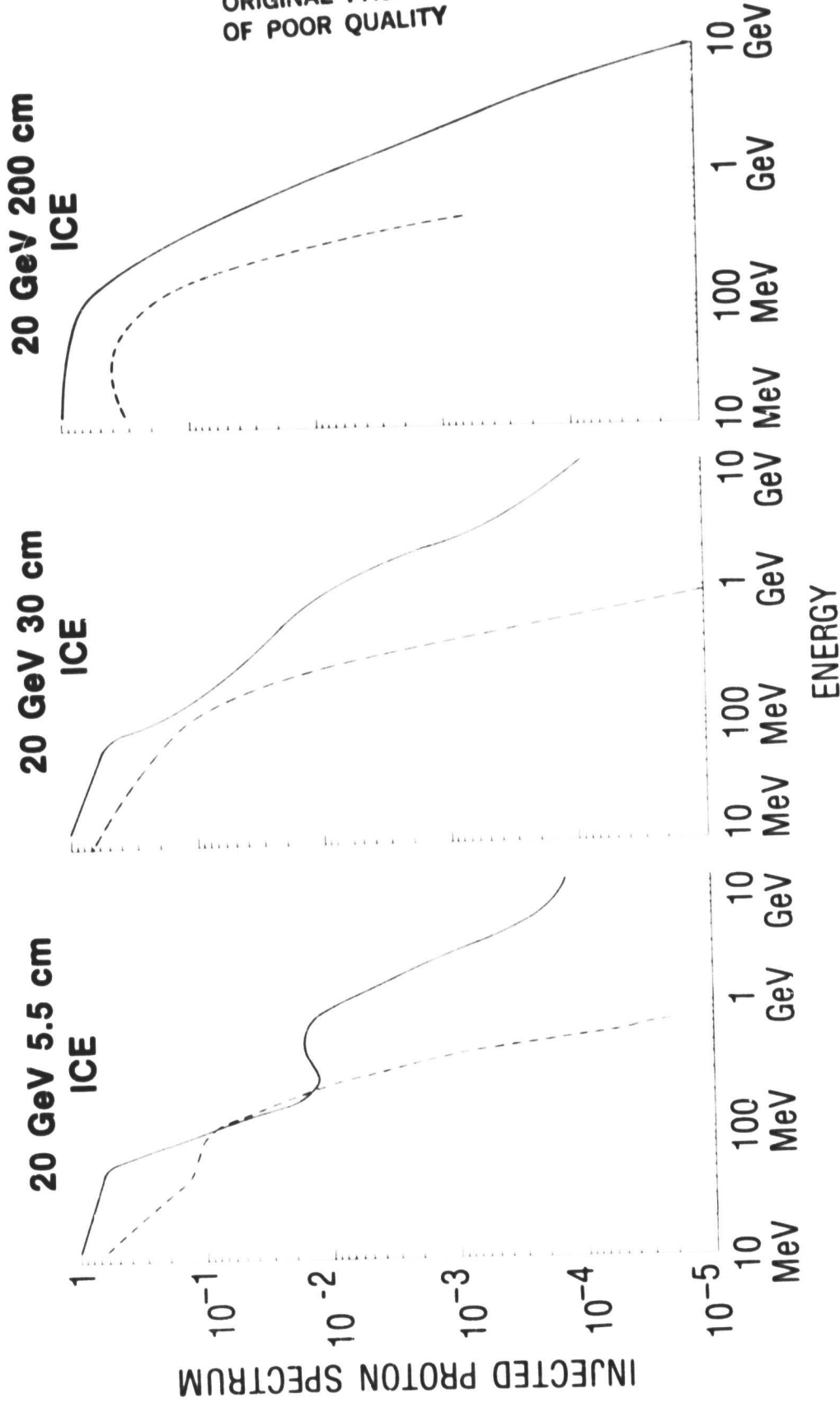ICE

INJECTED PROTON SPECTRUM

ENERGY

86

Fig. 41. A. Counting rate of 7 to 17 MeV electrons and flux of > 3.4 MeV
              electrons (right scale) in the inner magnetosphere.
          B. The corresponding electron density in phase space calculated for
              an E^{-4} spectrum. The reversal of the expected phase space
              density gradient remains even for spectra as steep as E^{-7}.
              Caution is required in interpreting the 7-17 MeV counting rate
              because the counter telescope was near saturation, and its
              response was almost certainly non-linear (courtesy of McKibbin
              and Simpson, 1980).

FLUX (CM² SEC)⁻¹ — $\text{FLUX (CM}^2\text{ SEC)}^{-1}$

10^8 10^7 10^6 10^5 10^4

THE UNIVERSITY
OF CHICAGO

(A)

>3.4 MeV ELECTRONS — >3.4 MeV ELECTRONS

1979S2

F-RING

MIMAS

7–17 MeV ELECTRONS

$f(\mu_o,L)$=PHASE SPACE DENSITY

(B)

S541

ASSUMED SPECTRUM:
$dJ/dE=AE^{-4}$

L OF PIONEER 11

10^3 10^2 10^1 10^0 10^{-1}

COUNTING RATE (SEC⁻¹) — COUNTING RATE (SEC^{-1})

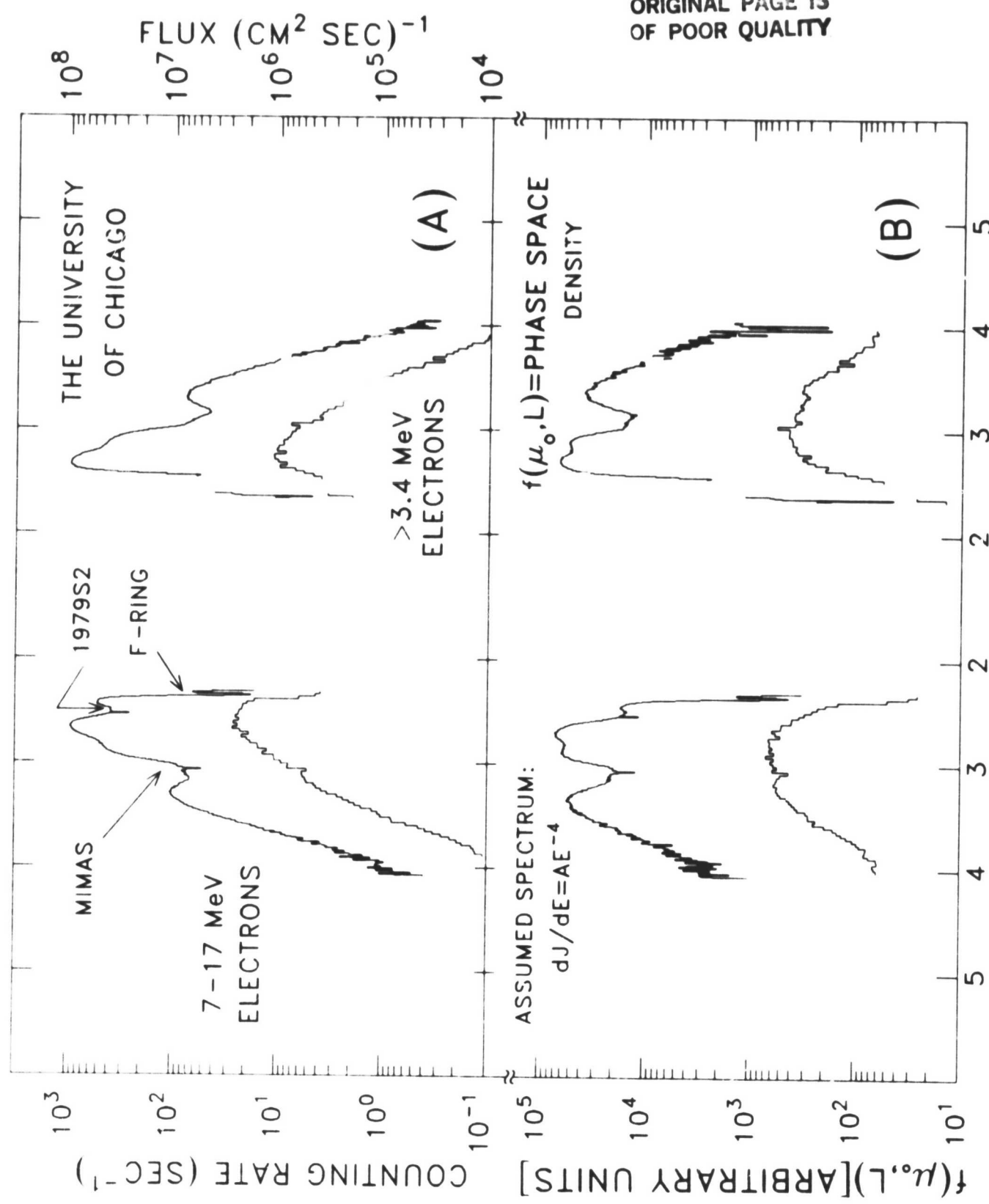10^5 10^4 10^3 10^2 10^1

$f(\mu_o,L)$[ARBITRARY UNITS]

Fig.41

Fig. 42. A. Macro- and micro-absorption features of charged particles at
              Mimas. The quasi-periodic variations in the counting rates are due
              to scanning through an anisotropic pitch angle distribution.
              Outside the Mimas absorption gap, the proton counter responded
              primarily to > 30 MeV protons (Simpson et al., 1981; courtesy of
              Simpson et al., 1980b).

THE UNIVERSITY OF CHICAGO
PIONEER 11

SPACECRAFT TIME (UT), DAY 244, 1979

COUNTING RATE (SEC^{-1})

ELECTRONS 7 - 17 MeV

PROTONS 0.5 - 1.8 MeV

MIMAS
(L = 3 03 - 3.15)

L = 2.81 JANUS?

L=3.3 L=3.2 L=3.1 L=3.0 L=2.9 L=2.8
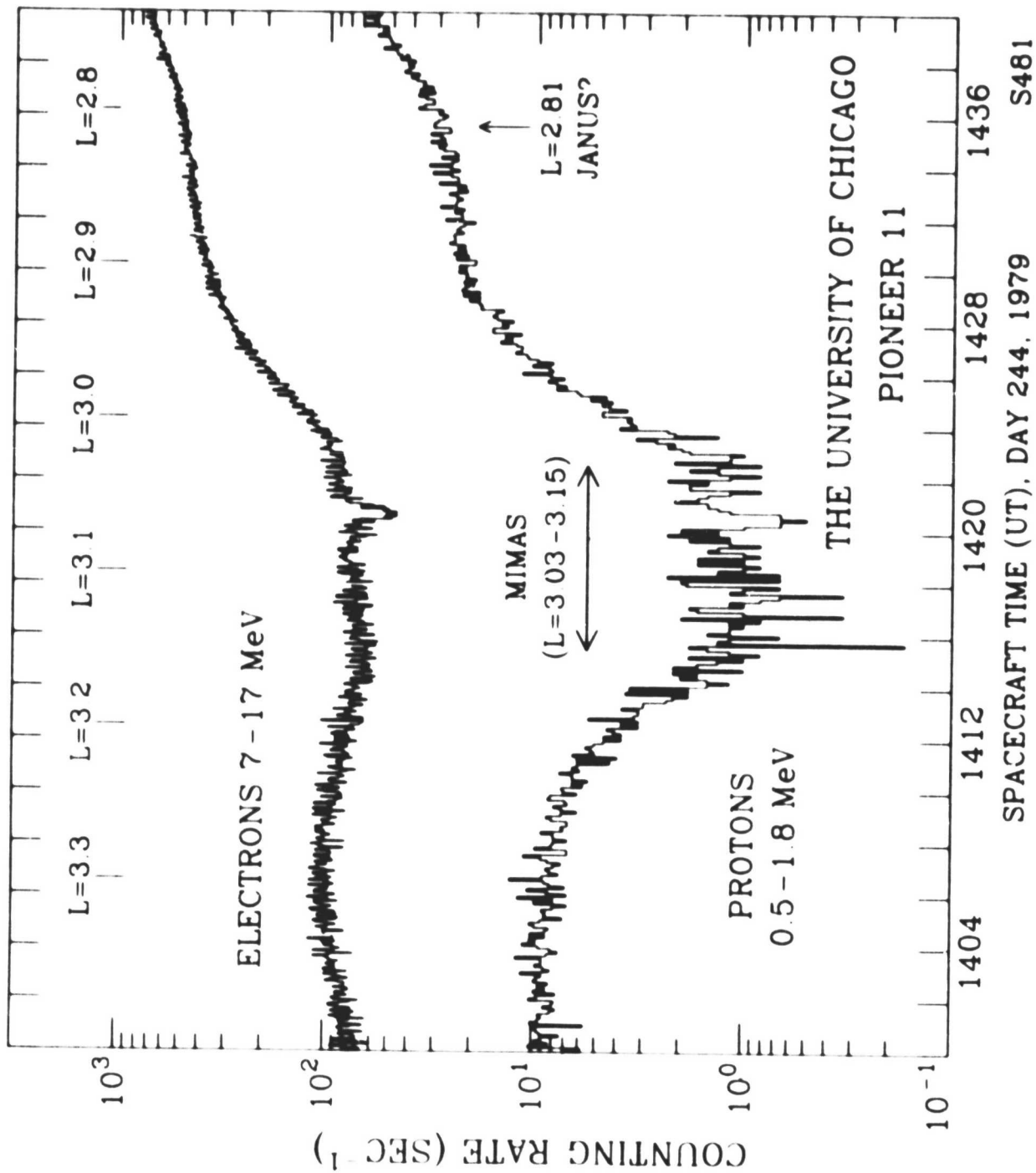
S481

Fig. 42A

Fig. 42. B. Normalized profile of the electron micro-absorption signature in
            detectors A, B, and C observed in the Mimas gap. The solid
            curve is the best fit result of a simple one-dimensional
            diffusion model of satellite sweep-up and refilling process.
            This model does not take into account dispersion due to the
            energy dependence of the drift velocity (courtesy of Van Allen
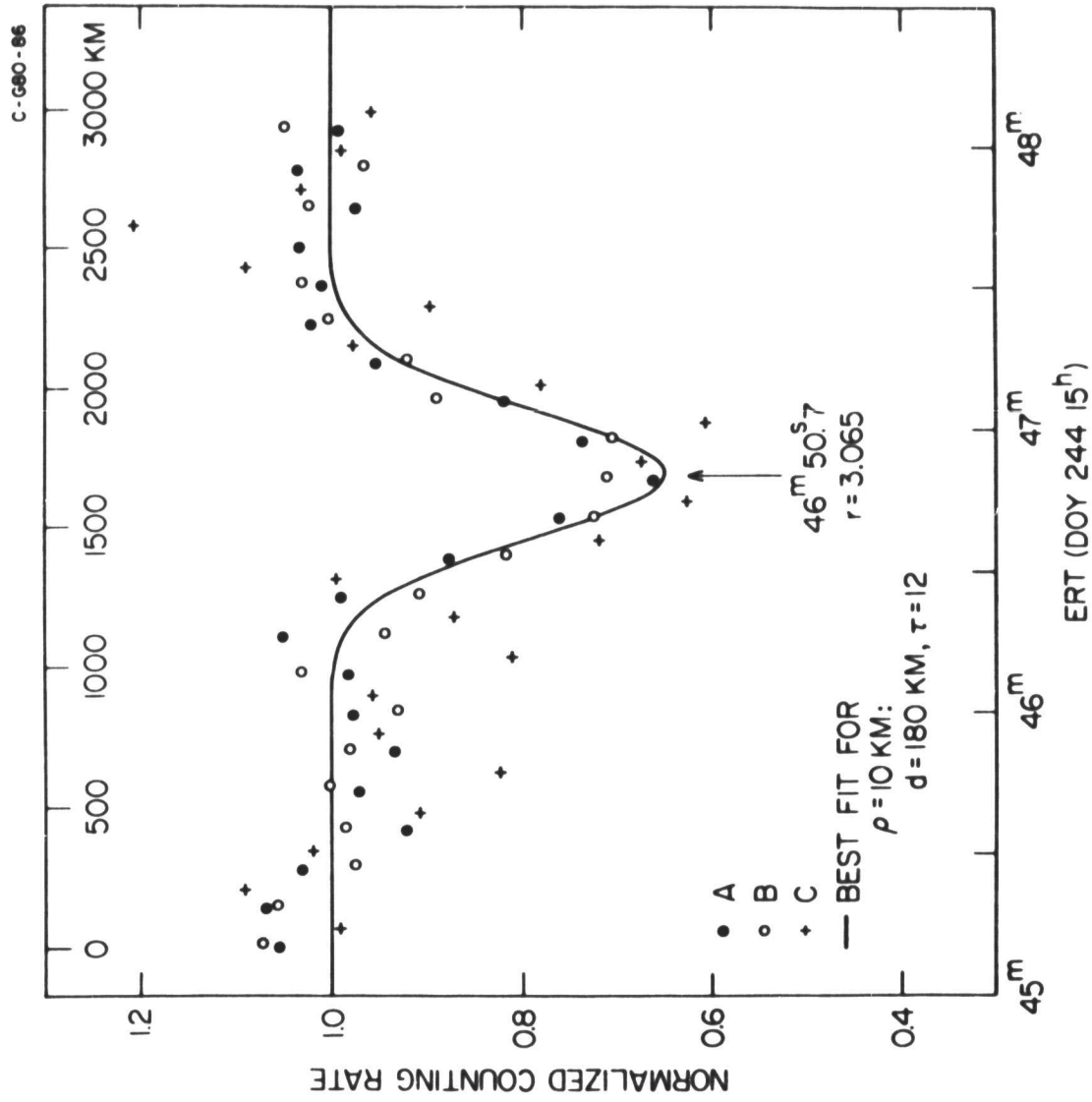   et al., 1980c).

Fig.
42B

Fig. 43. Calculated drift periods of electrons (upper two curves) and protons
          (lower two curves) relative to Enceladus as a function of kinetic
          energy of the particles. Of particular interest is the resonant, or
          synchronous, energy for electrons of 1.00 MeV at 90° pitch angle and
          1.21 MeV at 30°. Because protons drift in the opposite direction
          from the satellite motion, they cannot be in resonance at any energy
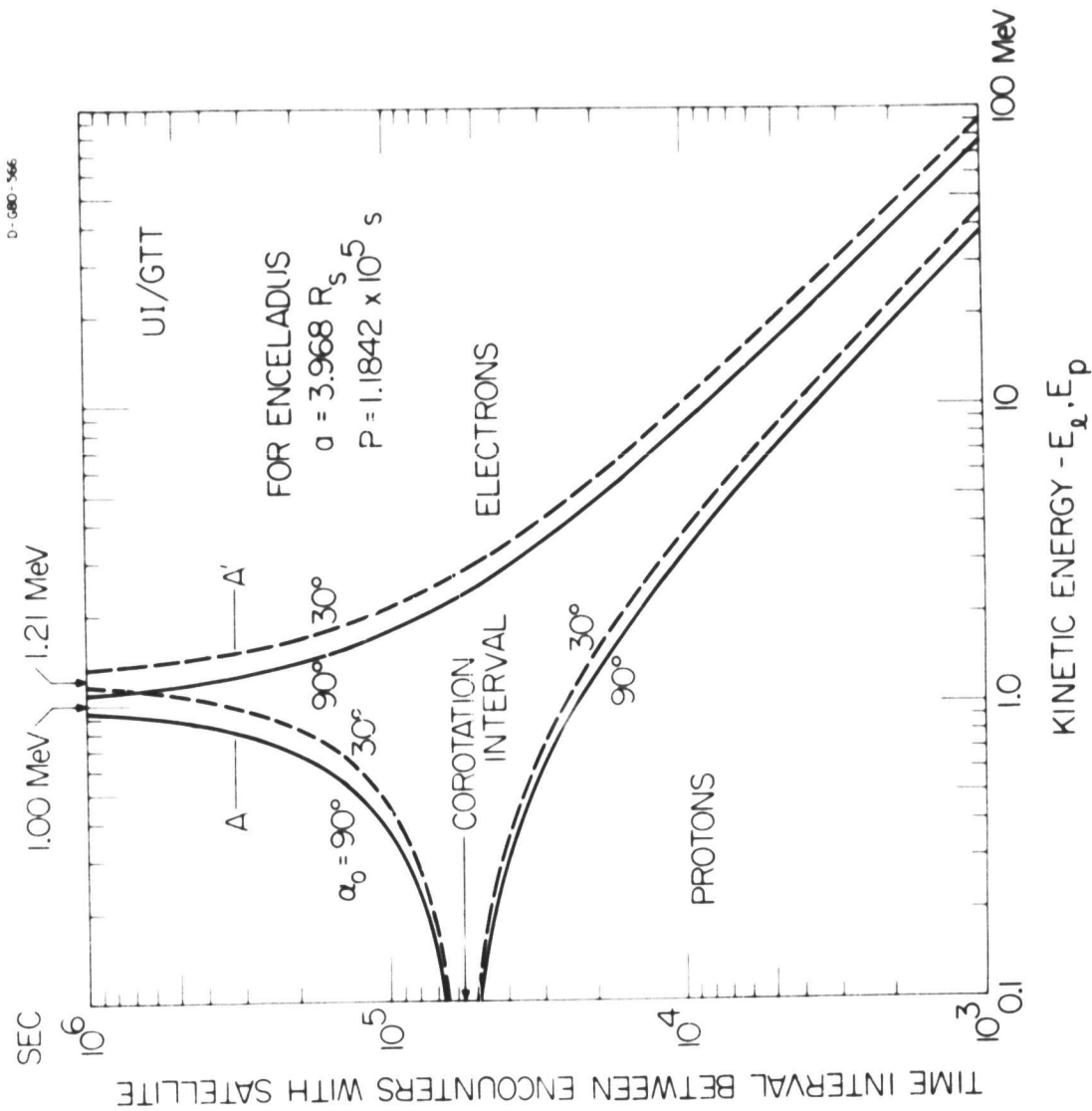   (courtesy of Van Allen et al., 1980c).

Fig. 43

Fig. 44. Counting rate (20 minute average) of 7-10 MeV electrons under the ring plane. The solid line superimposed on the observations gives the expected $L^{2.8}$ dependence and counting rate if the electrons result from the $\pi \rightarrow \mu \rightarrow e$ decay of pions produced by cosmic ray interaction with the rings (courtesy of Chenette et al., 1980).
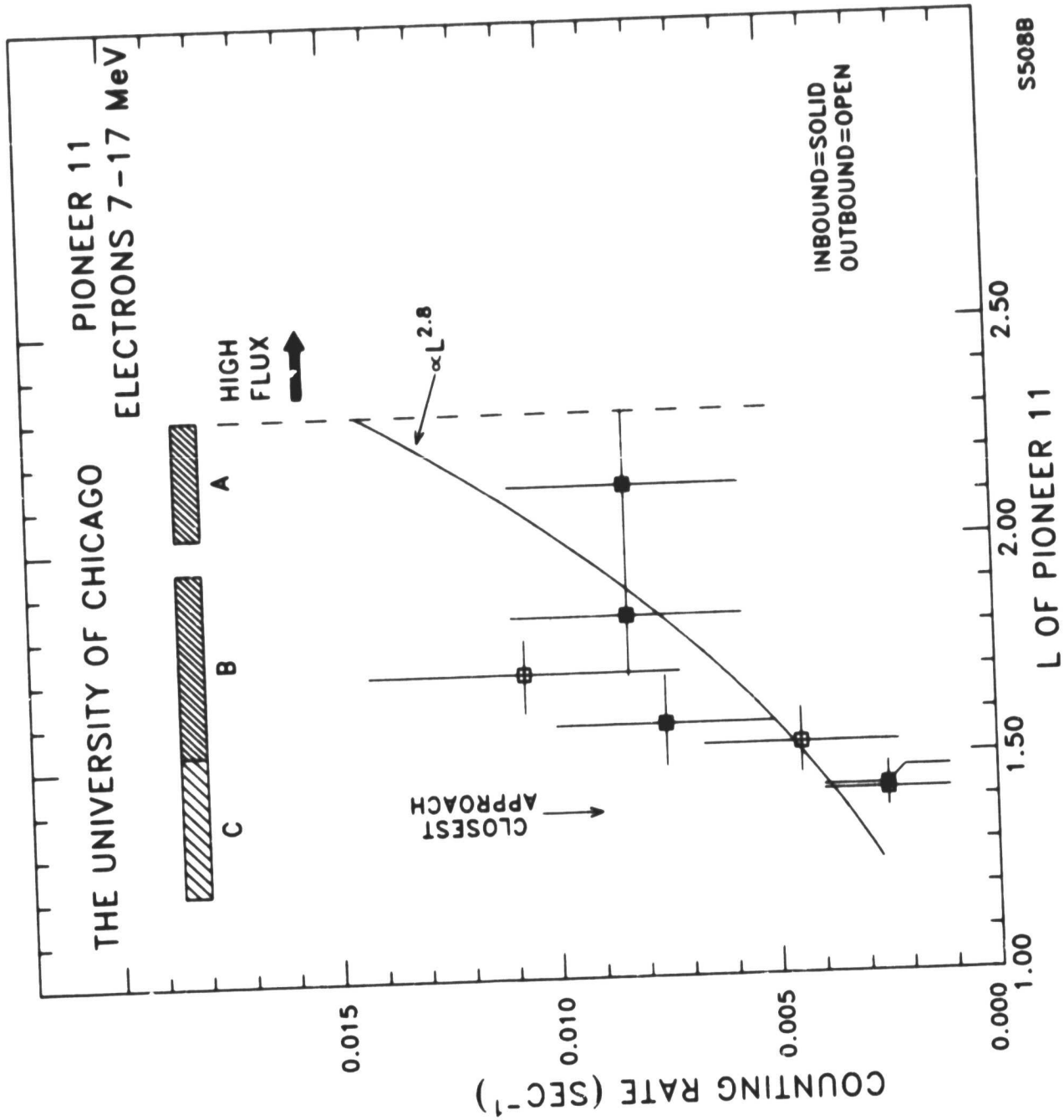
Fig. 44

Fig. 45. The angular velocity of spoke features in the B ring taken from Smith et al. (1981). The magnetic field corotation velocity of 810.76° per day is independent of radial distance, while the Keplerian angular velocity is proportional to $R^{-3/2}$. The dashed lines show the angular velocity for charged particles having the indicated charge to mass ratios, coul/kg (courtesy of Thomsen et al., 1982).
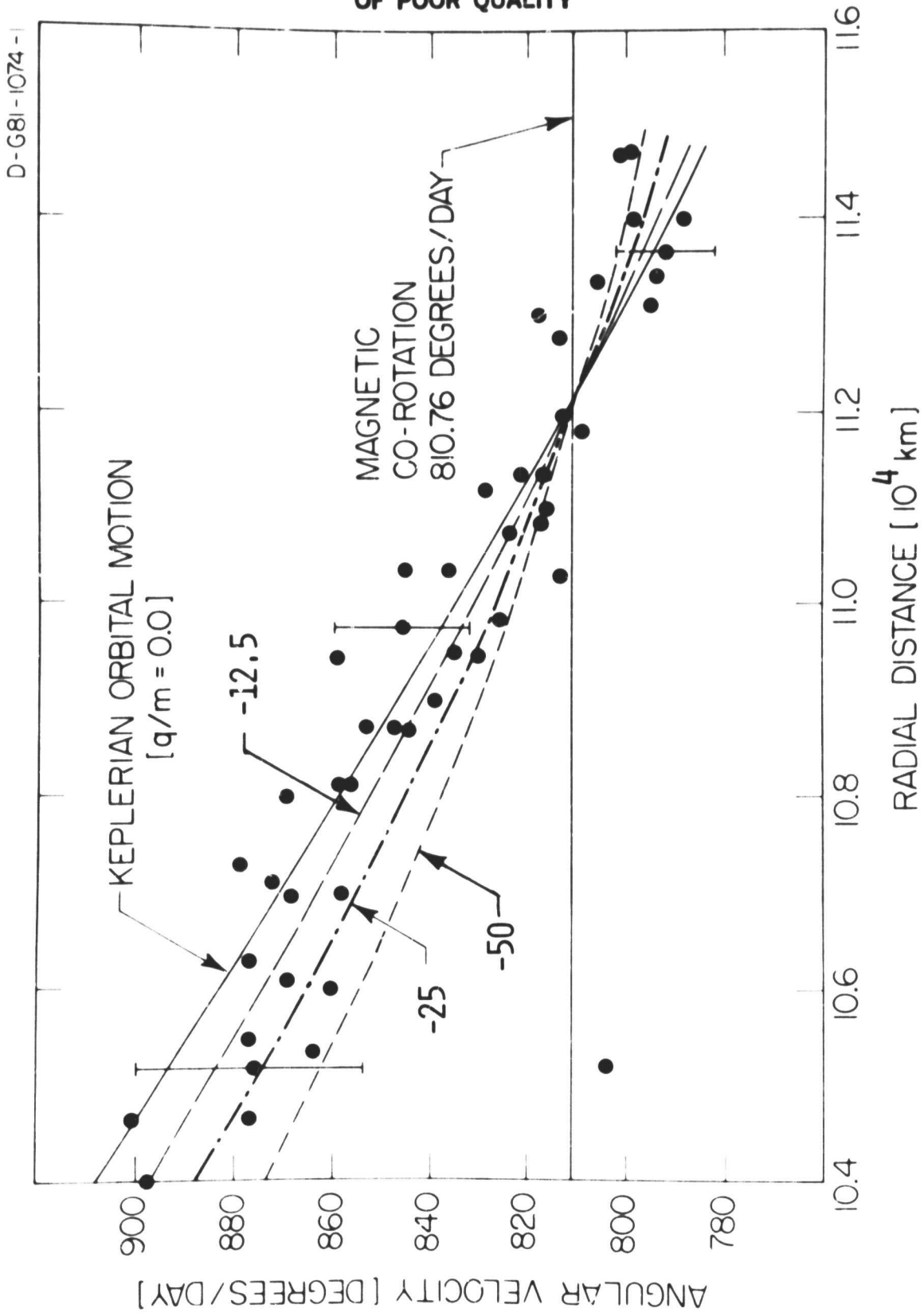
Fig. 45

92

Fig. 46.   Voyager 1 picture of Saturn's rings in forward scattered light (132°
phase angle) from Smith et al. (1981). The increase in the optical
depth of the B ring at 1.63 R$_S$ has been explained in terms of the
stability limit of highly charged submicron dust grains (courtesy of
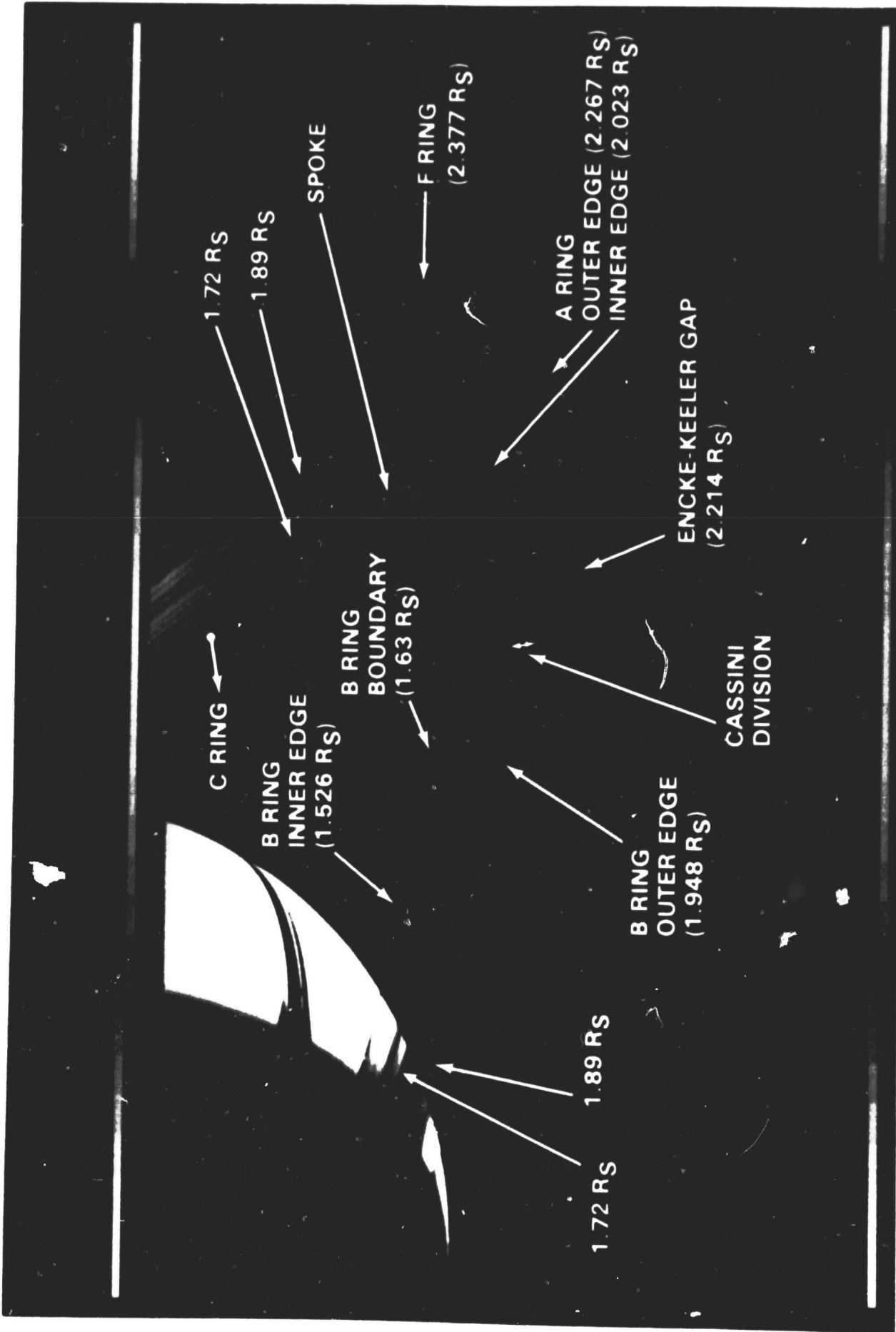Northrop and Hill, 1982).

C RING

B RING
INNER EDGE
(1.526 Rs)

B RING BOUNDARY
(1.63 Rs)

1.72 Rs

1.89 Rs

SPOKE

F RING
(2.377 Rs)

A RING
OUTER EDGE (2.267 Rs)
INNER EDGE (2.023 Rs)

ENCKE-KEELER GAP
(2.214 Rs)

CASSINI
DIVISION

B RING
OUTER EDGE
(1.948 Rs)

1.89 Rs

1.72 Rs

Fig. 46